Expanding the scope of the crystallisation-driven self-assembly of polylactone-containing polymers

Bo Li

Submitted for the degree of Doctor of Philosophy

Department of Chemistry

February 2021

Table of Contents

List of Schemes

List of Figures

List of Tables

Acknowledgements

Submitting my thesis during this pandemic, it reminds me of the difficult time I experienced during my PhD. I couldn't have gone through it without all the unconditional support from my supervisor, Professor Rachel O'Reilly. As such, I would love to express my sincere appreciation to her, not only for invaluable guidance throughout my research but also for the support when I'm overwhelmed with my personal life. I would also like to thank my second supervisor Professor Andrew Dove for all the advice during my PhD studies, especially for the opportunity of collaborating with Professor Alejandro Müller. It has been an honour to work with you in both groups.

My next thank goes to both of the amazing O'Reilly and Dove group members to make my PhD enjoyable. I'd like to thank the minority Chinese group: Dr Yujie Xie, Dr Jin Huang, Dr Zan Hua, Dr Wei Yu and Dr Bo Dong for all the laugh and joy during all meals we had together. I would also like to thank all the wonderful friends in our group: Miss Marjolaine Thomas, Matthieu Miclotte, Dr Robert Keogh, Dr Charlotte Zammit, Dr Spyridon Varlas, Dr Steuhn Jimaja, Dr Stefan Lawrenson, Miss Anissa Khalfa, Miss Cinzia Clamor for all the company in and out the lab. I would like to give my special thank to Dr Matthieu Tschan and Dr Kayla Chiaie for answering all my stupid ROP questions. Also huge thanks to Dr Amanda Pearce for helping me warp up my PhD during this pandemic. I would like to give my biggest thank to Mr Tianlai lai, which would be agreed upon between both groups. Thank you for both helping me in the lab with heavy duties and warming my life with your continued optimism.

Finally, None of these would happen without my parents: Mingyu and David Li. Thank you both for the love, support and pushing me to do a PhD since I was born. I hope reading this thesis could be your happiest moment like what you have been continuously giving me in my life.

Declaration of Authorship

This thesis is submitted to the University of Warwick in support of my application for the degree of Doctor of Philosophy. It has been composed by myself and has not been submitted in any previous application for any degree. The work presented (including data generated and data analysis) was carried out by the author except in the cases outlined below:

The DSC data in Chapters 4 was obtained and analysed by Asier Olmos and Maira Caputo;

The quantitive ^{13}C NMR was obtained by Dr Dr Cécile LE Duff.

List of Abbreviations

1D	One-dimensional
2D	Two-dimensional
3D	Three-dimensional
4VP	4-vinylpyridine
Å	Angstrom(s)
a_0	Contact area of the hydrophilic headgroup interface
AIBN	2,2-Azobis(2-methylpropionitrile)
AM	Acrylamide
ATRP	Atom transfer radical polymerisation
BCP	Block copolymer
BHT	2,6-di-tert-butyl-4-methylphenoxide
c	Concentration
$CDCl_3$	Deuterated chloroform
CDSA	Crystallisation-driven self-assembly
CEPA	4-cyano-4-(((ethylthio)carbonothioyl)thio)pentanoic acid
CHPET	2-cyano-5-hydroxypentan-2-yl ethyl carbonotrithioate

CLSM	Confocal laser scanning microscopy
CRP	Controlled radical polymerisation
Cryo	Cryogenic
CTA	Chain transfer agent
d	Diameter
d	Doublet
DBDS	Dibenzoyl disulfide
DBU	1,8-diazabicyclo[5.4.0]undec-7-ene
DCC	Dicyclohexylcarbodiimide
DCM	Dichloromethane
$Đ_M$	Molar-mass dispersity
DMA	*N*,*N*-dimethlyacrylamide
DMAEMA	2-(dimethylamino)ethyl methacrylate
DMAP	4-dimethylaminopyridine
DMF	*N*,*N*-Dimethyl formamide
DP	Number average degree of polymerisation
DPP	Diphenyl phosphate
DSC	Differential scanning calorimetry

Eq.	Equivalents
EtOH	Ethanol
GO	Graphene oxide
I	Initiator
IR	Infrared
J	Coupling constant in NMR spectroscopy
kDa	Kilodaltons
LAM	Less activated monomer
l_c	Length of hydrophobic block
L_i	Length of each counted particle
L_n	Number-average length
LP	Living polymerisation
L_w	Weight-average length
m	Multiplet
M	Monomer
m/z	Mass to charge ratio
MA	Methyl acrylate
MAM	More activated monomer

MeOH	Methanol
mg	Milligram(s)
mL	Millilitre(s)
MMA	Methyl methacrylate
mmol	Millimole(s)
M_n	Number average molecular weight
mol	Mole(s)
MS	Mass spectrometry
M_w	Weight average molecular weight
N_i	Number of micelles of length L_i
NIPAm	*N*-isopropylacrylamide
NMP	Nitroxide-mediated polymerisation
NMR	Nuclear magnetic resonance
NVC	*N*-vinyl carbazole
NVP	*N*-vinyl pyrrolidone
OPV	Oligo(*p*-phenylenevinylene)
p	Packing parameter
P2VP	Poly(2-vinylpyridine)

P3DSe	Poly(3-decylselenophene)
P3HT	Poly(3-hexylthiophene)
PAA	Poly(acrylic acid)
PC	Photoredox catalyst
PCL	Poly(*ε*-caprolactone)
PDHF	Poly(di-*n*-hexylfluorene)
PDMA	Poly(*N,N*-dimethlyacrylamide)
PDMAEMA	Poly(2-(dimethylamino)ethyl methacrylate)
PDMS	Poly(dimethylsiloxane)
PE	Poly(ethylene)
PEG	Poly(ethylene glycol)
PEO	Poly(ethylene oxide)
PET	Poly(ethylene terephthalate)
PFS	Poly(ferrocenyldimethylsilane)
PFTMC	Poly(spiro[fluorene-9,5'-[1,3]-dioxan]-2'-one)
PIP	Polyisoprene
PiPrOx	Poly(2-isopropyl-2-oxazoline)
PISA	Polymerisation-induced self-assembly

PLA	Poly(lactide)
PLLA	Poly(L-lactide)
PMMA	Poly(methyl methacrylate)
P_n	Polymer with a degree of polymerisation of n
ppm	Parts per million
PS	Polystyrene
q	Quartet
RAFT	Reversible addition-fragmentation chain transfer
RDRP	Reversible deactivation radical polymerisation
RI	Refractive index
ROMP	Ring-opening metathesis polymerisation
ROP	Ring-opening polymerisation
RT	Room temperature
s	Singlet
SEC	Size exclusion chromatography
St	Styrene
t	Time
t	Triplet

TBD	1,5,7-triazabicyclo[4.4.0]dec-5-ene
T_c	Crystallisation temperature
TEA	Triethanolamine
TEM	Transmission electron microscopy
T_g	Glass transition temperature
THF	Tetrahydrofuran
T_m	Melting temperature
TMS	Trimethylsilane
TTC	Trithiocarbonates
TTDS	Tetraethylthiuram disulfide
UA	Uranyl acetate
UV	Ultraviolet
v	Volume of hydrophobic segment
VAc	Vinyl acetate
W_n	Number-average width
wt. %	Weight percent
W_w	Weight-average width
αClεCL	α-Chloro-ε-caprolactone

β-PL	β-Propiolactone
γ-BL	γ-Butyrolactone
δ-VL	δ-valerolactone
ε-CL	ε-caprolactone
ζ-HL	ζ-Heptalactone
PDL	ω-pentadecalactone
θ	Angle
λ	Wavelength
$\lambda_{abs.}$	Wavelength of absorption
µg	Microgram(s)
µL	Microlitre(s)
µmol	Micromole(s)
l_c	Length of a hydrophobic block
v	Volume
γ	Interfacial tension

Chapter One - Introduction

1.1 Abstract

Aiming at expanding the scope of crystallisation-driven self-assembly with polylactone based copolymers, a number of block copolymers have been synthesised using a combination of reversible addition-fragmentation chain transfer polymerisation (RAFT) and ring-opening polymerisation (ROP). As it is fundamental to this work, this chapter briefly describes the main concepts of controlled polymerisations to build synthetic block copolymers. Ring-opening polymerisation of both small ring lactones and macrolactones is then explored, followed by an introduction to synthetic methods for utilising crystalline core-forming blocks. Methods for solution self-assembly are then summarised to compare their different characteristics. Crystallisation-driven self-assembly (CDSA) is then discussed as a key approach for preparing micelles of controlled size and dimension. Furthermore, a few fundamental characterisation techniques are discussed to give some insight into understanding the CDSA of lactone-based polymers.

1.2 Synthesis of block copolymers

Polymers play a crucial role in nature, including information storage in nucleic acids and catalysing biochemical reactions in cells.[1] The overall properties of natural polymers are typically reserved by the organisation of the units. For synthetic polymers, the way different monomer units distribute themselves along a polymer chain, such as statistically, gradient or grouped into blocks, can also play a significant role in determining their properties (**Figure 1.1**). These various polymer architectures can be obtained by many polymerisation methods, such as free radical polymerisation, reversible-deactivation radical polymerisation and ring-opening polymerisation, utilising thousands of different monomers. However, to build well-defined block polymers with precise polymer composition and narrow molecular weight distribution, 'living' polymerisation and 'controlled' polymerisation are the most used methods.

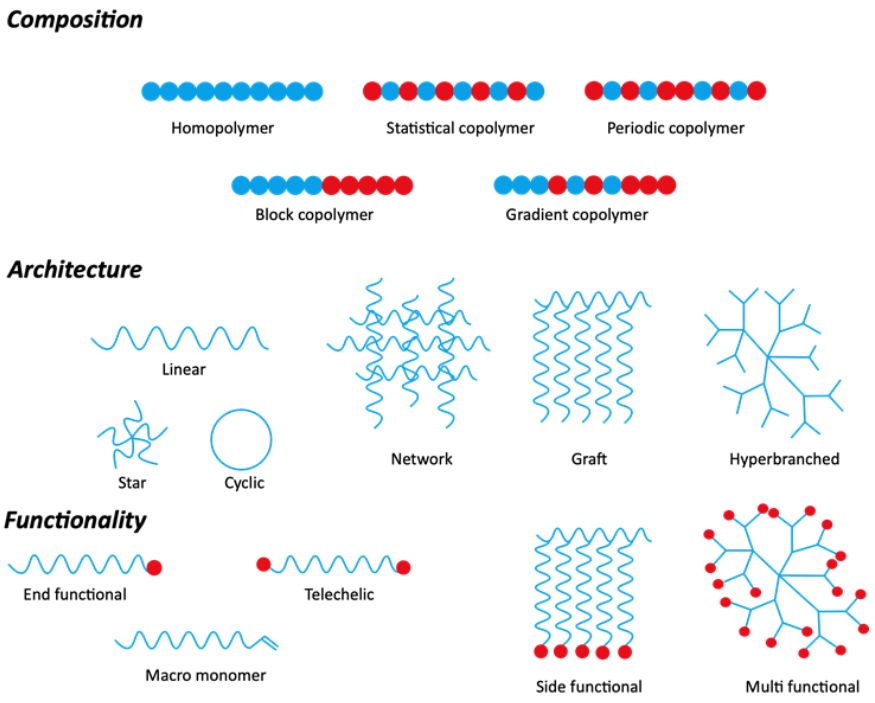

Figure 1.1 Examples of polymer architecture-composition, topology, and function, where blue and red indicate different monomers.

1.2.1 Living polymerisation

The concept of living polymerisation is where all polymer chains grow irreversibly and at the same rate, in the absence of termination. [2] This concept was first postulated by Flory in 1940 for the polymerisation of ethylene oxide, and was later supported by experimental data from Perry and Hibbert, which laid the foundation for further exploration of living polymerisation.[3, 4] In 1992, seven experimental criteria were proposed by Quirk and Lee to diagnose a living polymerisation:[5]

1. Polymerisation proceeds until all of the monomers have been consumed. Further addition of monomer results in continued polymerisation.
2. The number average molecular weight and monomer conversion express a linear relationship.
3. The number of growing polymer chains and active centres is constant and independent of conversion.
4. Targeted DP can be controlled by the ratio of monomer to the initiator.
5. Polymers of low polydispersity are produced.
6. Block copolymers can be prepared by sequential monomer addition.
7. Chain-end functionalised polymers can be prepared in quantitative yield.

Unfortunately, stringent conditions are often necessary in order to be able to perform truly living polymerisation. For example, the living cationic polymerisation of vinyl monomers could only proceed in the absence of oxygen and water.[6] Therefore, polymerisation methods, such as deactivation radical polymerisation (RDRP), have been developed to fulfil the need for controlled polymerisation under less stringent conditions.

1.2.2 Deactivation radical (RDRP) Polymerisation

Deactivation radical polymerisation (RDRP) is a method for controlled polymerisation where there is only limited occurrence of termination or chain-transfer reactions, meaning it retains many of the criteria of living polymerisation, such as low polydispersity and efficient chain-end functionality, but is able to tolerate much milder conditions. The development of RDRP has received great interest since the 1990s when controlled radical polymerisation using nitroxide agents was first reported.[7, 8] This method, termed nitroxide-mediated radical polymerisation (NMP), has then been widely expended to styrene derivatives and acrylates.[9] NMP gains its living polymerisation nature from persistent radical effect. [10] The persistent radical effect is when a radical is favourable to form, due to its stability compared to other radical couples. In the case of NMP, the nitroxide species act as persistent radical. This ensures the growing end of the polymer chain from the binding and unbinding of nitroxides. The chain continues to grow to consume any available monomers under suitable conditions unless thermally deactivated. (**Scheme 1.1**)

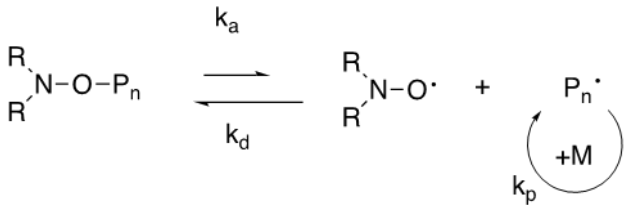

Scheme 1.1 Accepted mechanism of nitroxide-mediated polymerisation.

In 1995, a record deactivation radical polymerisation was demonstrated, known as atom transfer radical polymerisation (ATRP).[11] ATRP also relies on the persistent radical effect to achieve controllable polymerisation. In this case, the persistent radical is generated by the oxidation of a transition metal. (**Scheme 1.2**) As such, a transition metal complex

is employed during ATRP, with a range of transition metals having been reported, such as Cu, Fe, Ru, Ni, and Os.[11-13] In ATRP, termination could occur by the transition metal complex shifting to a lower oxidation state. The number of initiators determines the number of polymer chains in ATRP, meaning each chain has the same probability to propagate with monomers as a living process. However, the presence of metal catalyst has limited its general applicability due to the difficulty in conducting ATRP in aqueous media.

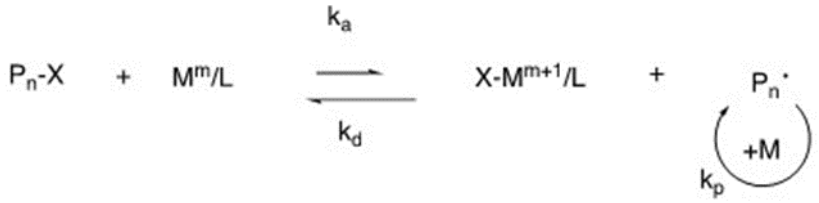

Scheme 1.2 Accepted mechanism of atom transfer radical polymerisation.[11]

1.2.3 Reversible addition-fragmentation chain transfer (RAFT) Polymerisation

A third major RDRP method, reversible addition-fragmentation chain-transfer (RAFT) polymerisation, was developed by Chiefari, et al. in 1998.[14] Here, a thiocarbonyl chain transfer agent (CTA) is employed during RAFT to control the molecular weight and dispersity during a free radical polymerisation. In general, RAFT polymerisation requires the presence of monomer that is capable of undergoing a radical polymerisation, a radical source and a RAFT agent in the form of thiocarbonate compound. The polymerisation starts with initiation by a free radical source. The free radical could be obtained from the decomposition of an initiator, such as azobisisobutyronitrile (AIBN). This then reacts with the monomer to yield a propagating polymeric radical (P_1•, **Scheme 1.3**). A longer propagating polymeric radical P_n• was then formed by capturing

monomers. The polymeric radical P_n• will then associate with CTA to form a RAFT adduct radical. The RAFT adduct radical could then yield either a radical (R•, **Scheme 1.3**), a polymeric RAFT agent (S=C(Z)S-P_n•, **Scheme 1.3**), or the starting radical and CTA, establishing a pre-equilibrium. The released radical R• then undergoes another initiation to generate a new propagating polymeric radical (P_m•, **Scheme 1.3**). Subsequently, all present radicals undergo a rapid interchange, leaving chains the equal opportunity to grow during the main equilibrium process. Termination is then able to occur when two polymeric radicals react to form chains that cannot react further, known as dead polymer chains. Ideally, termination reactions are minimised during RAFT by choosing a suitable CTA (**Scheme 1.3**).

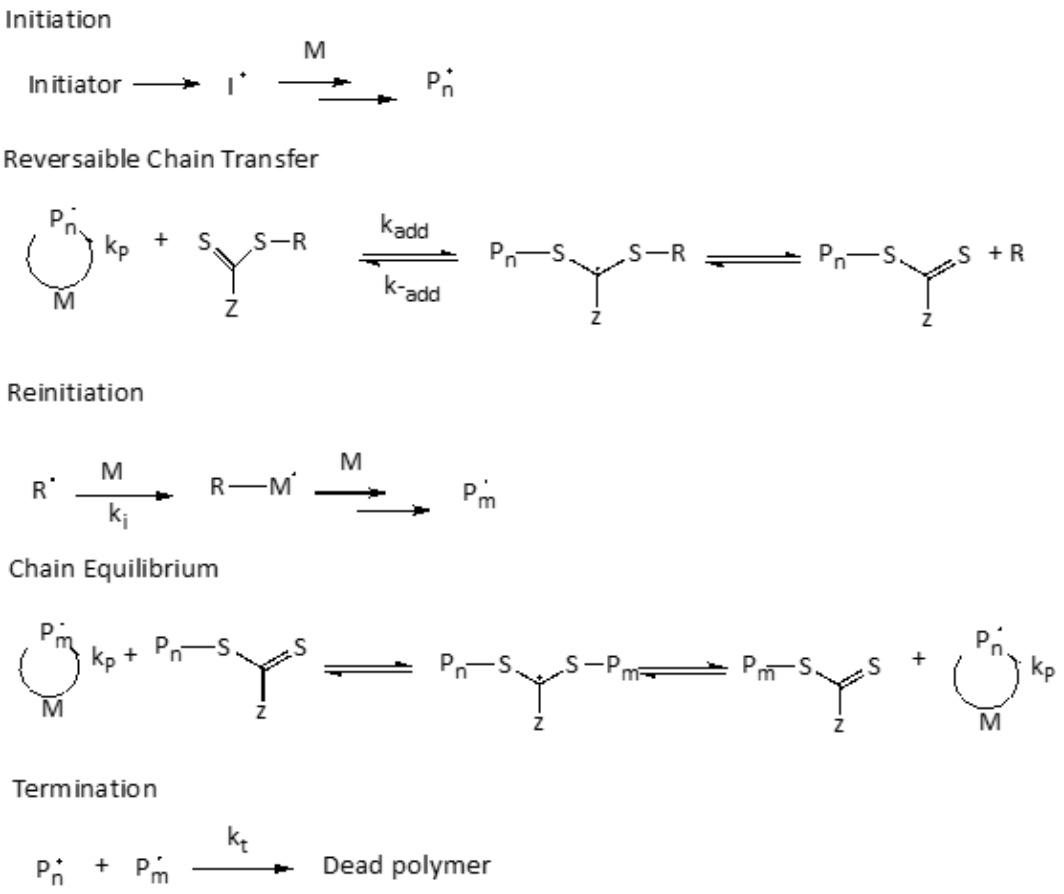

Scheme 1.3 Mechanism of reversible addition-fragmentation chain-transfer polymerisation.[14]

The successful choice of CTA for RAFT polymerisation can yield polymers of predictable molecular weight and low dispersity with maintained end group functionality. The addition and fragmentations rates can be significantly affected by the free radical leaving group (R) and the Z group, which means each must be carefully considered with the monomer used. The Z group must have moderate stability to be able to form the radical intermediate. In a general concept to select the Z group, a strong electron-donating Z group is required for less active monomers such as vinyl acetate (VAc), *N*-vinyl carbazole (NVC) and *N*-vinyl pyrrolidone (NVP), to enable polymeric radicals to be released from the thiocarbonyl intermediate radicals.[15] On the other hand, more active monomers, for example, methyl methacrylate (MMA), styrene (St), methyl acrylate (MA), acrylamide (AM) and acrylonitrile (AN), require an electron-withdrawing, or weakly electron-donating Z group to stabilise the thiocarbonyl intermediate radical. (**Scheme 1.4**)

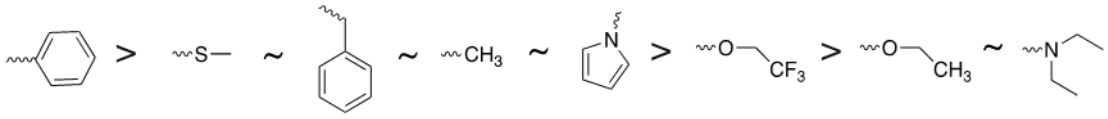

Scheme 1.4 A guide for the selection of RAFT CTA Z group. The addition rate decreases but fragmentation rates increase from left to right.[15]

A desirable R group must be a good leaving group and a good radical for initiating polymerisation when in the R• form. This allows radicals formed from less active monomers to be more prone to react during reinitiation. A general guide for the reactivity of the R group is listed below (**Scheme 1.5**):

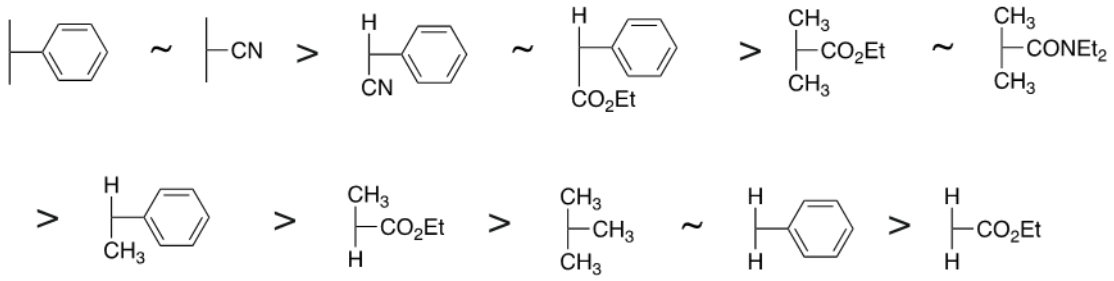

Scheme 1.5 Relative stability/ability to reinitiate for RAFT CTA R groups.[15]

RAFT polymerisation has been successfully applied in the synthesis of a wide range of functional polymers with good control owing to its high tolerance of functional group.[15-17] However, end-functionalised polymers is also achievable by ATRP and NMP using selected functional CTAs. A major advantage of RAFT is it can be carried out in a range of conditions, including aqueous media. As such, RAFT polymerisation has been considered as one of the most versatile and robust methods in polymer synthesis. A variety of architectures including block copolymers,[18] star-shaped polymers[19] and hyperbranched polymers[20] have been delivered by RAFT polymerisation.

1.2.4 Ring-opening polymerisation

Ring-opening polymerisation of cyclic monomers such as cyclic alkenes, [21] epoxides, [22] lactides, [23, 24] lactones, [25, 26] carbonates, [27, 28] etc. has been studied intensively to synthesise polymers with various architectures and useful functionality, including renewability, degradability and biocompatibility. As a consequence, different ROP techniques have been developed, such as ring-opening metathesis polymerisation (ROMP), [21] cationic ROP (CROP), [29] anionic ROP (AROP), [30] enzymatic ROP (eROP), [31-33] 'immortal' ROP (iROP) [33-35] and ring-opening copolymerisation (ROCOP).[36]

The ability of cyclic monomers with an ROP functional group to undergo ring-opening is largely due to the thermodynamics of ring-opening polymerisation. Based on the assumption that every polymer chain exhibits an equal reactivity, considered independently from the degree of polymerisation, the Gibbs free-energy of ring-opening can be defined as:

$$\Delta G_{RO} = \Delta H_{RO}^{\theta} - T(\Delta S_{RO}^{\theta} + Rln[M])$$

Equation 1.1 Gibbs free-energy of ring-opening polymerisation.

where ΔG is the Gibbs free-energy, ΔH^{θ} is the standard enthalpy of ring-opening, T is the temperature, ΔS^{θ} is the standard entropy of ring-opening, R is the gas constant and [M] is the concentration of monomer.[37] The ring-opening polymerisation is only possible when the Gibbs free energy is negative, when a mechanism of ring-opening polymerisation is required, generally facilitated by a catalyst.

Ring-opening polymerisation is a chain-growth process where both polymerisation and depolymerisation are generally competing at the same time. The overall polymerisation proceeds only when the rate of polymerisation (k_p) is higher than the rate of depolymerisation (k_d). During ROP, the monomer concentration will decrease during polymerisation, resulting in an increase in the rate of depolymerisation. As a consequence, the rate of polymerisation (k_p) is equal to the rate of depolymerisation (k_d) when the concentration of monomer and polymer has reached equilibrium. To enable ring-opening polymerisation, the concentration of monomer is required to be above a critical value, as below this concentration, the equilibrium is shifted in favour of the monomer. The critical monomer concentration is accounted for in the **equation 1.1**.

1.2.4.1 Lactone polymerisation

Lactone monomers are cyclic esters of different ring sizes varying from three to as large as sixteen. Cyclic esters with functional side chains are also considered as lactones, such as alkyl functionalised δ-decalactone (δDL), γ-caprolactone and halo-functionalised α-chloro-ε-caprolactone (**Figure 1.2**). The majority of lactones can be sourced from various plants and animals, where they have been widely applied in many different industries, such as food additives (δ-decalactone), perfume and flavouring agents (PDL), and as renewable and biocompatible materials.

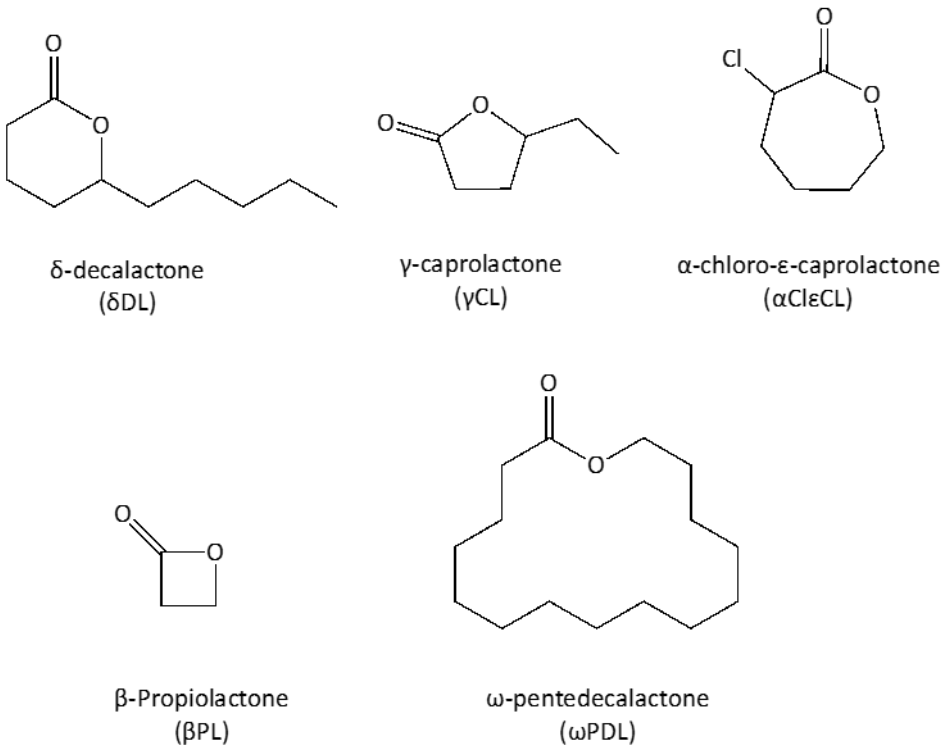

Figure 1.1 Examples of substituted lactones, small lactones and macrolactones.

Lactones can also be synthesised from other renewable materials. Baeyer-Villiger oxidation, since it was first demonstrated in 1899, has been the most used method for preparing lactones from cyclic ketones. The presence of peroxy acid attacks the carbonyl

of cyclic ketones leading a Criegee rearrangement to form a lactone and acid, resulting in good yields.[38] The mechanism is shown in **Scheme 1.6**.

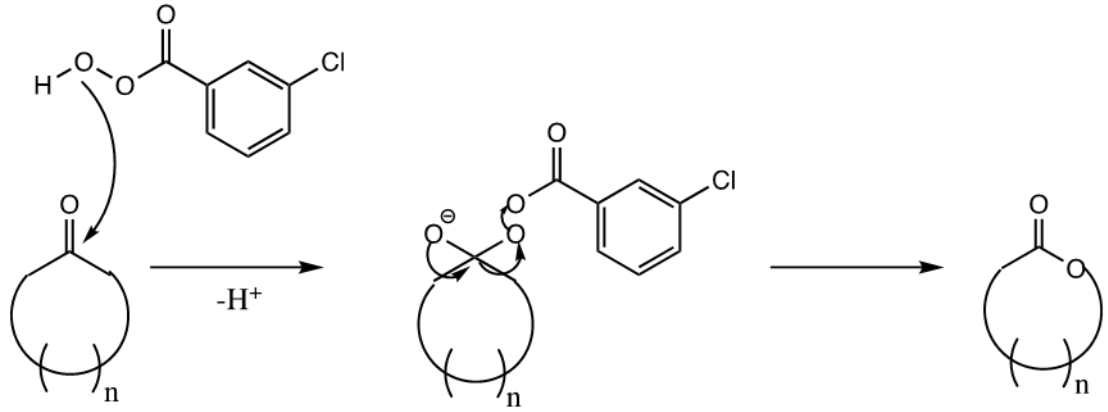

Scheme 1.6 Baeyer-Villiger oxidation of cyclic ketones to lactones.

In regard to the ring-opening polymerisation of cyclic lactones, most of the small ring lactones (4-, 6- and 7-membered rings) possess conformational ring-strain, undergoing an exothermic process due to a highly negative ΔH^{θ}. (**Table 1.1**)[37] In such a case, a negative Gibbs free-energy is achievable, which allows the ring-opening polymerisation. As for the 5-membered γ-butyrolactone (γBL), the low ring strain results in a positive ΔH^{θ}, which is not able to cancel the large negative entropic contribution ΔS^{θ}. This results in a positive Gibbs free energy, making the polymerisation challenging. Although there have been reports on the copolymerisation γBL and ε-caprolactone (εCL),[39] in 2015, the first successful example of homopolymerisation of γBL was reported by Chen.[40] The polymerisation was performed under relatively extreme conditions (-40 °C) to reduce the entropic penalty of the ROP. This also applies to other small lactones as free movement is limited after the monomer is incorporated into the polymer chain, providing a negative change in entropy. As a result, ring-opening polymerisation of small ring-size lactones often requires low temperature and high concentration to limit the

entropic penalty. Notably, except γBL, most ring-opening polymerisation of other small ring-size lactones is achievable above 0 °C.

Table 1.1 Standard enthalpies and entropies of ring-opening of small lactones.

	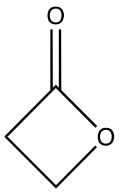 **β-propiolactone (βPL)**	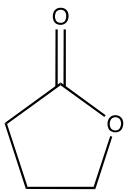 **γ-butyrolactone (γBL)**	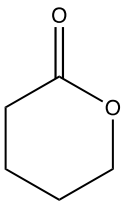 **δ-valerolactone (δVL)**	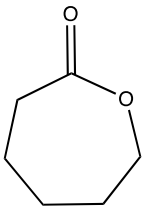 **ε-caprolactone (εCL)**
ΔH^{θ}(kJ mol^{-1})	-82.3	5.1	-27.4	-28.8
ΔS^{θ}(J mol^{-1} K^{-1})	-74.0	-29.9	-65.0	-53.9

In comparison, the ΔH^{θ} of macrolactones, having ring sizes of eight or above, is normally positive. This is as a result of the strain decrease due to the limited strained bond angles inside a large ring, describe as 'strainless'.[41] Although an entropic gain is possible for macrolactones from less hindered chain rotation when ΔS^{θ} is positive. As a consequence, the ROP of macrolactones is generally performed under high temperatures and lower concentrations to offset this change in enthalpy.

To achieve controlled ROP of lactones, understanding the possibility of transesterification side reactions is also essential. There are two different transesterification reactions that may occur during ROP; intermolecular and intramolecular. Intermolecular transesterification is between the chain end of one polymer chain and the ester functional group of another polymer chain. (**Scheme 1.7a**) This will result in an extension of the former polymer chain and a shortening of the latter

chain, increasing the overall dispersity of the polymerisation. Intramolecular transesterification is between the chain end of one polymer chain and an ester functional group within the same polymer chain. (**Scheme 1.7b**)

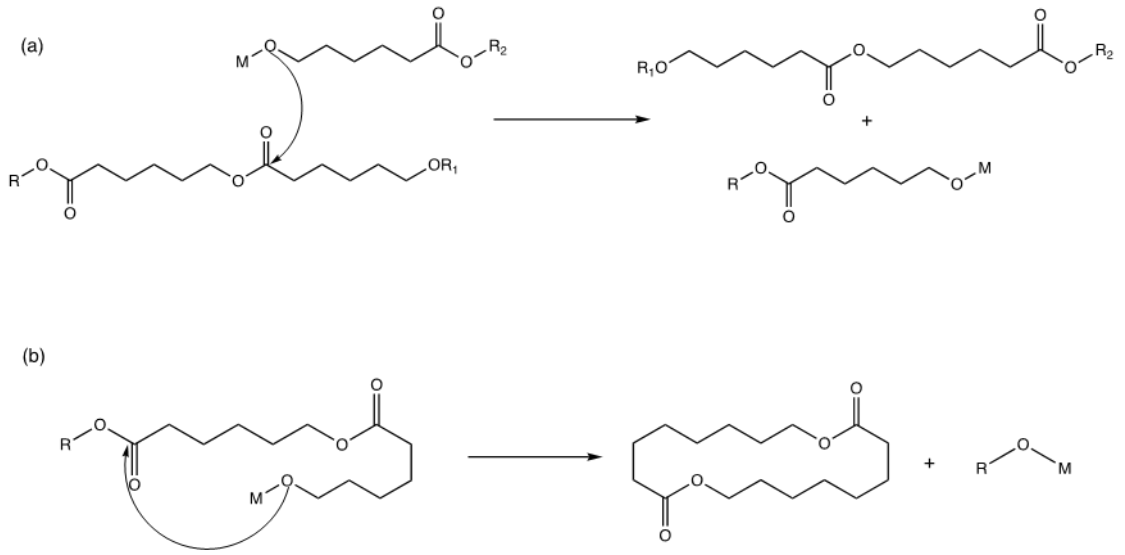

Scheme 1.7 (a) Intermolecular and (b) intramolecular transesterification side reactions during lactone polymerisation.

This will generate cyclic esters and a shorter polymer chain, again increasing the dispersity of the polymerisation. During the polymerisation of small ring-size lactones such as δVL or εCL, the ring-opening is much more favourable than transesterification, meaning transesterification generally only occurs when the monomer reaches high conversion. Thus, a controlled polymerisation is accessible by termination before transesterification can occur at a specific conversion.[42] As in for macrolactones, such as PDL, the chain strain leads to higher energy being required for ROP. This means that, ROP is not preferable to transesterification, making control of the polymerisation challenging as transesterification and polymerisation are both likely to occur, leading to large dispersities.[41]

1.2.4.2 Pentadecalactone polymerisation

Pentadecalactone (PDL) is a lactone monomer that could be either sourced from angelica root oil or produced synthetically from cyclotetradecanone, which makes it a promising renewable material.[43] As a sixteen-membered ring macrolactone with no side chain, the polymerisation of PDL exhibits high crystallinity from the repeating long alkyl chain. The polymer poly(pentadecalactone) (PPDL) also displays high melting and crystallisation temperatures (T_m and T_c) as a consequence of the long aliphatic backbone. These properties often lead to a comparison between PPDL and low-density Polyethylene (LDPE).[44, 45] Although the extra ester group (adding an ester group into PE) has allowed for the degradation of PPDL. However, the degradation has proved to be more difficult than other polymerised lactones, due to the high hydrophobicity of the long alkyl chain. The degradation of PPDL has only been demonstrated under highly acidic or basic conditions or in the presence of enzyme.[31, 46]

Similar to most macrolactones, PDL exhibits a ΔH^{θ}= +3 kJ mol^{-1} as a consequence of the 'strainless' large ring and an ΔS^{θ}= - 23 J mol^{-1} K^{-1} from the gain in free rotation. As such, a negative Gibbs free energy for the polymerisation is achievable when performed under high temperature so that $-T\Delta S^{\theta}$ would be able to offset the positive enthalpy.

The first successful example ROP of PDL was catalysed by Novozyme 435 in 1996.[47] However, water is required to activate the enzyme during polymerisation, which could also initiate PDL, resulting in polymer chains with different end groups when using another initiator. As an industrially interesting material, the polymerisation of PDL has also been studied widely using commercially available organocatalysts.[26] Among the studied organocatalysts, the polymerisation of PDL could only reach high conversion

when catalysed by 1,5,7-triazabicyclo[4.4.0]dec-5-ene(TBD), with other organocatalysts showing either oligomer formation or no polymerisation. Organometallic catalysts with various metal centres were also shown to successfully catalyse the polymerisation of PDL, including Al,[36, 48] Sn, [48] Zn,[49] Ca,[49] and Mg.[34](**Figure 1.3**) High molecular weights of PPDL were accessible with these catalysts. Furthermore, a catalyst/chain transfer agent (CTA) complex is generated to propagate polymerisation, which usually requires equimolar organometallic catalyst with initiator. This meant the PPDL molecular weights could be defined by the molar ratio of monomer-to-initiator-to-catalyst as in 'classic' ROP. In particular, the $Mg(BHT)_2(THF)_2$ species has been shown the ability to catalyse the reaction in 'air'. This could reduce the cost when producing PPDL in industrial scale compared to the inert environment required by other organometallic catalysts. However, as a macrolactone, the formation of cyclic species of PDL from intramolecular transesterification side reaction could not be prevented with any of the catalysts above, leading to a high polydispersity.

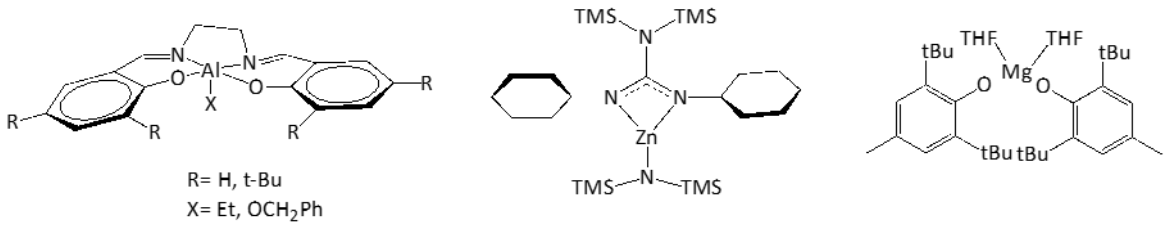

Figure 1.2 Examples of organometallic catalysts used in ROP of PDL.

1.3 Block copolymer self-assembly in solution

Amphiphilic block copolymers containing both hydrophobic and hydrophilic blocks are able to self-assemble in aqueous solvents. For example, water has been the most studied for such self-assembly as a selective solvent for the hydrophobic block. The assembly of amphiphilic block copolymers seeks to minimise the unfavourable interactions between the hydrophobic block and the aqueous solvent, resulting in various self-assembled structures.[50]

1.3.1 Morphology of block copolymer self-assembly in solution

There is a wide range of morphologies that can be obtained from amphiphilic block copolymer self-assembly, including spherical micelles, rods, bicontinuous structures, lamellae, vesicles, large compound micelles (LCMs) and large compound vesicles (LCVs).[50] The formation of these morphologies is typically determined by three main characteristics: the flexibility of the core-forming block, the interfacial tension between the micelle core and the solvent, and the repulsive interactions among corona-forming chains.[51] Herein, the morphologies can be adjusted by introducing factors that are relevant to these three characteristics, such as copolymer composition,[51] copolymer concentration in solution,[52, 53] nature of the common solvent,[54, 55] and the presence of additives.[51, 56]

To better understand the transition of morphologies of BCP self-assembly in solution, a packing parameter, p, has been used as a predictive tool using the influence of molecular curvature.[57] In a hydrophilic solvent, $p = v/a_0 l_c$, where v is the volume of the hydrophobic block, l_c is the length of the hydrophobic block, and a_0 is the optimal area of the interface. Based on this, spherical micelles are formed when p ≤ ⅓, cylinders between ⅓

< p ≤ ½ and vesicles or bilayers with low curvature are formed when ½ < p ≤ 1. (**Figure 1.4**) To date, spherical micelles have been the most commonly reported and studied morphology, as they are easily accessible due to the small packing parameter. Vesicles or bilayers form from a reduced volume of the hydrophilic block in a hydrophilic solvent, leading to a low curvature than spherical micelles. Such morphologies exhibit a structure that the hydrophobic block resides between hydrophilic core and a hydrophilic corona, showing great potential in applications such as encapsulating water-soluble external molecules in an aqueous media.[58]

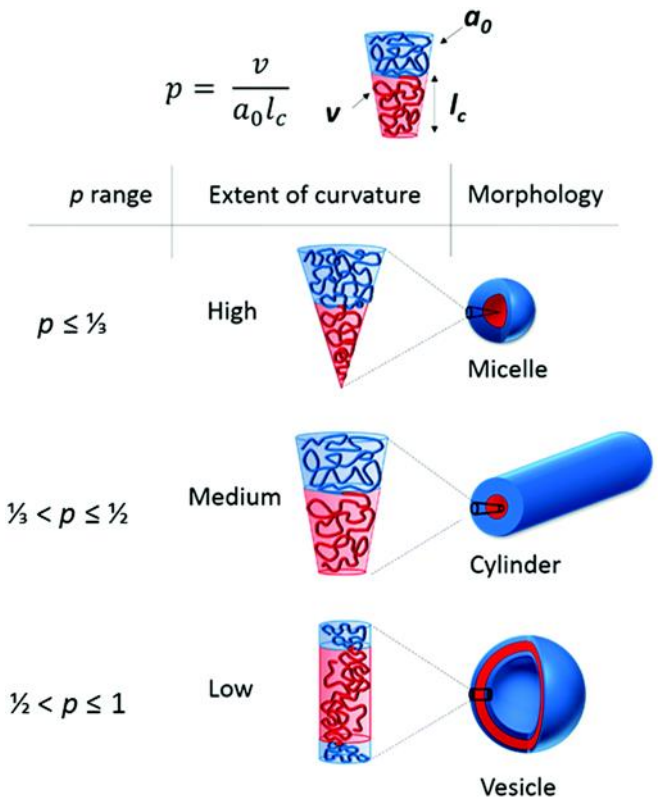

Figure 1.3 Predicting different morphologies based on the block copolymer packing parameters in a hydrophilic solvent, red structures represent hydrophobic blocks and blue structures represent hydrophilic blocks.[59]

In regard to the formation of cylindrical morphologies, this morphology is often observed as a mixture alongside either spherical or vesicular morphologies. Theoretically, pure cylindrical structures are more challenging to access due to the narrow packing parameter window making it a transition between the other two morphologies. However, cylinders have been suggested to offer a significant advantage in biomedical applications.[59, 60] For example, cylinders have been shown to exhibit higher rate during cell uptake studies and undergo a much longer in vivo circulation time, compared to spherical morphologies. [61-63] Interest in block copolymer (BCP) self-assembly to form cylindrical morphologies has therefore seen a variety of interest.

1.3.2 Methods of block copolymer self-assembly in solution

Anisotropic nanoscale structures have long been interested in their unique properties in applications such as photonics and drug delivery. [64, 65] Self-assembly of synthetic block copolymers in solution has been the most common access to afford highly anisotropic nanoparticles.[50] Block copolymer self-assembly through a solvent switch method is considered the most straightforward approach to forming micellar structures. Typically, a selective solvent is added to a polymer solution followed by removal of the good solvent. However, access to cylindrical micelles by this method always results in mixed morphologies.[50] A few alternative methods have therefore been developed for achieving pure cylindrical morphologies during BCP self-assembly. Polymerisation-induced self-assembly (PISA) has been proved to be a powerful tool for this purpose. For aqueous PISA, a water-miscible monomer is polymerised onto a water-soluble homopolymer through controlled polymerisation techniques, including ATRP, [66, 67] RAFT,[68-70] ROMP.[71] As the second block grows, it becomes insoluble in the media during

the polymerisation, driving self-assembly into higher-order morphologies, such as worms and vesicles. A wide range of monomers can be utilised for PISA, with the advantage that a variety of controlled polymerisation approaches can be used. However, it has only been proven that PISA can be used to control the dimension of vesicles and spherical micelles, which limits its use for biological applications.[72]

In this regards, other self-assembly approaches such as the morphological transformation process (MORPH) has been reported, which allows for the access to pure and dimensionally-controlled cylindrical micelles.[73] Here, worm growth is driven by the formation of supramolecular bonds and is proceeded with the added polymer incorporated into the cylindrical structure. However, the successful example has been limited to a single report of nucleobase monomers with complicated synthetic steps.

Alternatively, self-assembly of block copolymers composed of a crystalline block which could be prepared from a wide range of monomers has been the most successful method accessing precisely size-controlled cylindrical morphologies. Such a process is described as crystallisation-driven self-assembly (CDSA).

1.4 Crystallisation-driven self-assembly

1.4.1 Polymer crystallisation

The crystallisation of a polymer could be understood as a chain folding process. This theory was first suggested by Storks back in 1938. It was then demonstrated by the successful preparation of a single crystal of polyethylene, characterised by selected area electron diffraction in 1957. [74] During chain folding, the remaining polymer chain length (L) could be defined as $L = L_0 - ml$, where L_0 represents the polymer chain length, m are the overall folds in the crystal, and the l represents folded chain length in the crystal. As a single crystal, the crystallinity could reach 100% when $L = 0$, meaning no polymer chain remains as unfolded. However, with a high polydispersity, nonuniform polymer chains lead to a positive L, reducing crystallinity. This is important to understand as it affects not only how the polydispersity impacts polymer crystallisation but also unmasks the fact that most of the reports in this field have concentrated on homopolymer crystallisation, as they are the closest to monodisperse polymers. However, the accessible morphology of a homopolymer single crystal has been mostly limited to lamellae and spherulite structures. (Figure 1.5)

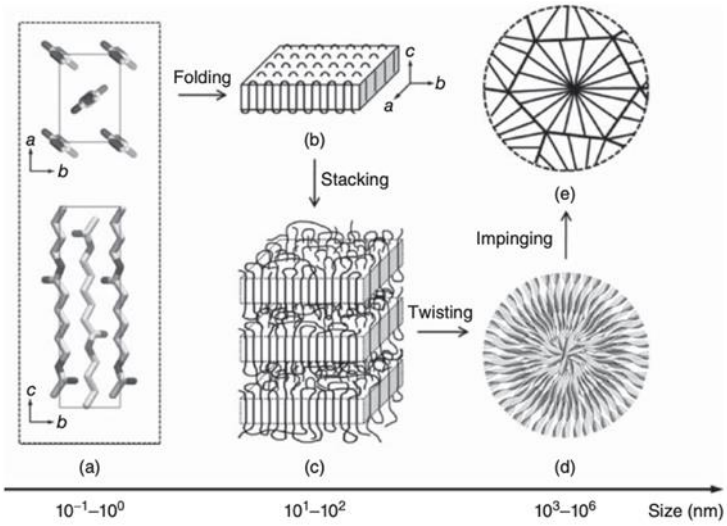

Figure 1.4 Schematic illustration showing a hierarchical structure formed in crystalline homopolymers when quenched from a homogeneous melt. (a) Crystal structure, (b) crystalline lamella, (c) lamellar morphology, (d) spherulite, and (e) spherulite structure.[75]

To afford various morphologies, crystalline block copolymers were studied with the expectation that the structures were driven by two forces, including crystalline-crystalline and crystalline-amorphous interactions. A range of morphologies could be achieved such as spheres, cylinders, lamellae and bilayer lamellae.[76-79] Concerning the interest of these higher-order self-assembled morphologies from crystalline-amorphous polymers, Vilgis and Halperin purposed a theoretical prediction that a thermodynamic equilibrium state can be achieved.[80] In this model, chain-folding of the insoluble crystalline block obtained a sharp interface excluding the other block from the crystal, forming the soluble amorphous upper and lower layers. This model has revealed the possibility of crystallisation-driven self-assembly in solution towards the preparation of different morphologies.

1.4.2 Crystallisation-driven self-assembly

An early report of the formation of worm-like micelles prepared from poly(ferrocenyldimethylsilane)-*b*-poly(dimethylsiloxane) was reported in 1998,[81] showing a distinct mechanism of block copolymer self-assembly in solution. The novel approach of semi-crystalline block copolymers self-assembly in solution is driven by the chain folding of a crystalline block generating a certain space based on folds, which the non-crystalline block will occupy. The process has since been recognised as crystallisation-driven self-assembly (CDSA).

1.4.2.1 Self-assembly through thermal nucleation

For all polymer crystallisation, the presence of nuclei is compulsory. During crystallisation-driven self-assembly the nuclei often result as a consequence of the fast-cooling process. Crystalline-coil polymers are heated above melting temperature and cooled down below the crystallisation temperature of the crystalline block. The nuclei are therefore produced from a portion of polymer crystallisation. A secondary crystallisation will then be allowed for the polymers in solution to grow on the nuclei resulting in micelles (**Figure 1.6**). Other than the thermal process, a solvent switch can also facilitate the formation of nuclei, where nuclei are generated from introducing a selective solvent to a polymer solution.

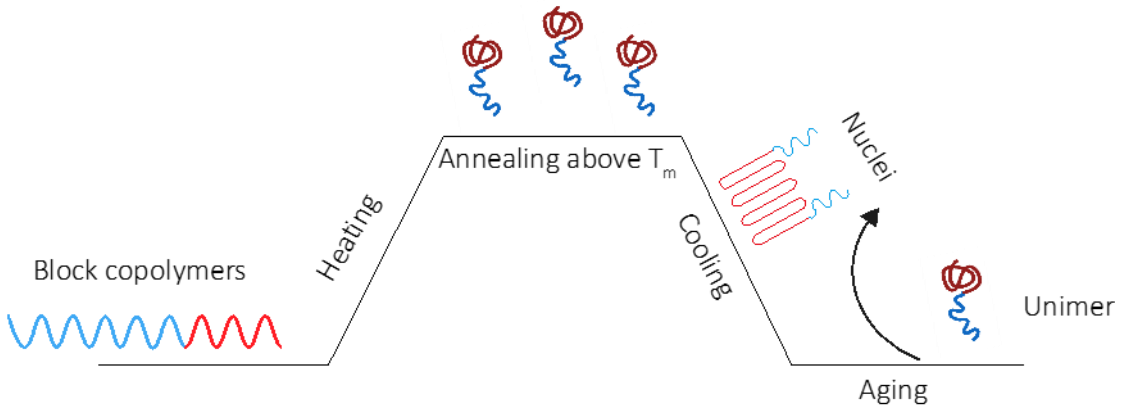

Figure 1.5 A general process for thermal self-nucleation for a semi-crystalline copolymer.

To date, a few semi-crystalline polymers have been successfully demonstrated for CDSA, these include: poly(ferrocenyldimethylsilane) (PFS),[82-84] poly(3-decylselenophene) (P3DSe),[85] poly(3-hexylthiophene) (P3HT),[86] oligo(*p*-phenylenevinylene) (OPV),[87] poly(di-*n*-hexylfluorene) (PDHF),[88] poly(perfluoroethyloctyl methacrylate) (PFMA),[89] poly(ethylene) (PE),[90-93] poly(ethylene oxide) (PEO),[94] poly(ε-caprolactone) (PCL),[95] poly(L-lactide) (PLLA),[96, 97] poly(spiro[fluorene-9,5'-[1,3]-dioxan]-2'-one) (PFTMC).[98] Despite the crystallinity, the various properties of these polymers have allowed exploration in different applications such as surface modification and optical and electronic study.[87, 99] However, owing to spontaneous homogeneous nucleation, size-controlled micelles formed through polymer self-nucleation could not be achieved.

1.4.2.2 Living crystallisation-driven self-assembly

In an effort to address the problem regarding the formation of micelles in a controlled manner, living crystallisation-driven self-assembly was proposed by Manners and Winnik in 2007. [100] Living CDSA could be defined as an epitaxial growth mechanism where dissolved polymer unimers crystallise on pre-existed seeds. Sonicated self-nucleated micelles with an exposed crystalline surface were used as external nuclei.

Micelles with a specific size could then be formed by introducing a certain amount of unimer into the fragment micelles solution, through an epitaxial growth mechanism. (**Figure 1.7**)

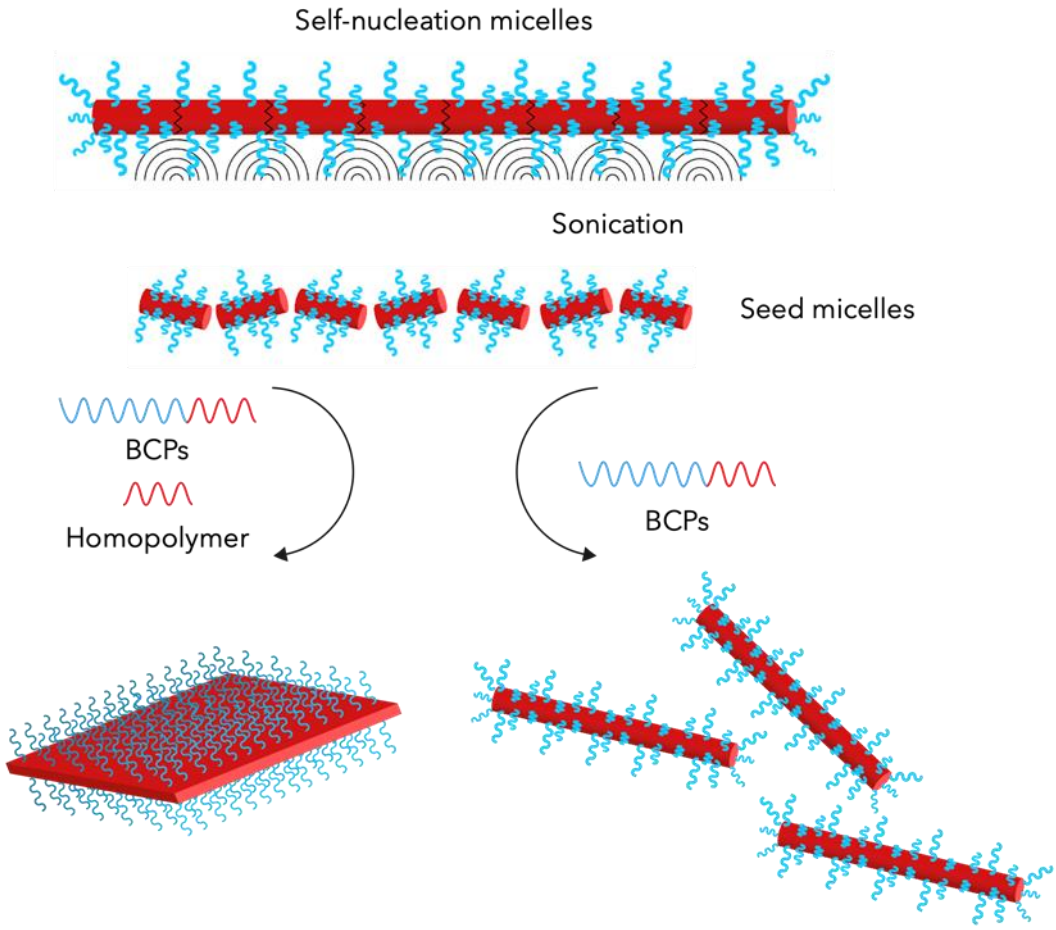

Figure 1.6 A general process of living CDSA.

This has successfully demonstrated a pathway for the preparation of crystalline micelles with morphological and dimensional control. As a consequence, 1D, 2D, complex and hierarchical micelles prepared by living CDSA have since been reported.[101-104] Among those crystalline micelles, PFS block copolymers have received the most extensive study. Access to highly monodisperse cylindrical micelles was reported as early as 2010, where a cylindrical micelle was prepared by self-nucleation of polyferrocenylsilane-*b*-

polyisoprene(PFS-*b*-PI) in *n*-hexane with a length dispersity greater than 1.4.[105] Different amounts of unimer were then added into the sonicated PFS-*b*-PI cylinders as 'seeds' to undergo an epitaxial growth. For instance, different length cylinders could be formed with a dispersity as low as 1.03 by controlling the unimer to seeds ratio. (**Figure 1.8a**) The formation of a size-controlled poly(ferrocenyldimethylsilane)-*b*-poly[bis(trifluoroethoxy)phosphazene] (PFS-b-PP) 2D nanosheet has also been demonstrated by living CDSA.[103] Seed micelles were prepared by sonication of PFS_{34}-*b*-$P2VP_{272}$ cylinder micelles obtained by self-nucleation. Unimer solution of PFS_{54}-*b*-$P2VP_{290}$ with an increased ratio of core-forming block was then added into the seeds to afford 2D platelets with a narrow size distribution. (**Figure 1.8c**) Poly(*L*-lactide) (PLLA)-based 2D platelets have also been prepared in a similar seeded growth process.[106] Sequential addition of homopolymer or homopolymer and BCP blends into PLLA seeds solution yields concentric 'diamond' platelet patchy micelles, which could be selectively crosslinked in spatially specific regions, allowing the disassembly of un-cross-linked regions to form hollow 'diamond' platelets in a good solvent. (**Figure 1.8d**) As a consequence of their biocompatibility, other crystalline materials such as PCL have also been studied in living CDSA. [95] Cylinders were prepared by self-nucleation of both PCL_{50}-*b*-$PDMA_{180}$ and PCL_{50}-*b*-$PMMA_{20}$-*b*-$PDMA_{200}$. Precisely controlled monodisperse cylinder micelles were then produced by living CDSA of both pre-sonicated cylinders. (**Figure 1.8b**) In particular, the micelles prepared by PCL_{50}-*b*-$PMMA_{20}$-*b*-$PDMA_{200}$ were done so in an aqueous environment, showing great potential in bioapplications.

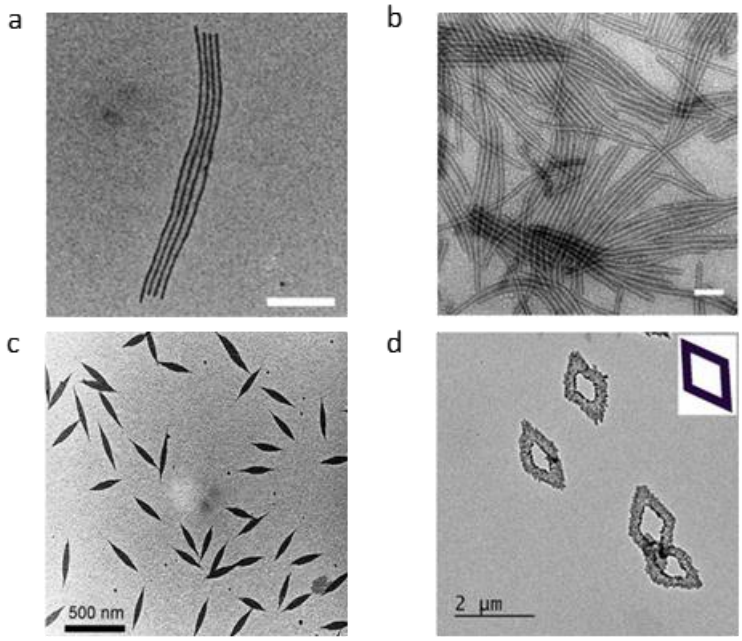

Figure 1.7 Seeded growth of (a) PFS-b-P2VP cylinder micelles, (b) PCL- b-PDMA cylinder micelles, (c) PFS-b-P2VP 2D platelets (d) (PLLA)-based 'diamond' hollow platelets scale bar 500nm. [95,103,106]

1.4.2.3 Main factors of crystallisation-driven self-assembly

Unlike coil-coil block copolymer self-assembly, where a solvophobic interaction drives phase separation, phase separation of block copolymers undergoing crystallisation-driven self-assembly is driven by both solvophobic interactions and core crystallisation. This complicates the number of parameters that can be influencing CDSA and living CDSA. However, the main parameters that are investigated typically include the ratio of the blocks, solvent conditions and temperature, based on the current understanding of CDSA.

It is widely accepted that 1D cylindrical micelles are generally obtained with a high corona-core block ratio from CDSA.[107] On the contrary, low corona-core block copolymers produce 2D micelles.[83] This is based on the space to accommodate the

corona chain provided by folded crystalline chain. As more space is required, this promotes a more elongated structure. Notably, CDSA of poly(*N*,*N*-dimethylacrylamide)-*b*-poly(L-lactic acid) (PDMA-b-PLLA) has been an exception to this rule, where 2D micelles were formed with a very high corona-core ratio (corona:core=20).[108] Here, a mechanism has been proposed that the increased solubility caused by a long corona block preserves unimer at a higher temperature, where unimer favour the core crystallisation.

Unlike coil-coil BCPs self-assembly, the selected solvent in CDSA assists the crystallisation of core-forming block. If the core-forming block becomes too soluble in a solvent, failed crystallisation leads to spherical micelles with an amorphous core. In comparison, the core-forming block is able to crystallise in a selective solvent, and homogenous structures are formed by core crystallisation-driven micellisation. However, if microphrase separation occurs before crystallisation, the core-forming block crystallises under confinement, resulting in intermediate morphologies.[107]

As a thermally controlled process, it is essential for CDSA of crystalline-coil BCPs is performed under a suitable temperature where the polymer is considered to melt in a solvent. Notably, it's been demonstrated that the addition of good solvent can reduce the dissolution temperature of core-forming blocks.[109] As such, the temperature should not be considered as an independent parameter during CDSA as it is largely based on the selective solvent.

1.5 Analysis of CDSA particles

Particles of various morphologies and dimensions can be prepared using CDSA. Microscopy has been the most common way to visualise these particles and determine

a representative morphology. Besides standard polymer characterisation techniques such as nuclear magnetic resonance (NMR) spectroscopy and size-exclusion chromatography (SEC), it is also important to study the thermal behaviour of coil-crystalline block copolymers to understand the formation of different morphologies.

1.5.1 Transmission electron microscopy

Transmission electron microscopy (TEM) is a microscopy technique which can be used to image features at the nanoscale level. Since this method was first demonstrated in 1931, it has developed as one of the main characterisation techniques in material science. The main concept of TEM is that a beam of electrons is transmitted through a specimen. Images can then be formed from the interaction between the electrons and the atoms of the structure. These images are then seen by projecting onto a phosphorescent screen. Digital images can then be captured through a charge-coupled device (CCD) camera positioned underneath the screen. (**Figure 1.9a**) Notably, to ensure the electrons do not collide with gas atoms is it essential to operate TEM under vacuum. This requires that the self-assembled sample solution is dried prior to characterisation by TEM. This could cause changes in size and morphology. The collapses of the solvated block in the dry state often lead to smaller nanostructure size comparing to other copolymer self-assembly solution analysis methodologies.[110] Therefore, it is essential to combine TEM with other characterisation methods to conclude the particle size and morphology. An electron microscopy technique called cryogenic transmission electron microscopy (cryo-EM) is commonly used to avoid these drawbacks. By rapidly cooling an aqueous sample to cryogenic temperatures on a thin substrate, frozen particles in solution could be imaged while both size and morphology could be reserved. (**Figure**

1.9b) However, cryo-TEM is mainly used in an environment of vitreous water which limits its application in analysing self-assembly samples.[111]

Sample preparation in TEM can be varied based on the nature of materials such as small organisms, viruses, or nanotubes. Crystallisation-driven self-assembly samples are easily prepared by depositing a diluted solution onto films on support girds, followed by solvent removal.

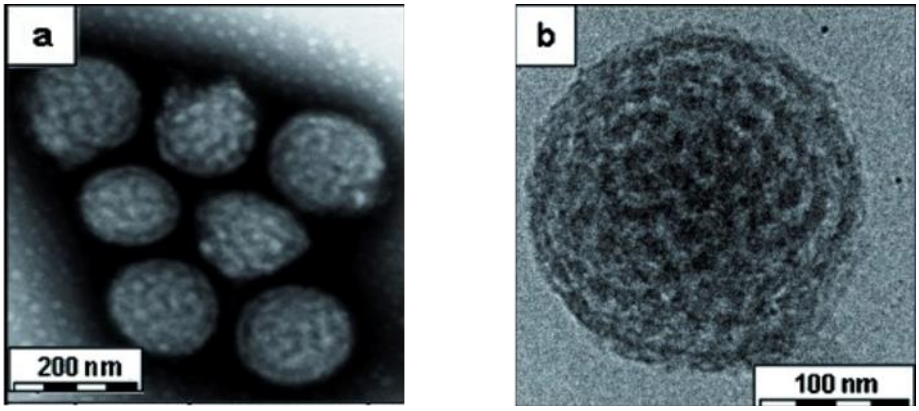

Figure 1.8 Aggregates of peptide-based diblock copolymers analysed by (a) TEM (stained with uranyl acetate), and (b) cryo-TEM.[112]

To build a good contrast which is contributed by the difference between electrons travelling through thick features and mean free path, a certain thickness of the specimen is typically required to obtain good quality images of samples. Another approach to enhance contrast is using high atomic number stains, as they absorb electrons or scatter part of the electron beam. Formed by a chain folding mechanism, particles generated by CDSA are generally thin features with a thickness of less than 50 nm. As such, staining is required for most of the sample preparation when characterising CDSA nanoparticles. There are two main stains established in TEM: positive stain and negative stain. A negative stain is a method where the background is stained with actual specimen

untouched, while a positive stain is the actual specimen is stained. The most commonly used stains include ammonium molybdate, uranyl acetate, uranyl formate, phosphotungstic acid and osmium tetroxide. The observed contrast in TEM by staining is often affected by the interaction between specimen and stains. Comparison among different stains and preparation methods is essential to obtain the best possible images.

1.5.2 Differential scanning calorimetry

Differential scanning calorimetry (DSC) is widely used to determine the crystallisation of polymers. When the samples undergo a physical transition, a comparable difference in heat flow can be observed between the sample and a reference, depending on whether the process is exothermic or endothermic. A heat flux versus temperature curve, therefore, can be produced from a DSC experiment. Thermal transitions, such as crystallisation temperature and melting temperature, can be observed from the curve. Enthalpies of the transitions could also be calculated from the curves.

DSC is the most commonly used technique to characterise the degree of crystallinity, which determines the mechanical properties of semi-crystalline polymers such as impact resistance and dimensional stability. [113] In most studies of crystallisation-driven self-assembly, the polymer's crystallisation in solution is different from bulk crystallisation. DSC has only been limited as a technique to determine a temperature window for the self-assembly to further carry out in solution. However, the core-forming block could be polymerised from commercially available or synthetic monomers. Prior to CDSA, a comprehensive crystallisation study of a polymer is important to confirm the thermal properties is in line with literature.

1.5.3 Nano Differential scanning calorimetry

Nano differential scanning calorimetry (Nano DSC) is designed to measure the absorbed or released heat of bio-molecules undergoing a thermal transition. The heat exchange from processes such as bio-molecules unfolding could be measured by Nano DSC. Nano DSC delivers superior high sensitivity and reproducibility of data while requiring less sample than DSC. (**Figure 1.10**) As a differential scanning calorimetry technique operating with high sensitivity, Nano DSC can be used to determine polymer crystallisation and melting in solution, where the heat exchange is contributed by the crystalline polymer chain folding and unfolding. In comparison to dry state DSC, this technique has a great advantage giving more accurate information of polymer crystallisation in solution as such process could be associate by solvents.

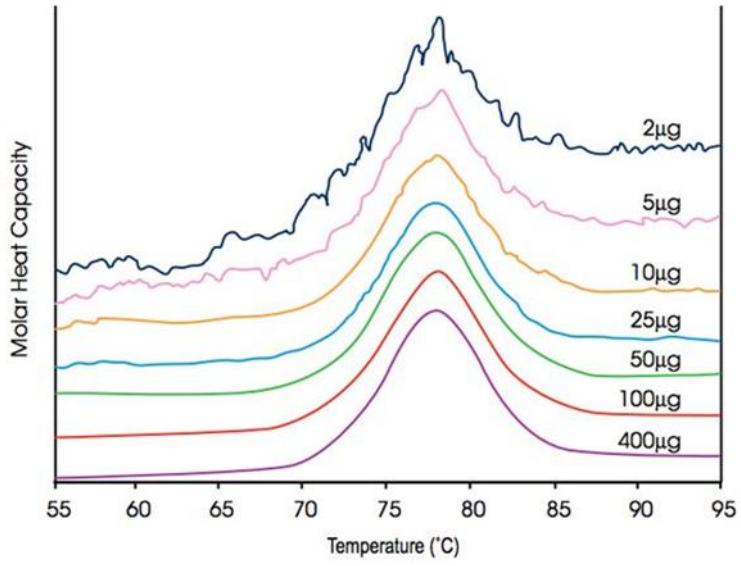

Figure 1.9 Example of protein stability analysed by Nano DSC.[114]

An early example of characterisation CDSA with Nano DSC is reported by Schmalz.[90] Crystallisation and melting temperatures of polyethylene-based block copolymers were determined by Nano DSC showing different values in each solvent. This technique has

also been applied in CDSA studied in mineral oil.[115] The thermal transition of poly(behenyl methacrylate) (PBeMA)-based block copolymers has been measured in Nano DSC. Interestingly, two signal peaks were captured during the cooling scanning of Nano DSC. It has been purposed by the author that one peak is the crystalline chain folding, and the other represents the aggregation of nanoparticles as observed in TEM.(**Figure 1.11**) This has revealed the ability of Nano DSC to determine other macromolecular and nanoparticle activities than crystallisation during CDSA. No doubt this could provide a pathway to understand CDSA. Although this technique has not been widely used in reported CDSA studies, in this thesis, it has acted as a main characterisation to understand CDSA of different lactone polymers.

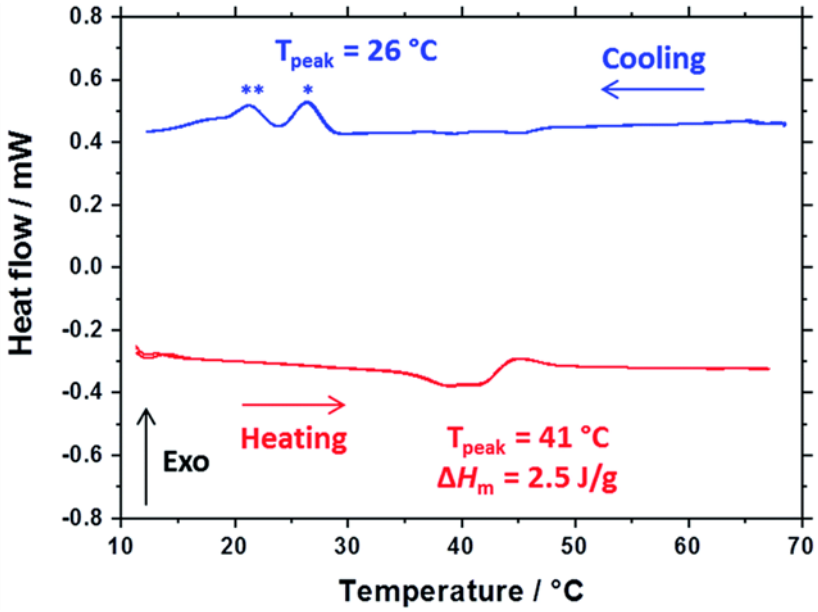

Figure 1.10 Differential scanning calorimetry (DSC) experiments conducted at a cooling/heating rate of 2 °C min^{-1} for PBeMA-based block copolymers in mineral oil.* Indicates the crystallization within individual (isolated) nanoparticles. ** Indicates the secondary crystallisation (aggregation) between PBeMA nanoparticles.[115]

1.6 Summary

Aiming at block copolymer crystallisation-driven self-assembly, a few concepts regarding polymer synthesis and self-assembly were introduced. Initially, methods of polymerisation were discussed to synthesise well-defined block copolymers. In particular, ring-opening polymerisation of different lactones was focused on building semi-crystalline core-forming blocks studied in this thesis. Following this, various methods for self-assembly of block copolymer in solution were compared, emphasising the remaining challenge on delivering precisely size-controlled anisotropic nanoparticles. Crystallisation-driven self-assembly is highlighted with the advantage of achieving high ordered and precisely size-controlled morphologies. The development of various morphologies afforded by polymer crystallisation has also been briefly introduced followed by an overview of crystallisation-driven self-assembly of diblock copolymers with a crystallisable core block. Finally, a summary of characterisation methods used for crystallisation-driven self-assembly particles in this thesis is outlined.

1.7 Reference

1. G. Pasparakis, N. Krasnogor, L. Cronin, B. G. Davis and C. Alexander, *Chem. Soc. Rev.*, 2010, **39**, 286-300.

2. R. B. Grubbs and R. H. Grubbs, *Macromolecules*, 2017, **50**, 6979-6997.

3. P. J. Flory, *J. Am. Chem. Soc.*, 1940, **62**, 1561-1565.

4. S. Perry and H. Hibbert, *J. Am. Chem. Soc.*, 1940, **62**, 2599-2604.

5. R. P. Quirk and B. Lee, *Polym. Int.*, 1992, **27**, 359-367.

6. S. Aoshima and T. Higashimura, *Macromolecules*, 1989, **22**, 1009-1013.

7. C. J. Hawker, *J. Am. Chem. Soc.*, 1994, **116**, 11185-11186.

8. C. J. Hawker, *Acc. Chem. Res.*, 1997, **30**, 373-382.

9. B. B. Wayland, G. Poszmik, S. L. Mukerjee and M. Fryd, *J. Am. Chem. Soc.*, 1994, **116**, 7943-7944.

10. D. Bertin, D. Gigmes, S. R. A. Marque and P. Tordo, *Chem. Soc. Rev.*, 2011, **40**, 2189-2198.

11. M. Kato, M. Kamigaito, M. Sawamoto and T. Higashimura, *Macromolecules*, 1995, **28**, 1721-1723.

12. J.-S. Wang and K. Matyjaszewski, *J. Am. Chem. Soc.*, 1995, **117**, 5614-5615.

13. W. A. Braunecker, W. C. Brown, B. C. Morelli, W. Tang, R. Poli and K. Matyjaszewski, *Macromolecules*, 2007, **40**, 8576-8585.

14. J. Chiefari, Y. K. Chong, F. Ercole, J. Krstina, J. Jeffery, T. P. T. Le, R. T. A. Mayadunne, G. F. Meijs, C. L. Moad, G. Moad, E. Rizzardo and S. H. Thang, *Macromolecules*, 1998, **31**, 5559-5562.

15. S. Perrier and P. Takolpuckdee, *J Polym Sci A Polym Chem*, 2005, **43**, 5347-5393.

16. C. Barner-Kowollik and S. Perrier, *J Polym Sci A Polym Chem*, 2008, **46**, 5715-5723.

17. G. Moad, E. Rizzardo and S. H. Thang, *Aust. J. Chem.*, 2005, **58**, 379-410.

18. A. M. Bivigou-Koumba, J. Kristen, A. Laschewsky, P. Müller-Buschbaum and C. M. Papadakis, *Macromol. Chem. Phys.*, 2009, **210**, 565-578.

19. J. F. Quinn, R. P. Chaplin and T. P. Davis, *J Polym Sci A Polym Chem*, 2002, **40**, 2956-2966.

20. J. Xu, L. Tao, J. Liu, V. Bulmus and T. P. Davis, *Macromolecules*, 2009, **42**, 6893-6901.

21. C. W. Bielawski and R. H. Grubbs, *Prog. Polym. Sci.*, 2007, **32**, 1-29.

22. Y. Li, J. Hong, R. Wei, Y. Zhang, Z. Tong, X. Zhang, B. Du, J. Xu and Z. Fan, *Chem.*, 2015, **6**, 1530-1536.

23. P. K. Kuroishi and A. P. Dove, *ChemComm*, 2018, **54**, 6264-6267.

24. B. Orhan, M. J. L. Tschan, A.-L. Wirotius, A. P. Dove, O. Coulembier and D. Taton, *ACS Macro Lett.*, 2018, **7**, 1413-1419.

25. Y. Y. Svirkin, J. Xu, R. A. Gross, D. L. Kaplan and G. Swift, *Macromolecules*, 1996, **29**, 4591-4597.

26. M. Bouyahyi, M. P. F. Pepels, A. Heise and R. Duchateau, *Macromolecules*, 2012, **45**, 3356-3366.

27. J. Huang, J. C. Worch, A. P. Dove and O. Coulembier, *ChemSusChem*, 2020, **13**, 469-487.

28. S. M. Guillaume and J.-F. Carpentier, *Catal. Sci. Technol.*, 2012, **2**, 898-906.

29. A. E. Neitzel, T. J. Haversang and M. A. Hillmyer, *Ind. Eng. Chem.*, 2016, **55**, 11747-11755.

30. S. J. Jeon, M.-y. Jung and J. Y. Do, *React Funct Polym"*, 2016, **100**, 37-43.

31. I. van der Meulen, M. de Geus, H. Antheunis, R. Deumens, E. A. J. Joosten, C. E. Koning and A. Heise, *Biomacromolecules*, 2008, **9**, 3404-3410.

32. M. Eriksson, L. Fogelström, K. Hult, E. Malmström, M. Johansson, S. Trey and M. Martinelle, *Biomacromolecules*, 2009, **10**, 3108-3113.

33. C. Vaida, H. Keul and M. Moeller, *Green Chem.*, 2011, **13**, 889-899.

34. J. A. Wilson, S. A. Hopkins, P. M. Wright and A. P. Dove, *Polym. Chem.*, 2014, **5**, 2691-2694.

35. M. Endo, T. Aida and S. Inoue, *Macromolecules*, 1987, **20**, 2982-2988.

36. M. P. F. Pepels, M. Bouyahyi, A. Heise and R. Duchateau, *Macromolecules*, 2013, **46**, 4324-4334.

37. in *Handbook of Ring-Opening Polymerization*, 2009, DOI: https://doi.org/10.1002/9783527628407.ch1, pp. 1-51.

38. A. Baeyer and V. Villiger, *Chem. Ber.*, 1899, **32**, 3625-3633.

39. A. Bhaw-Luximon, D. Jhurry, S. Motala-Timol and Y. Lochee, *Macromol. Symp.*, 2005, **231**, 60-68.

40. M. Hong and E. Y. X. Chen, *Nat. Chem.*, 2016, **8**, 42-49.

41. M. P. F. Pepels, P. Souljé, R. Peters and R. Duchateau, *Macromolecules*, 2014, **47**, 5542-5550.

42. L. van der Mee, F. Helmich, R. de Bruijn, J. A. Vekemans, A. R. Palmans and E. Meijer, *Macromolecules*, 2006, **39**, 5021-5027.

43. J. Panten and H. Surburg, in *Ullmann's Encyclopedia of Industrial Chemistry*, 2015, DOI: https://doi.org/10.1002/14356007.a11_141.pub2, pp. 1-9.

44. J. Cai, C. Liu, M. Cai, J. Zhu, F. Zuo, B. S. Hsiao and R. A. Gross, *Polymer*, 2010, **51**, 1088-1099.

45. M. de Geus, I. van der Meulen, B. Goderis, K. van Hecke, M. Dorschu, H. van der Werff, C. E. Koning and A. Heise, *Polym. Chem.*, 2010, **1**, 525-533.

46. Y. Nakayama, N. Watanabe, K. Kusaba, K. Sasaki, Z. Cai, T. Shiono and C. Tsutsumi, *J. Appl. Polym. Sci.*, 2011, **121**, 2098-2103.

47. H. Uyama, H. Kikuchi, K. Takeya and S. Kabayashi, *Acta Polym.*, 1996, **47**, 357-360.

48. A. Kumar, K. Garg and R. A. Gross, *Macromolecules*, 2001, **34**, 3527-3533.

49. L. Jasinska-Walc, M. Bouyahyi, A. Rozanski, R. Graf, M. R. Hansen and R. Duchateau, *Macromolecules*, 2015, **48**, 502-510.

50. Y. Mai and A. Eisenberg, *Chem. Soc. Rev.*, 2012, **41**, 5969-5985.

51. L. Zhang and A. Eisenberg, *J. Am. Chem. Soc.*, 1996, **118**, 3168-3181.

52. L. Zhang and A. Eisenberg, *Macromolecules*, 1999, **32**, 2239-2249.

53. L. Zhang, H. Shen and A. Eisenberg, *Macromolecules*, 1997, **30**, 1001-1011.

54. Y. Yu, L. Zhang and A. Eisenberg, *Macromolecules*, 1998, **31**, 1144-1154.

55. P. Bhargava, J. X. Zheng, P. Li, R. P. Quirk, F. W. Harris and S. Z. D. Cheng, *Macromolecules*, 2006, **39**, 4880-4888.

56. L. Zhang, K. Yu and A. Eisenberg, *Science*, 1996, **272**, 1777-1779.

57. J. N. Israelachvili, D. J. Mitchell and B. W. Ninham, *Biochim Biophys Acta Biomembr.*, 1977, **470**, 185-201.

58. A. Blanazs, S. P. Armes and A. J. Ryan, *Macromol. Rapid Commun.*, 2009, **30**, 267-277.

59. K. E. B. Doncom, L. D. Blackman, D. B. Wright, M. I. Gibson and R. K. O'Reilly, *Chem. Soc. Rev.*, 2017, **46**, 4119-4134.

60. S. E. Gratton, P. A. Ropp, P. D. Pohlhaus, J. C. Luft, V. J. Madden, M. E. Napier and J. M. DeSimone, *PNAS*, 2008, **105**, 11613-11618.

61. Y. Geng, P. Dalhaimer, S. Cai, R. Tsai, M. Tewari, T. Minko and D. E. Discher, *Nat. Nanotechnol*, 2007, **2**, 249-255.

62. R. Toy, P. M. Peiris, K. B. Ghaghada and E. Karathanasis, *Nanomedicine*, 2014, **9**, 121-134.

63. X. Huang, X. Teng, D. Chen, F. Tang and J. He, *Biomaterials*, 2010, **31**, 438-448.

64. F. E. Alemdaroglu, N. C. Alemdaroglu, P. Langguth and A. Herrmann, *Macromol. Rapid Commun.*, 2008, **29**, 326-329.

65. N. D. Burrows, A. M. Vartanian, N. S. Abadeer, E. M. Grzincic, L. M. Jacob, W. Lin, J. Li, J. M. Dennison, J. G. Hinman and C. J. Murphy, *J. Phys. Chem. Lett.*, 2016, **7**, 632-641.

66. G. Wang, M. Schmitt, Z. Wang, B. Lee, X. Pan, L. Fu, J. Yan, S. Li, G. Xie, M. R. Bockstaller and K. Matyjaszewski, *Macromolecules*, 2016, **49**, 8605-8615.

67. G. Wang, Z. Wang, B. Lee, R. Yuan, Z. Lu, J. Yan, X. Pan, Y. Song, M. R. Bockstaller and K. Matyjaszewski, *Polymer*, 2017, **129**, 57-67.

68. E. Guégain, C. Zhu, E. Giovanardi and J. Nicolas, *Macromolecules*, 2019, **52**, 3612-3624.

69. G. Mellot, J.-M. Guigner, L. Bouteiller, F. Stoffelbach and J. Rieger, *Angew. Chem. Int.*, 2019, **58**, 3173-3177.

70. C. A. Figg, A. Simula, K. A. Gebre, B. S. Tucker, D. M. Haddleton and B. S. Sumerlin, *Chem.*, 2015, **6**, 1230-1236.

71. J. C. Foster, S. Varlas, B. Couturaud, J. R. Jones, R. Keogh, R. T. Mathers and R. K. O'Reilly, *Angew. Chem. Int.*, 2018, **57**, 15733-15737.

72. S. Pearce and J. Perez-Mercader, *Polym. Chem.*, 2021, **12**, 29-49.

73. Z. Hua, J. R. Jones, M. Thomas, M. C. Arno, A. Souslov, T. R. Wilks and R. K. O'Reilly, *Nat. Commun.*, 2019, **10**, 5406.

74. A. Keller, *Philos. Mag.*, 1957, **2**, 1171-1175.

75. S. Nojima and H. Marubayashi, in *Polymer Morphology*, 2016, DOI: https://doi.org/10.1002/9781118892756.ch10, pp. 165-180.

76. D. J. Quiram, R. A. Register, G. R. Marchand and D. H. Adamson, *Macromolecules*, 1998, **31**, 4891-4898.

77. H.-L. Chen, S.-C. Hsiao, T.-L. Lin, K. Yamauchi, H. Hasegawa and T. Hashimoto, *Macromolecules*, 2001, **34**, 671-674.

78. L. Zhu, S. Z. D. Cheng, B. H. Calhoun, Q. Ge, R. P. Quirk, E. L. Thomas, B. S. Hsiao, F. Yeh and B. Lotz, *J. Am. Chem. Soc.*, 2000, **122**, 5957-5967.

79. S. Hong, L. Yang, W. J. MacKnight and S. P. Gido, *Macromolecules*, 2001, **34**, 7009-7016.

80. T. Vilgis and A. Halperin, *Macromolecules*, 1991, **24**, 2090-2095.

81. J. Massey, K. N. Power, I. Manners and M. A. Winnik, *J. Am. Chem. Soc.*, 1998, **120**, 9533-9540.

82. H. Qiu, Y. Gao, C. E. Boott, O. E. C. Gould, R. L. Harniman, M. J. Miles, S. E. D. Webb, M. A. Winnik and I. Manners, *Science*, 2016, **352**, 697-701.

83. Z. M. Hudson, C. E. Boott, M. E. Robinson, P. A. Rupar, M. A. Winnik and I. Manners, *Nat. Chem.*, 2014, **6**, 893-898.

84. H. Zhou, Y. Lu, M. Zhang, G. Guerin, I. Manners and M. A. Winnik, *Macromolecules*, 2016, **49**, 4265-4276.

85. E. L. Kynaston, A. Nazemi, L. R. MacFarlane, G. R. Whittell, C. F. J. Faul and I. Manners, *Macromolecules*, 2018, **51**, 1002-1010.

86. J. B. Gilroy, D. J. Lunn, S. K. Patra, G. R. Whittell, M. A. Winnik and I. Manners, *Macromolecules*, 2012, **45**, 5806-5815.

87. D. Tao, C. Feng, Y. Cui, X. Yang, I. Manners, M. A. Winnik and X. Huang, *J. Am. Chem. Soc.*, 2017, **139**, 7136-7139.

88. X.-H. Jin, M. B. Price, J. R. Finnegan, C. E. Boott, J. M. Richter, A. Rao, S. M. Menke, R. H. Friend, G. R. Whittell and I. Manners, *Science*, 2018, **360**, 897-900.

89. X. Li, B. Jin, Y. Gao, D. W. Hayward, M. A. Winnik, Y. Luo and I. Manners, *Angew. Chem. Int.*, 2016, **55**, 11392-11396.

90. J. Schmelz, A. E. Schedl, C. Steinlein, I. Manners and H. Schmalz, *J. Am. Chem. Soc.*, 2012, **134**, 14217-14225.

91. J. Schöbel, M. Karg, D. Rosenbach, G. Krauss, A. Greiner and H. Schmalz, *Macromolecules*, 2016, **49**, 2761-2771.

92. J. Schöbel, C. Hils, A. Weckwerth, M. Schlenk, C. Bojer, M. C. A. Stuart, J. Breu, S. Förster, A. Greiner, M. Karg and H. Schmalz, *Nanoscale*, 2018, **10**, 18257-18268.

93. J. Schmelz, M. Karg, T. Hellweg and H. Schmalz, *ACS Nano*, 2011, **5**, 9523-9534.

94. Y. Geng and D. E. Discher, *J. Am. Chem. Soc.*, 2005, **127**, 12780-12781.

95. M. C. Arno, M. Inam, Z. Coe, G. Cambridge, L. J. Macdougall, R. Keogh, A. P. Dove and R. K. O'Reilly, *J. Am. Chem. Soc.*, 2017, **139**, 16980-16985.

96. Z. Li, Y. Zhang, L. Wu, W. Yu, T. R. Wilks, A. P. Dove, H.-m. Ding, R. K. O'Reilly, G. Chen and M. Jiang, *ACS Macro Lett.*, 2019, **8**, 596-602.

97. Y. He, J.-C. Eloi, R. L. Harniman, R. M. Richardson, G. R. Whittell, R. T. Mathers, A. P. Dove, R. K. O'Reilly and I. Manners, *J. Am. Chem. Soc.*, 2019, **141**, 19088-19098.

98. J. R. Finnegan, X. He, S. T. G. Street, J. D. Garcia-Hernandez, D. W. Hayward, R. L. Harniman, R. M. Richardson, G. R. Whittell and I. Manners, *J. Am. Chem. Soc.*, 2018, **140**, 17127-17140.

99. J. Cai, C. Li, N. Kong, Y. Lu, G. Lin, X. Wang, Y. Yao, I. Manners and H. Qiu, *Science*, 2019, **366**, 1095-1098.

100. X. Wang, G. Guerin, H. Wang, Y. Wang, I. Manners and M. A. Winnik, *Science*, 2007, **317**, 644-647.

101. T. Gädt, N. S. Ieong, G. Cambridge, M. A. Winnik and I. Manners, *Nat. Mater*, 2009, **8**, 144-150.

102. G. Molev, Y. Lu, K. S. Kim, I. C. Majdalani, G. Guerin, S. Petrov, G. Walker, I. Manners and M. A. Winnik, *Macromolecules*, 2014, **47**, 2604-2615.

103. A. Presa Soto, J. B. Gilroy, M. A. Winnik and I. Manners, *Angew. Chem. Int.*, 2010, **49**, 8220-8223.

104. S. F. Mohd Yusoff, M.-S. Hsiao, F. H. Schacher, M. A. Winnik and I. Manners, *Macromolecules*, 2012, **45**, 3883-3891.

105. J. B. Gilroy, T. Gädt, G. R. Whittell, L. Chabanne, J. M. Mitchels, R. M. Richardson, M. A. Winnik and I. Manners, *Nat. Chem.*, 2010, **2**, 566-570.

106. X. He, Y. He, M.-S. Hsiao, R. L. Harniman, S. Pearce, M. A. Winnik and I. Manners, *J. Am. Chem. Soc.*, 2017, **139**, 9221-9228.

107. T. Gädt, F. H. Schacher, N. McGrath, M. A. Winnik and I. Manners, *Macromolecules*, 2011, **44**, 3777-3786.

108. M. Inam, G. Cambridge, A. Pitto-Barry, Z. P. L. Laker, N. R. Wilson, R. T. Mathers, A. P. Dove and R. K. O'Reilly, *Chem.*, 2017, DOI: 10.1039/C7SC00641A.

109. J. Qian, Y. Lu, A. Chia, M. Zhang, P. A. Rupar, N. Gunari, G. C. Walker, G. Cambridge, F. He, G. Guerin, I. Manners and M. A. Winnik, *ACS Nano*, 2013, **7**, 3754-3766.

110. Y. Talmon, *J. Colloid Interface Sci.*, 1983, **93**, 366-382.

111. H. Friedrich, P. M. Frederik, G. de With and N. A. Sommerdijk, *Angew. Chem. Int.*, 2010, **49**, 7850-7858.

112. A. L. Parry, P. H. Bomans, S. J. Holder, N. A. Sommerdijk and S. C. Biagini, *Angew. Chem. Int.*, 2008, **120**, 8991-8994.

113. Y. Kong and J. N. Hay, *Polymer*, 2002, **43**, 3873-3878.

114. C. T. Choma, *Calorimetry Sciences Corporation*, 2006.

115. M. J. Derry, O. O. Mykhaylyk, A. J. Ryan and S. P. Armes, *Chem.*, 2018, **9**, 4071-4082.

Chapter Two – Determination of solvent effects on the self-nucleation of novel poly(ω-pentadecalactone) copolymers in crystallisation-driven self-assembly

2.1 Abstract

Polymer nanostructures of highly controlled size and morphology is a current area of high interest yet remains a significant challenge. Crystallisation-driven self-assembly (CDSA) has been developed as an accessible method to prepare 1D and 2D nanomaterials from various crystalline polymers. However, owing to the spontaneous nucleation of polymer crystallising in solution, nanostructures prepared by CDSA often resulted in a high size dispersity. Therefore, studying the self-nucleation of polymers is critical to allow control over the dimensions and dispersity of these nanostructures. Herein, the preparation of biocompatible and biodegradable Poly(pentadecalactone)(PPDL) 1D (cylindrical) micelles in several solvents and its self-nucleation in each solvent are studied. Nano differential scanning calorimetry and TEM have been used to examine the thermal transition of PPDL block copolymers in different solvents. A correlation between solvent polarity and polymer melting temperature has been revealed, suggesting an interesting solvent effect in 'controlling' self-nucleation activities.

2.2 Introduction

2.2.1 Block polymer self-assembly

Block copolymers are of great interest as a result of their ability to undergo self-assembly and form various nanostructures such as spheres, wormlike micelles, platelets, and vesicles, in a broad range of aqueous and organic solvents.[116, 117] In the last decades, spherical micelles, in particular, have been studied most intensively, as a result of their simple production methods and ability to be assembled from a broad range of polymers.[51, 118] These studies have drawn interest from across the biomedical and mechanical fields, with applications in drug delivery, antibacterial, and lubrication.[119-121] More recently, cylindrical or wormlike micelles have gained increasing attention in these applications, driven by the competitive advantages in properties of these elongated structures. For example, elevated cell uptake rates and prolonged blood circulation times have been observed for wormlike micelles, and hence they are promising candidates to replace spherical particles for the purpose of drug delivery.[122] When considering the different self-assembly approaches commonly employed, PISA (Polymerization-induced self-assembly) has been one of the most popular approaches for producing wormlike self-assembly structures. Of note, PISA can be performed at a very high weight percentage of block copolymers (BCPs), and therefore is an industrially relevant process.[123, 124] Unfortunately, PISA suffers from a significant drawback in that precise dimensional control remains challenging with this method, and thus micelle length cannot be reliably predicted. This can limit the application of these nanostructures. However, the ability to precisely direct the dimension of elongated

nanostructures would open up significant possibilities for their application in areas including drug delivery[125] and optochemical sensors.[126]

2.2.2 Crystallisation-driven self-assembly

An alternative approach to PISA is using solution crystallization of block copolymers to form nano/microparticle morphologies with low interfacial curvature. The self-assembly of platelet structures from diblock poly(ethylene oxide)-*b*-polystyrene (PEO-*b*-PS) with a crystalline PEO block was initially reported in the 1960s, which inspired subsequent studies investigating the influence of polymer crystallinity on BCPs self-assembly. [127] To date, successful progress in this area has led to the field of crystallisation-driven self-assembly (CDSA), whereby crystallisable BCPs are heated above the polymer melting temperature in solution, followed by a cooling process to enable the polymer to crystallise and chain fold. In comparison to traditional coil-coil self-assembly, block copolymers which are comprised of at least one crystallising block, which allows for crystallisation during self-assembly, more favourably form high order morphologies such as platelets and cylinders. Initially, the random homogeneous nucleation of the crystalline polymer chains allows further crystallization upon cooling, which ultimately results in the formation of micelles with a broad dispersity. Subsequent external sonication can yield small, uniform seed micelles, and with this, the exposure of crystalline faces. The further addition of unimer solution or self-seeding can then lead to controlled growth from the uniform seeds, producing micelles with a narrow size dispersity. This precise dimensional control is a distinct feature and indeed the major advantage of CDSA as a self-assembly technique.[128] Nonetheless, understanding the

initial self-nucleation process during CDSA, particularly for less well-known crystallising polymer systems, is an interesting area of research.

The mechanism of CDSA requires that the core-forming block be crystalline or semi-crystalline in nature, and therefore to date only a select number of polymers have been extensively studied, including polyferrocenylsilane (PFS), poly(caprolactone) (PCL), and polyethylene (PE).[93, 95, 129] Manners and Winnik *et al*. have pioneered this field, particularly in the assembly of PFS block copolymers. Of note, they have extensively investigated the assembly of crystallizing PFS block copolymers with different corona chemistries, producing complex structures with precise size-control such as 'patchy' corona cylinders, charged-end platelets, and allowing brushy growth on the surfaces.[99, 130, 131]

2.2.3 Crystallisation-driven self-assembly of PE

Polyethylene has been an extensively studied polymer over past decades as a result of its commercial availability and widespread use in industry.[132, 133] Of relevance, Schmalz et al. reported the formation of wormlike micelles from the crystallisation-driven self-assembly of triblock co- and terpolymers with a semi-crystalline PE middle block. They examined the one-dimensional CDSA of these PE polymers at different temperatures, while the crystallisation and melting in solution was monitored by Nano DSC. [134] When applying different crystallisation temperatures during the CDSA process, they observed that the length of wormlike micelles could be altered as a result of a decreased population of nucleation events at higher temperatures. Finally, they could perform a growth mechanism starting from spherical PE-core micelles as initial 'seeds' micelles, to

form controlled elongated wormlike PE-core micelles by epitaxial growth, when suitable conditions (solvent environments and temperature) were employed.[90]

2.2.4 Crystallisation-driven self-assembly of polylactones

To increase the versatility of CDSA and extend its application into the biological field, biodegradable and biocompatible polylactide and polycaprolactone have more recently been studied as the crystalline core segments of self-assembling copolymers.[97, 135] The majority of studies in this domain have focused on polylactide copolymers. For example, when varying the volume of the hydrophilic block, a morphology change from cylinder to platelets was demonstrated.[108] This work has provided a simple and reproducible protocol for preparing well-defined 2D materials. Interestingly, a unimer exchange mechanism between poly(*L*-lactide) and poly(*D*-lactide) BCP cylinders was shown, resulting in disassembly of cylinders.[136] This has opened up great potential for biological applications. Among these studies, our group has previously reported a precise size-controlled one-dimensional morphology formed by PCL diblock copolymers, through the growth of unimers onto sonicated uniform cylinders (generally described as 'living CDSA') in water, which allowed for direct translation into biological applications.[95] A different mechanism of 2D platelet prepared by CDSA was also reported by Eisenberg et al., where a homopolymer blending technique of PCL polymers in aqueous conditions to enable the lamella to grow from a one-dimensional rod structure.[137]

2.2.5 Crystallisation of PDL

Our group is particularly interested in exploring and expanding the scope of CDSA, by investigating novel polymers with wide-ranging properties, giving the potential for exploiting the unique advantages of CDSA in a range of possible applications. As such,

we have set our eyes on an interesting material: ω-pentadecalactone (PDL). This polymer is commonly used as a food-grade flavouring, and the monomer can be produced from angelica root oil, which makes it a green and sustainable resource. With the increasing attention on PDL, different catalysts (organometallic catalysts, organocatalysts, and enzymes) have been reported for the ring-opening polymerization of this monomer.[26, 138, 139] Among these, an 'immortal' ring-opening polymerization of PDL under atmospheric conditions has been demonstrated by our group, giving the polymerisation process considerable potential for industrial scale-up production. [140] Exhibiting a 14-carbon chain in each repeat unit, poly(ω-pentadecalactone) (PPDL) has shown comparable tensile properties to low-density polyethylene (LDPE) as a consequence of its hydrophobicity.[141] Importantly, as a polyester, PPDL shows a considerable advantage over PE in that it is biodegradable, and as such is often referred to as "degradable PE". This makes PDL attractive for a variety of applications where both mechanical properties and degradation are beneficial, such as in biological applications or in packaging. In addition, compared to other widely used polyesters such as PCL, PPDL shows much slower hydrolytic degradation rates due to its high hydrophobicity, and could therefore be of benefit in applications where a more extended degradation period is required.[31]

Although there has been an increasing number of studies on CDSA over recent years, certain fundamental questions – such as the effect of solvent choice on the crystallisation process – still remain unanswered. This is mainly the consequence of each investigated polymer having unique crystallisation behaviour during the CDSA process, and therefore studies on one will not necessarily be relevant to another. Hence, a

fundamental study of the crystallisastion behaviour of polymers in CDSA would contribute significantly to the overall knowledge of the field.

Based on this, in this Chapter, we demonstrate for the first time the CDSA of copolymers with a crystallising PPDL block. As an essential precursor stage in CDSA, we focused our study on understanding the self-nucleation of PPDL BCPs. We extensively examined the crystallisation phase of the PPDL copolymer in a range of organic solvents using Nano DSC. We were able to demonstrate a correlation between the PPDL copolymer CDSA morphologies and self-nucleations with respect to changing solvent and temperature. Furthermore, we were able to direct access to different lengths of wormlike micelles based on our understanding of PPDL copolymer self-nucleation rates in solution.

2.3 Result and discussion

Initially, the preparation of poly(ω-pentadecalactone) (PPDL) block copolymer was investigated in term of further studying crystallisation-driven self-assembly in solution. The solvent effect on self-nucleation of PPDL block copolymer was then revealed by Nano differential scanning calorimetry and transmission electron microscopy.

2.3.1 Synthesis of $Mg(BHT)_2(THF)_2$

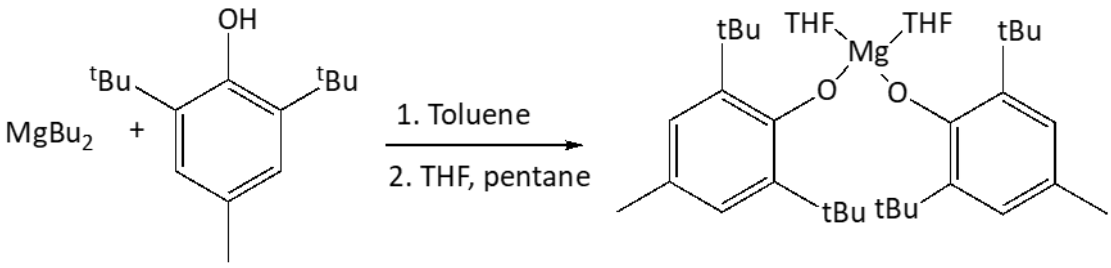

Scheme 2.1 Synthesis of $Mg(BHT)_2(THF)_2$.

Among all the reported ring-opening polymerisation of ω-pentadecalactone, $Mg(BHT)_2(THF)_2$ has been successfully demonstrated to catalyse in 'air' condition, showing the advantage in possible industrial scale application. The synthesis of $Mg(BHT)_2(THF)_2$ was performed following the reported procedure from the Ittel group (**Scheme 2.1**).[142] Under an N_2 environment, 2,6-di-*tert*-butyl-4-methylphenol (BHT) was dissolved in toluene, and $^nBu_2Mg$ (1 M in pentane) was then added dropwise. The volume of solvent was reduced in *vacuo* and the product recrystallised at -3°C. The purified crystals were separated and dried before characterization by ^1H NMR spectroscopy (**Figure 2.1**). Excess pentane was added to dissolve the dimer, followed by two molar equivalents of tetrahydrofuran. After stirring overnight, all solvents were removed without any further purification, and the white solid was stored in a glovebox.

The structure of the catalyst was confirmed by ^{1}H NMR and ^{13}C NMR spectroscopies, with the resonances corresponding to complexed THF seen around 1.2 ppm to the non-complexed reagent in deuterated benzene (C_6D_6) (**Figure 2.2**).

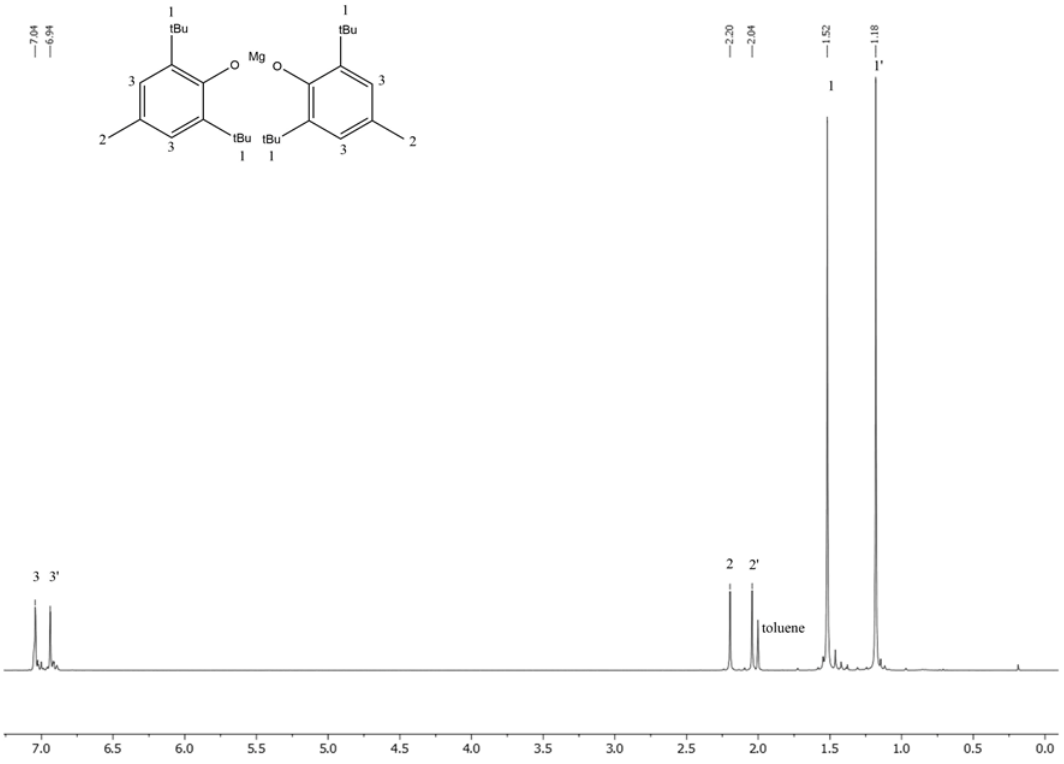

Figure 2.1 ^{1}H NMR spectrum (C_6D_6, 400 MHz) of $Mg_2(BHT)_4$.

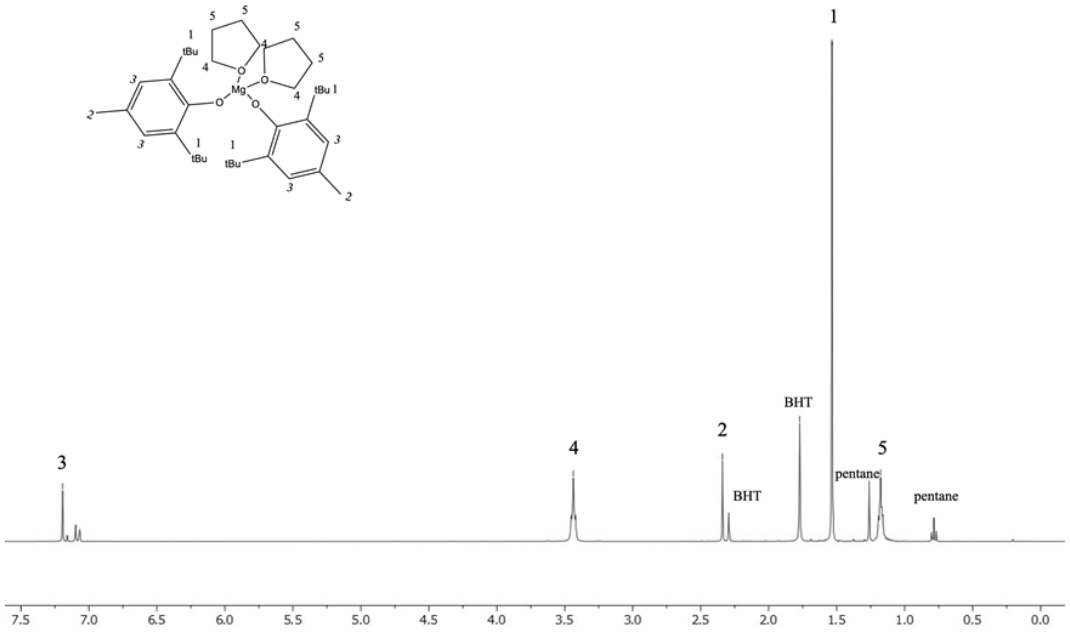

Figure 2.2 ^{1}H NMR spectrum (C_6D_6, 400 MHz) of $Mg(BHT)_2(THF)_2$.

2.3.2 Synthesis of PPDL polymers

In order to compare the crystallising behaviour of this novel system with the previous PCL work in our group, we synthesised a series of analogous diblock copolymers composed of poly(ω-pentadecalactone)-*b*-poly(*N,N*-dimethylacrylimade) (PPDL-b-PDMA), where the non-crystallising block was consistent with the reported PCL copolymers.[95] The polymers were synthesised using a combination of ring-opening polymerisation and reversible addition-fragmentation chain transfer (RAFT) polymerisation (**Scheme 2.2**).

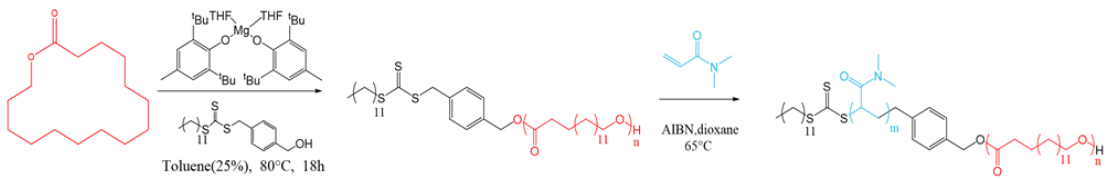

Scheme 2.2 Synthesis route of PPDL-b-PDMA copolymers.

The synthesis of PPDL was catalysed by $Mg(BHT)_2(THF)_2$ and initiated with a dual-functionality CTA to allow the further chain extension reaction by RAFT. As reported, the use of this catalyst allowed this reaction to be carried out in an atmospheric environment. This 'immortal' polymerisation is, therefore, a more effective process for large-scale synthesis, which highlights the industrial potential of this polymer. All reactants were mixed without pre-drying and then heated to 80 °C to improve the poor solubility of the PDL monomer in toluene. The PDL reached 80% conversion after 18 hours by monitoring the disappearance of the monomer CH_2OC=O resonance (δ = 4.15 ppm) and appearance of the polymer CH_2OC=O resonance (δ = 4.05 ppm) in agreement with previous literature.[143] The reaction was then quenched with the addition of 5% acidified methanol. After redissolution in chloroform, the polymer was precipitated into methanol to remove any residual PDL monomer. Two different DPs (10, 25) were targeted and were confirmed by analysing the purified products by ^{1}H NMR spectroscopy, comparing the ratio of SC$H_2C_6H_4$ resonance (δ=4.61) to the α-methylene resonance of PPDL (δ = 4.05 ppm) (**Figure 2.3**).

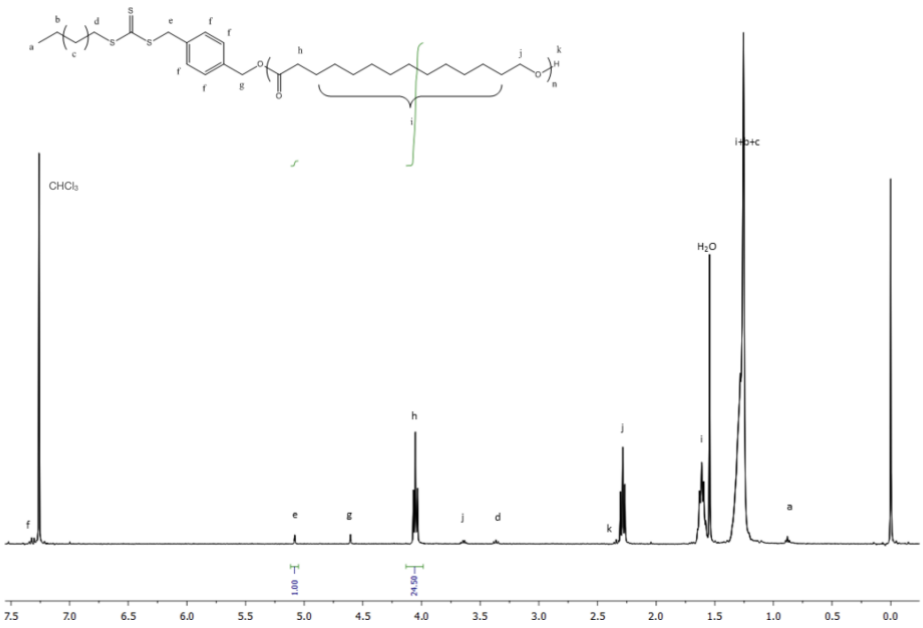

Figure 2.3 ^{1}H NMR spectrum ($CDCl_3$, 400 MHz) of $PPDL_{25}$.

Size exclusion chromatography (SEC) analysis revealed a good overlap of the refractive index (RI) and ultraviolet (UV) (λ = 309 nm, corresponding to the π-π* electronic transition of the thiocarbonyl moiety) peaks in the SEC traces signifies the retention of the RAFT end group. The broad dispersity of PPDL ($Đ_M$ = 1.9, 2.0) is in accordance with previous reports and is mainly the result of side esterification reactions owing to the chain restrain from the 16-member ring. (**Figure 2.4**)

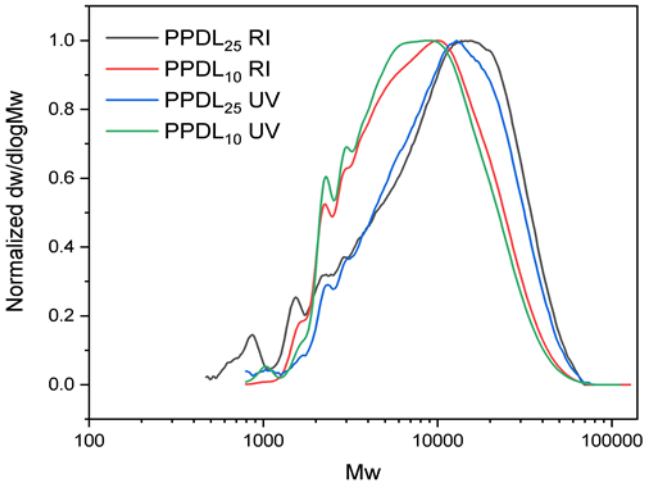

Figure 2.4 SEC chromatograms of PPDL homopolymers.

Subsequently, the homopolymers were used as a macromolecular chain transfer agent to mediate the polymerisation of DMA by RAFT. The polymerisation was carried out in toluene at 80 °C to ensure full solubilization of PPDL and using 2,2-azobis(2-methylpropionitrile) (AIBN) as a radical initiator. A chain extension of DP 110 of the DMA hydrophilic block was targeted for both of the PPDL homopolymers, in order to study the morphology changes with different crystallising block volumes. The polymer was purified by precipitation into hexane followed by centrifugation. The DP of DMA was confirmed by ^{1}H NMR spectroscopy, whereby the peak at δ = 2.90 ppm corresponds to the 6 protons of the dimethyl groups and the α-methylene resonance of PPDL (δ = 4.05 ppm) (**Figure 2.5**). SEC analyses in $CHCl_3$ were also used to characterise both polymers, where a molecular weight shift compared to the PPDL homopolymers could be observed. The retention of RAFT group was confirmed by the overlapping of the RI and UV traces (λ = 309 nm) (**Table 2.1**). Interestingly, we discovered a significantly narrower dispersity ($Đ_M$ =1.4) for the PPDL-*b*-PDMA from the SEC analysis following the RAFT polymerisation step. We attribute this as the result of the cyclic ester side product

produced during the ROP (which would therefore not engage in the chain extension reactions) being purified out as a result of the considerable difference of molecular weight compared to the diblock, as shown in the SEC traces (**Figure2.6**). Crystallisation-driven self-assembly of the resultant diblock copolymers was then studied.

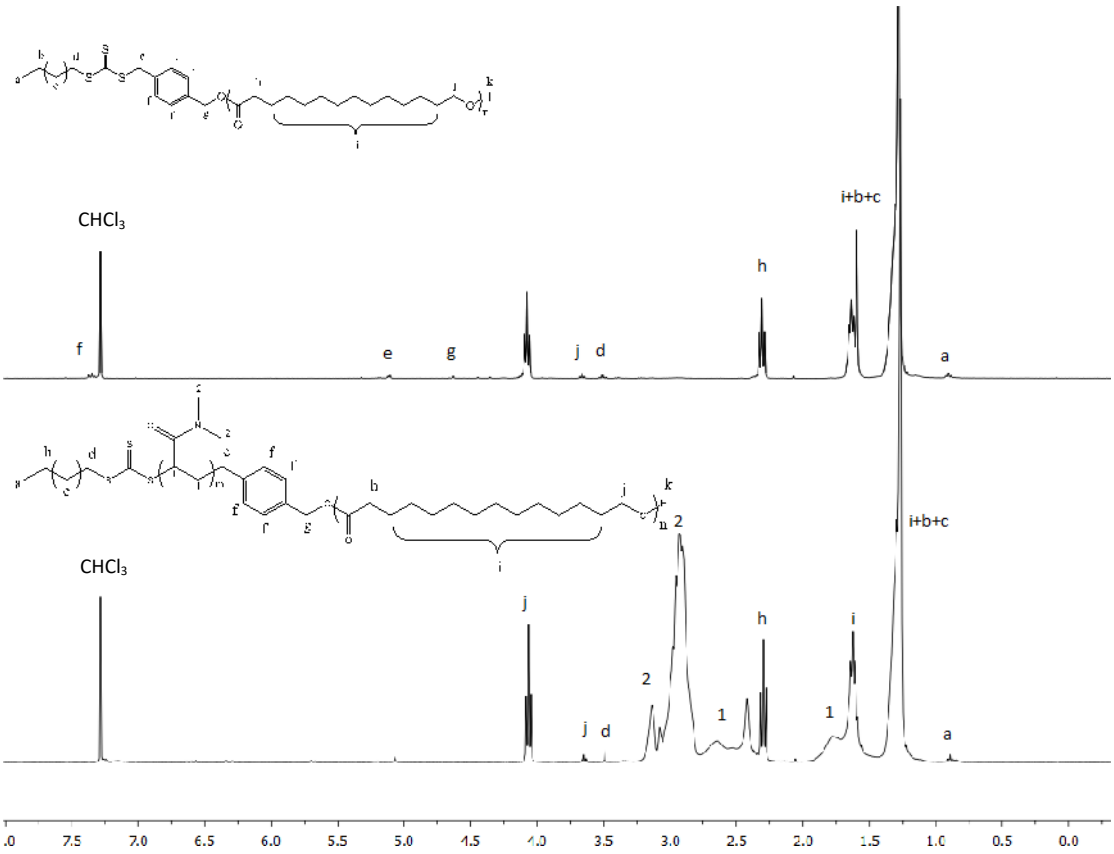

Figure 2.5 Stacked ^{1}H NMR spectra ($CDCl_3$ 400Hz) of $PPDL_{25}$-*b*-$PDMA_{110}$ block copolymers and homopolymer.

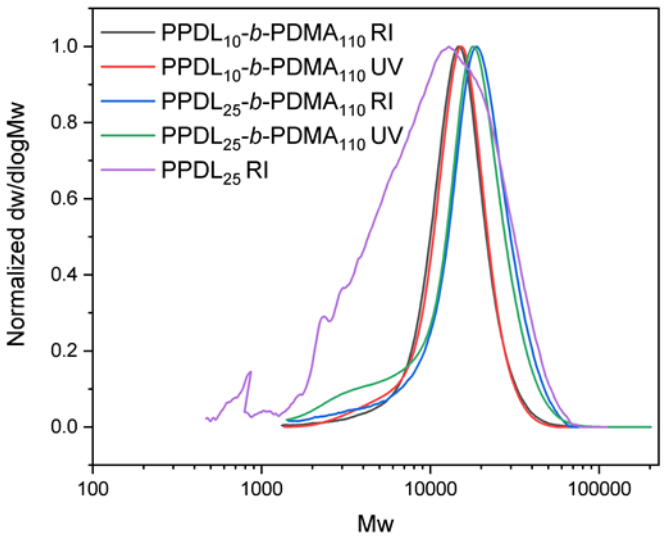

Figure 2.6 SEC chromatograms of PPDL homopolymer and PPDL BCPs using chloroform as an eluent.

Table 2.1 Summary of M_n (SEC and NMR) and $Đ_m$ of PPDL homo and block copolymers.

Polymer	**M_n SEC(g/mol)**	**M_n NMR(g/mol)**	**$Đ_m$**	**Hydrophobic wt.%**
$PPDL_{10}$	5420	2798	1.9	-
$PPDL_{25}$	12300	6398	2.1	-
$PPDL_{10}$-b-$PDMA_{110}$	14707	13704	1.4	18.1
$PPDL_{25}$-b-$PDMA_{110}$	22080	17303	1.3	35.5

2.3.3 Exploring crystallisation driven self-assembly conditions of PPDL copolymers

To understand the CDSA process for this novel polymer, CDSA of $PPDL_{25}$-*b*-$PDMA_{110}$ was examined in various solvents, initially with ethanol in order to be consistent with the PCL work reported by our group.[95] A solution of 5mg mL^{-1} PPDL BCP was heated to 70 °C for three hours to ensure full melting of the polymer. The solution was then cooled down to room temperature (23 °C), followed by ageing for three days to allow the unimer to fully crystallise. The sample was diluted ten times and examined by transmission electron microscope (TEM) (staining with a 1 wt% solution of uranyl acetate in 18.2 MΩ·CM water), which showed precipitated small crystals (**Figure 2.7**). This was postulated to be the result of the high melting temperature of PPDL, leading to a fast self-nucleation process without the complete melting of the polymer during heating. Following this, CDSA of PPDL BCPs in a mixed solvent ethanol/chloroform (3:1) was investigated by heating to the same temperature (70 °C) and annealing for three hours, before slowly cooling down to room temperature and ageing for three days to allow further crystallization. A majority morphology of cylinders was observed by TEM (**Figure 2.7**). From the observed morphology change, we hypothesized that the addition of chloroform, which is a good solvent for the core-forming block, helped to reduce the melting temperature and suppress self-nucleation rates. This observation of change of morphology in the presence of a suitable solvent for the core-forming block has provided an initial insight of PPDL copolymer crystallising behaviour in solution.

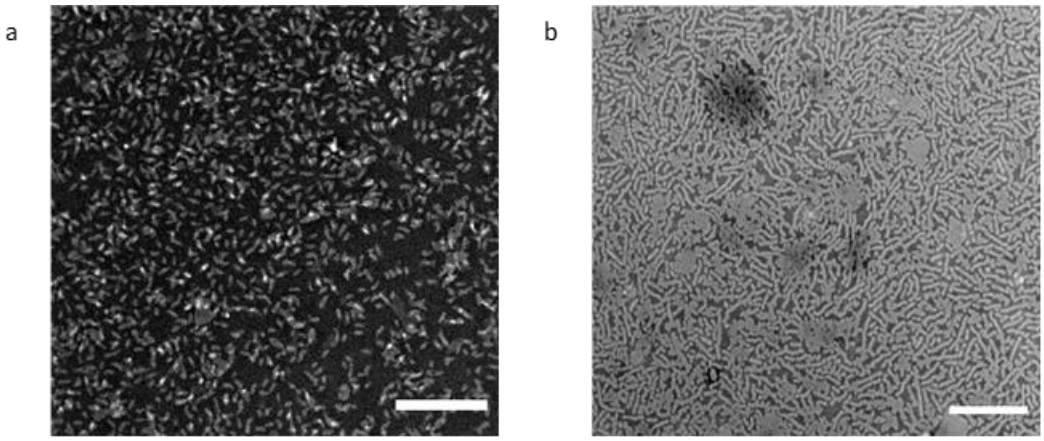

Figure 2.7 TEM micrographs of $PPDL_{25}$-*b*-$PDMA_{110}$ CDSA in (a) ethanol and (b) ethanol: chloroform (3:1) at 70°C for 3 hours and cooled down to room temperature. Samples were stained with uranyl acetate. Scale bar = 1 µm.

To gain further insights into suitable conditions for CDSA of PPDL BCPs, additional experiments were then performed in a range of solvents. Considering the high melting temperature of PPDL and solubility of DMA, the copolymers were firstly heated in n-butanol. The 5 mg mL^{-1} polymer solution was heated to 90 °C for 3 hours to allow the full melting of the PPDL block. After slowly cooling down to room temperature, the solution was left to age for three days to conclude the crystallisation. The CDSA structures were then determined by TEM (**Figure 2.8a**), where wormlike structures were observed from the $PPDL_{25}$-*b*-$PDMA_{110}$. To further understand the PPDL crystallisation in n-butanol, we performed a non-isothermal Nano Differential scanning calorimetry (NanoDSC) analysis, which, unlike dry state DSC, detects the phase transitions of polymers in solution. The solution was heated to 100 °C and cooled down to 0 °C at 1 °C/min. We observed that the temperatures of the melting and crystallization peaks were reduced compared to those in dry state DSC (**Figure 2.8d**), which was attributed to the plasticising effect of the solvent.

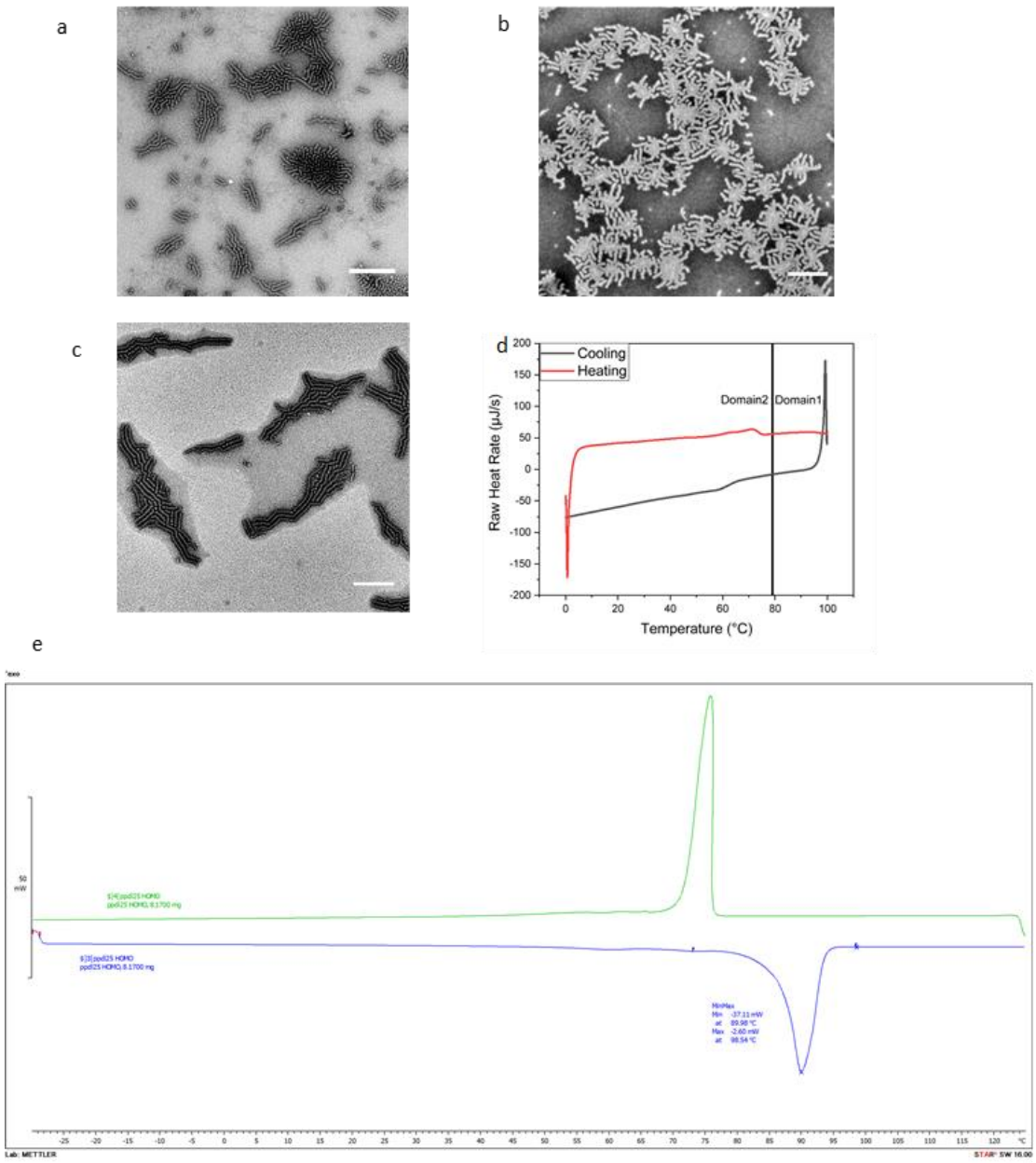

Figure 2.8 TEM micrographs of $PPDL_{25}$-*b*-$PDMA_{110}$ CDSA in n-butanol (a) at 70°C and (b) at 90°C for 3 hours and cooled down to room temperature. Samples were stained with uranyl acetate. Scale bar = 0.5 µm. NanoDSC scanning of $PPDL_{25}$-*b*-$PDMA_{110}$ in n-butanol at from 0 to 100°C at 1°C min^{-1}(c), dry state DSC scanning of $PPDL_{25}$-*b*-$PDMA_{110}$, second circle(d).

Different from other polylactones such as PCL, there were two distinct peaks present between 55-75 °C in the Nano DSC, indicating that there were two domains of self-nucleation, as explained below.

We hypothesized that there was a fast PPDL block self-nucleation throughout the domain one during the lower temperature range as a consequence of its high crystallinity. Repeated melting behaviour of those self-nucleation micelles from domain one was then recorded as the second peak by NanoDSC. To verify this theory, we examined a sample following the same procedure as initially, but instead only heating to 70 °C. The resultant morphology from this experiment was then analyzed by TEM. Interestingly, a unique 'spider' structure was formed, which had worms crystallized onto platelets (**Figure 2.8b**). This likely revealed the two domains of PPDL copolymers crystallising in n-butanol (**Figure 2.8d**). A fast self-nucleation forms the inner platelet structure during domain one, which is driven by part of PPDL BCPs reserved memory effect. The remained fully-melt polymers allow further self-assembly forming wormlike shielding structures. In contrast, a single self-nucleation produced neat wormlike structures when the thermal history of all polymers was removed in domain two (**Figure 2.9**). We next heated the 'spider-like' sample back to 90 °C, followed by a fast cooling down, which led to the observation of a single wormlike structure by TEM, indicating that the formation of the two structures is thermally reversible. (**Figure 2.8c**) A slightly less polar solvent, n-pentanol, was next utilised to establish the two domains which were observed in n-butanol during the CDSA of PPDL copolymers. Identical experiments were carried out as before, and similar results were obtained from both Nano DSC and TEM (**Figure 2.10**).

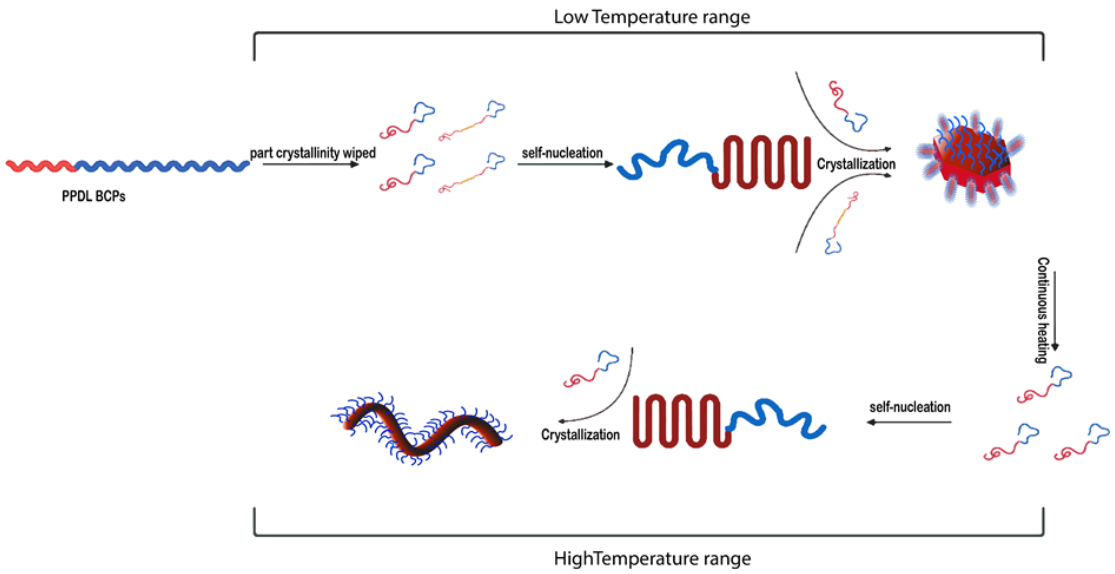

Figure 2.9 Scheme of PPDL BCPs CDSA in two different temperature domains.

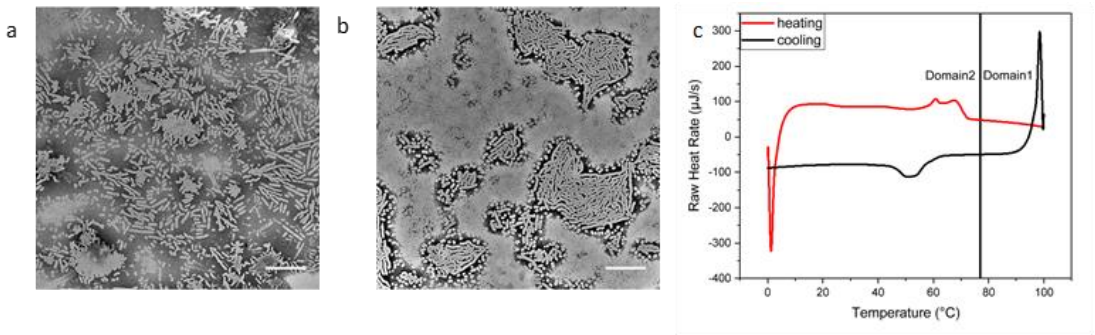

Figure 2.10 TEM micrographs of $PPDL_{25}$-*b*-$PDMA_{110}$ CDSA in n-pentanol (a) at 70°C and (b) at 90°C for 3 hours and cooled down to room temperature. Samples were stained with uranyl acetate. Scale bar = 0.5 µm. NanoDSC scanning of $PPDL_{25}$-*b*-$PDMA_{110}$ in n-pentanol at from 0 to 100°C at 1°C min^{-1}.

2.3.4 CDSA of PPDL copolymers in various solvents

During the preliminary study of PPDL copolymers crystallization behaviour in solution, it was noticed that the peak melting temperature (66°C) in n-pentanol was slightly reduced compared to that (71°C) in n-butanol. This encouraged us to take a closer look at how the solvent polarity affects PPDL copolymer crystallization in solution. Hence, a

range of CDSA experiments were performed using $PPDL_{25}$-*b*-$PDMA_{110}$ as the model polymer and a series of solvents with reducing solvent polarity, with examination by NanoDSC to investigate the melting and crystallization temperature in solutions. We firstly heated the polymer (5 mg mL^{-1}) in n-hexanol and cyclopentanol in the NanoDSC to 100 °C and cooled down to 0 °C at 1 °C min^{-1}. The melting and crystallisation peaks in these solvents were observed to continuously decrease by 10 °C as the polarity decreased compared to n-butanol (**Figure 2.11a, b**). To further investigate the polarity effect, we repeated the same experiment in less polar solvent 2-Methyltetrahydrofuran (2Me-THF), which has a higher boiling point than the more common solvent THF, to fulfil the need for a high-temperature range to accommodate the high melting temperature of the PPDL. Furthermore, 2-Me THF is an ether compared to the alcohols previously used, and thus was also a control experiment to exclude H bonding effects. In this case, the melting peak shifted to 42 °C and crystallization peak shifted to 30 °C according to the NanoDSC analysis, which is a significant change compared to those in n-butanol, n-pentanol, n-hexanol and cyclopentanol (**Figure 2.11c**). The observed transitions in different solvents confirm that melting and crystallization temperatures of PPDL copolymers decrease with the solvent polarity. Given that our interest is focused on the crystallization driven self-assembly of PPDL copolymers, we subsequently used TEM to demonstrate the morphologies formed in these solvents. PPDL was heated to the temperature above the melting range obtained from Nano DSC in each solvent, followed by cooling down to allow the CDSA to occur. Wormlike structures were observed in each sample, and therefore demonstrating the correlation between solvent polarity and PPDL polymer crystallization and melting temperatures in a more precise way than just a solvent plasticizing effect. From these results, we were able to determine that a similar

CDSA process of the PPDL copolymers could be achieved within different predicated temperature ranges as a function of changing the solvent polarity (**Figure 2.11d**). More importantly, this method could potentially translate to any polymers which crystallise in solution and therefore contribute a significant pathway gaining more insight into CDSA.

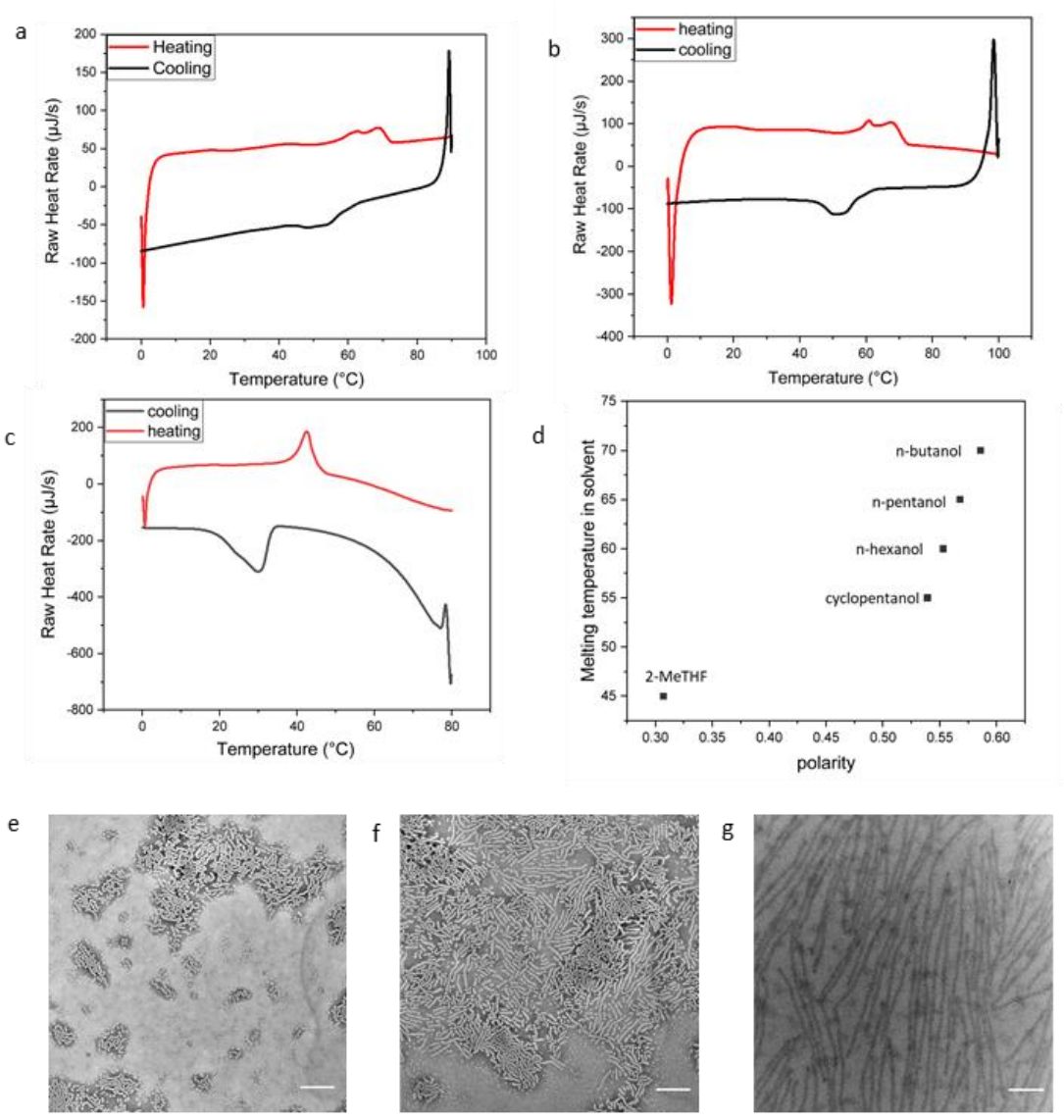

Figure 2.11 Nano DSC measurement of $PPDL_{25}$-*b*-$PDMA_{110}$ CDSA in n-hexanol (a), Cyclopentanol (b) and 2-MeTHF(c); TEM of PPDL-*b*-PDMA CDSA in n-hexanol (e), Cyclopentanol (f) and 2-MeTHF(g), Scale bar 500nm; CDSA temperature in different solvents associated with polarity (d).

2.3.5 Studying solvent effect of PPDL BCP with different core volume

Based on the results obtained from $PPDL_{25}$-*b*-$PDMA_{110}$ (35.5% hydrophobic weight percentage) CDSA in different solvents, we were next interested in investigating whether the core volume plays a role during the self-nucleation process. As such, $PPDL_{10}$-b-$PDMA_{110}$ of which the hydrophobic weight percentage is 18.1, was studied in each solvent (n-butanol, n-pentanol, n-hexane, cyclopentanol and 2-Me THF) as an extension from $PPDL_{25}$-*b*-$PDMA_{110}$. The polymer was heated in the NanoDSC to 100 °C and cooled down to 0 °C at 1 °C min^{-1} (**Figure 2.12a**). The results from each scan were calculated, which confirmed that the melting and crystallization temperatures were decreased to the same level in each solvent corresponding to those of $PPDL_{25}$-b-$PDMA_{110}$. As before, two melting peaks appeared in n-butanol, n-pentanol, n-hexanol and cyclopentanol, while a single melting peak was seen in 2-ME THF, indicating that the self-nucleation was suppressed in this solvent. This has shown, for BCPs having the same crystallisation block, self-nucleation in solution changes along with solvent regardless of the volume of crystallisation block.

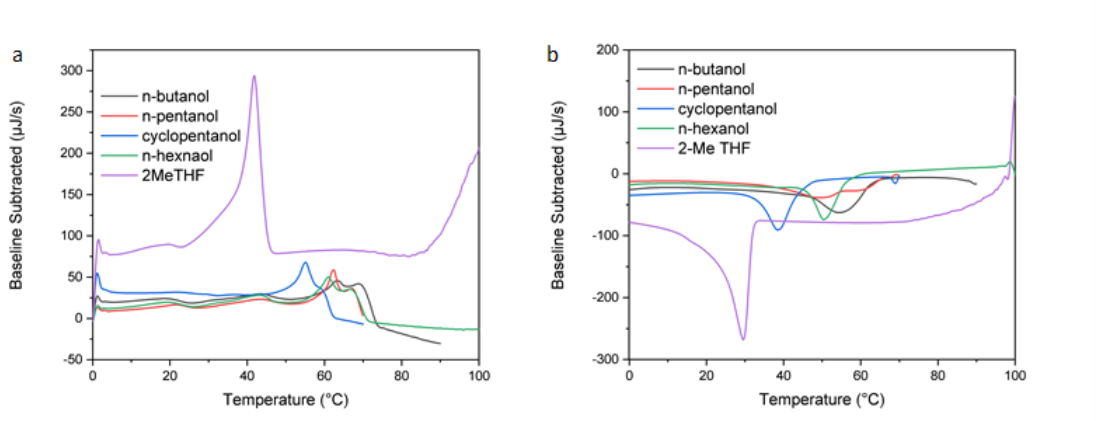

Figure 2.12 NanoDSC scanning of $PPDL_{10}$-*b*-$PDMA_{110}$ in different solvents from at 1°C/min heating(a), cooling(b).

2.3.6 Mechanism of Structure Formation

As a less polar semi-crystalline polymer, the effect of solvent in plasticising PPDL decreases with its polarity, which changes the self-nucleation rate of PPDL. By comparing the average length of the wormlike structures observed by TEM in different solvents, it was observed that there was a significant increase as the polarity was reduced. This was particularly so in 2-Me THF, where the resulting Nano DSC melting trace only showed a single peak, suggesting that the self-nucleation micelles remelting was not detected by NanoDSC. This indicates that when the melting temperature of PPDL in solution is primarily reduced, the fast self-nucleation can be minimized, resulting in increased length of cylinders. This suggests that the self-nucleation rate is an essential parameter that determines the length of the cylinders. A fast self-nucleation of PPDL enables a vast population of micelles, and therefore less unimer left in solution to further crystallise onto these micelles. As a result, shorter cylinders are produced.

In contrast, in a less polar solvent such as 2-Me THF, where the PPDL experiences a much slower self-nucleation, fewer micelles are formed during the cooling down process. Over time, more unimer is then able to crystallise on these self-nucleation sites leading to longer cylinder growth. Thus, the second crystallisation phase dominates the formation of cylinders (**Scheme 2.3**). Despite the nature of random homogenous nucleation, the length variations of the resultant cylinders that could be achieved in the different solvents have demonstrated an interesting solvent effect in 'controlling' self-nucleation activities. Therefore, these findings have allowed us to define precise temperature ranges for different PPDL CDSA behaviour in solution. Furthermore, this has introduced a new approach to tune the length of PPDL CDSA structures simply by exploiting

different solvent polarities. Notably, the solution crystallisation of polymers is generally thermally controlled, where the solvent effect has proven to be a crystallization parameter corresponding to the free energy.[80] This approach, hence, could be applied in all-polymer solution crystallisation theoretically.

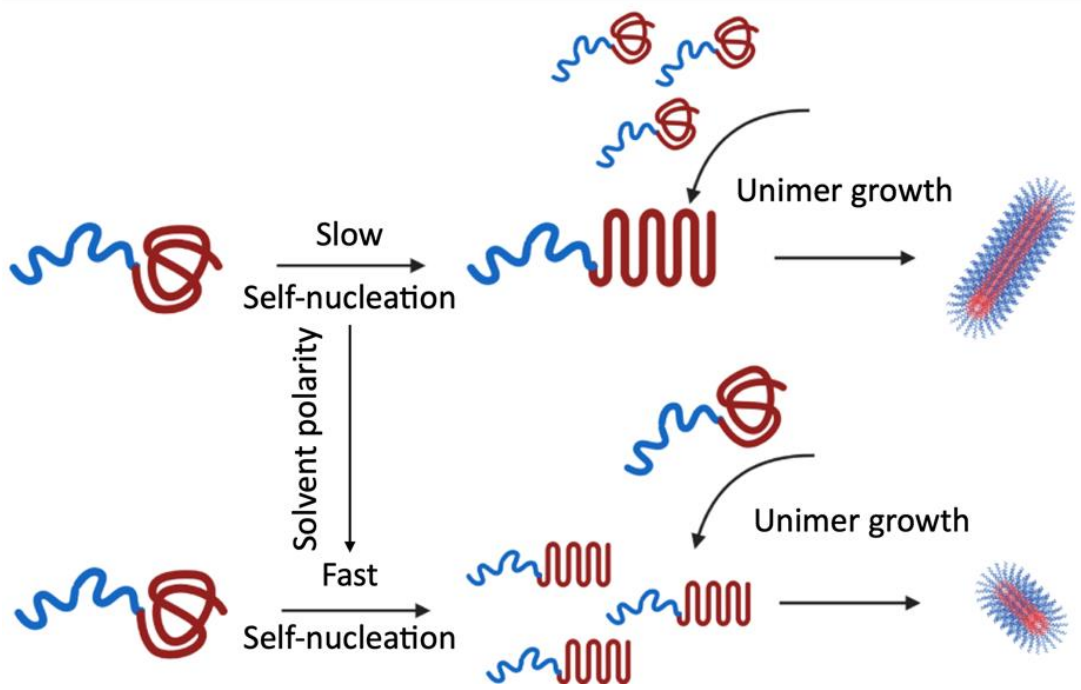

Scheme 2.3 Mechanism of different length cylinders formation.

2.4 Conclusion

PPDL block copolymers were synthesised using a combination of ring-opening polymerisation (ROP) and RAFT. And CDSA of PPDL BCPs into wormlike and complex 'spider' structures have been established for the first time. It is proposed that the unique 'spider' self-assembly structure is initiated by a fast self-nucleation nature of PPDL within its melting process. Subsequently, we utilised NanoDSC as a critical technique to determine the self-nucleation for PPDL polymers in a particular solvent. This scheme has revealed different PPDL self-nucleation domains in polar solvents, where different self-nucleation kinetics were associated with its melting temperature due to hydrophobicity and crystallinity. The results obtained indicate the annealing temperature in CDSA that could drive PPDL BCPs towards each morphology.

The relationship between the polarity of the solvent and PPDL self-nucleation is then determined, whereby self-nucleation rates adjusted by different solvent polarities, could allow for tuning of the length of cylinders. Furthermore, in 2-Me THF, two distinct melting peaks due to the nature of PPDL's fast self-nucleation in other solvents have emerged from NanoDSC measurements. This proves the self-nucleation has been largely slowed down in this least polar solvent and corresponds to the length of the cylinder formed.

By studying the $PPDL_{10}$-*b*-$PDMA_{110,}$ which comprises the smaller PPDL molecular weight percentage, we could further confirm that the fast self-nucleation determined by NanoDSC is due to the nature of PPDL. The polymer underwent the same decrease in melting and crystallisation temperatures as the $PPDL_{25}$-*b*-$PDMA_{110}$. This revealed that

the process was primarily controlled by the properties of the material itself, while the hydrophobic weight percentage played no role.

The process of studying the self-nucleation of PPDL BCPs in this work has overall drawn a pathway to both determine precise thermal conditions and manipulate the self-nucleation rates in CDSA, purely by changing the solvent. Therefore, this method shows great potential for understanding and expanding the CDSA of different and novel polymers.

2.5 Experimental

2.5.1 Materials

Chemicals and solvents were purchased from Sigma Aldrich, Acros, Fluka, Fisher Chemical, Alfa Aesar, or VWR. Dry solvents were purified using MBRAUN SPS solvent purification system. ω-Pentadecalactone was dissolved in 75 wt.% toluene and dried overnight on molecular sieves. 1,4-Dioxane, *N,N*-dimethylacrylamide (DMA) and 2,2'-azobis(2-methylpropionitrile) (AIBN) was recrystallised twice from methanol and stored in the dark at 4 °C.

2.5.2 Instrumentation

^{1}H and ^{13}C nuclear magnetic resonance (NMR) spectra were recorded at 400 MHz on a Bruker DPX-400 spectrometer in $CDCl_3$ unless otherwise stated. Chemical shifts are reported as δ in parts per million (ppm) downfield from the internal standard trimethylsilane.

Size exclusion chromatography (SEC) was performed on an Agilent 390-MDS on PLgel Mixed-D type columns in series with refractive index (RI) detection. Weights were calculated using a calibration curve determined from poly(styrene) standards with chloroform (0.5% NEt_3) as eluent flowing at 1.0 $mL.min^{-1}$ and sample concentration 3 $mg.mL^{-1}$.

Differential scanning calorimetry (DSC) analysis was performed on a Mettler Toledo HP DSC827. Samples were run at a heating or cooling ramp series of 10 °C min^{-1} in triplicate under a nitrogen atmosphere using 40 μL aluminium crucibles. T_c and T_m of various

samples were obtained in the first runs and were taken as the midpoint of the inflection tangent.

Nano Differential scanning calorimetry (NanoDSC) was performed on a TA NanoDSC. 800µL samples were run at a heating or cooling ramp series of 1 °C min^{-1} in triplicate under a constant 3-atmosphere pressure. T_c and T_m of various samples were obtained in the second runs and were taken as the midpoint of the inflection tangent.

Samples for transmission electron microscopy (TEM) analysis were prepared by drop casting 10 µL of polymer in ethanol (0.5 mg mL^{-1}) onto a carbon/formvar-coated copper grid placed on filter paper. Samples were stained with a 1% uranyl acetate solution to facilitate imaging of the thin organic structures unless specified. Imaging for samples was performed on a Jeol 2100 transmission electron microscope operating at 120 kV. TEM images were analysed by ImageJ software.

2.5.3 Synthesis of $Mg(BHT)_2(THF)_2$

Using a modified version of the previously reported procedure, 2,6-di-*tert*-butyl-4-methylphenol (4.407 g, 20.0 mmol) was dissolved in dry toluene (20 mL). Di-n-butylmagnesium 1 M in heptane (10 mL, 10.0 mmol) was added dropwise with stirring at room temperature. The exotherm raised the temperature of the flask and did not peak above 60 °C. The solution was stirred for a further 2 hours before removing the solvent under vacuum. The remaining white solid was dissolved in dry pentane (25 mL) before dry tetrahydrofuran (5 mL) was added dropwise with stirring. The reaction was stirred for a further 2 hours before removing the solvent to yield a white solid (5.96 g, 9.8 mmol, 98%). The product was dried under vacuum overnight and stored in a glovebox. Characterising data was consistent with the previous report.

^{1}H NMR (400 MHz, 298 K, C_6D_6): δ = 7.01 (s, BHT Ar), 3.59 (t, $^{3}J_{H\text{-}H}$ = 6.4, THF CH_2CH_2O), 2.30 (s, BHT CH_3Ar), 1.48 (s, BHT $(CH_3)_3CAr$), 1.20 (m, THF CH_2CH_2O). ^{13}C NMR (125 MHz, 298 K, C_6D_6): δ = 159.0, 154.4, 139.5, 139.3, 130.0, 127.2, 123.1 (BHT Ar C), 72.6 (THF CH_2CH_2O), 37.5 (BHT $ArCH_3$), 34.0 (BHT $ArC(CH_3)_3$), 27.0 (THF CH_2CH_2O), 23.7 (BHT $ArC(CH_3)_3$) ppm.

2.5.4 Synthesis of dual-headed ROP initiator and chain transfer agent dodecyl 4-(hydroxymethyl) benzyl carbonotrithioate

Acetone (200 mL) was added to a mixture of dodecanethiol (1.53 mL, 6.4 mmol), potassium phosphate (1.48 g, 7.0 mmol) and carbon disulfide (1.15 mL, 20 mmol) and stirred for 2 hours at room temperature. After adding 4-chloromethylbenzyl alcohol (1.00 g, 6.4 mmol), the yellow solution was stirred for 72 hours. Acetone was removed in vacuo, and the resultant yellow solid was dissolved in CH_2Cl_2. The organic layer was washed with hydrochloric acid (1 M, 2 × 100 mL), deionised water (3 × 100 mL) and brine (2 × 100 mL). The yellow solution was dried over magnesium sulfate, filtered and concentrated in vacuo before purification by flash column chromatography (silica gel, 3:2 hexane/ethyl acetate). The solvent was removed in vacuo, and the resultant yellow solid was dried in a desiccator over P_2O_5 for two days (1.82 g, 72%). Rf (3:2 hexane:ethyl acetate): 0.48. 1H NMR ($CDCl_3$, 400 MHz): δ (ppm) 7.33 (m, 4H, Ar-*H*) 4.68 (d, 2H, $^{3}J_{H\text{-}H}$ = 5.9 Hz, C*H*$_2$OH) 4.61 (s, 2H, Ar-C*H*$_2$S) 3.36 (t, 2H, $^{3}J_{H\text{-}H}$ = 7.4 Hz, CH_2CH_2S) 1.70 (m, 2H, C*H*$_2$$CH_2S$) 1.63 (t, 1H, $^{3}J_{H\text{-}H}$ = 5.9 Hz, O*H*), 1.22-1.44 (m, 18H, $CH_3C_9H_{18}$) 0.87 (t, 3H, $^{3}J_{H\text{-}H}$ = 6.0 Hz, C*H*$_3$). ^{13}C NMR ($CDCl_3$, 150 MHz): δ (ppm) = 223.7 (S*C*(S)S), 140.4 (SCH_2C), 134.6 (OCH_2C), 129.5 (SCH_2CCH), 127.3(OCH_2CCH), 65.0 (OCH_2), 41.0 (SCH_2C), 37.1 (SCH_2CH_2), 32-22 ($CH_3C_{10}H_{20}$), 14.1 (CH_3).

2.5.5 General procedure of ω-pentadecalactone polymerisation

Using standard glovebox techniques, an ampoule was filled with $Mg(BHT)_2(THF)_2$ (40 mg, 66 µmol), dodecyl 4-(hydroxymethyl) benzyl carbonotrithioate (26.3mg, 66 µmol) and ω-pentadecalactone stock solution (75 wt.% toluene, 1.98 mmol). The ampoule was sealed and heated at 80 °C for a defined time period. The reaction was quenched with the addition of acidified (5 % HCl) methanol. Chloroform was added to dissolve any solids, and the polymer was precipitated in excess methanol. The resultant white polymer was filtered and dried under vacuum over P_2O_5 for two days.

1H NMR (300MHz, 298K, CDCl3): δ = 7.31-7.37 (m, 4H, Ar-*H*), 5.10 (s, 2H, SC*H*$_2$Ar), 4.69 (s, 2H, C=OOC*H*$_2$Ar), 4.05 (t, 52H, $^3J_{H-H}$ = 6.8 Hz, C*H*$_2$OC=O), 3.68 (t, 2H, $^3J_{H-H}$ = 7.3 Hz, C*H*$_2$OH) 3.37 (t, 2H, $^3J_{H-H}$ = 7.3 Hz, SC*H*$_2$CH$_2$) 2.28 (t, 50H, $^3J_{H-H}$ = 7.5 Hz, C*H*$_2$C=OO), 1.61, 1.25 and 0.79 (all remaining hydrogens) ppm. Yield: 80%.

2.5.6 Synthesis of poly(ω-pentadecalactone)-*b*-poly(*N,N*-dimethylacrylimade)

$PPDL_n$ (6.6 µmol), N,N-dimethylacrylamide, (108µl, 990 µmol) and AIBN (13 µL of a 10 mg mL^{-1} solution in toluene, 0.79 µmol) and toluene (1.0mL) were combine in a dried ampoule under nitrogen. After three freeze-pump-thaw cycles, the solution was sealed under nitrogen and heated for 3 hours at 80 °C. The reaction was quenched in liquid nitrogen and purified by precipitation three times into ice-cold diethyl ether. The resultant pale yellow solid was dried in vacuo before use. $PPDL_{25}$-b-$PDMA_{110}$: NMR ($CDCl_3$): δ (ppm) 4.05 (t, 52H, $^3J_{H-H}$ = 6.8 Hz, C*H*$_2$OC=O) 2.76-3.24 (660 H, m, N(*CH*$_3$)$_2$) 1.27-2.75 (all remaining hydrogens) 0.87 (t, 3H, $^3J_{H-H}$ = 6.9 Hz, CH$_2$C*H*$_3$).

2.5.7 Typical crystallisation-driven self-assembly method for poly(ω-pentadecalactone)-*b*-poly(*N,N*-dimethylacrylimade) block copolymers

$PPDL_{25}$-*b*-$PDMA_{110}$ (10 mg) was added to 2 mL of solvent (5.0 mg mL^{-1}) in a 7 mL vial. The samples were heated in an oil bath at different temperatures without stirring for a predetermined period of time before being removed from the oil bath and left to cool to room temperature. Samples were imaged after 3 days of ageing at room temperature.

2.6 Reference

1. T. H. Epps Iii and R. K. O'Reilly, *Chem Sci*, 2016, **7**, 1674-1689.

2. R. K. O'Reilly, C. J. Hawker and K. L. Wooley, *Chem Soc Rev*, 2006, **35**, 1068-1083.

3. L. Zhang and A. Eisenberg, *Journal of the American Chemical Society*, 1996, **118**, 3168-3181.

4. T. Azzam and A. Eisenberg, *Langmuir*, 2007, **23**, 2126-2132.

5. A.-V. Ruzette and L. Leibler, *Nat. Mater.*, 2005, **4**, 19-31.

6. M. J. Rymaruk, C. T. O'Brien, S. L. Brown, C. N. Williams and S. P. Armes, *Macromolecules*, 2020, **53**, 1785-1794.

7. L. Wang, C. Hu and L. Shao, *Int J Nanomedicine*, 2017, **12**, 1227-1249.

8. X. Huang, X. Teng, D. Chen, F. Tang and J. He, *Biomaterials*, 2010, **31**, 438-448.

9. S. Varlas, J. C. Foster and R. K. O'Reilly, *ChemComm*, 2019, **55**, 9066-9071.

10. S. Varlas, R. Keogh, Y. Xie, S. L. Horswell, J. C. Foster and R. K. O'Reilly, *J. Am. Chem. Soc.*, 2019, **141**, 20234-20248.

11. E. Hinde, K. Thammasiraphop, H. T. Duong, J. Yeow, B. Karagoz, C. Boyer, J. J. Gooding and K. Gaus, *Nat. Nanotechnol*, 2017, **12**, 81.

12. A. Setaro, S. Lettieri, P. Maddalena and L. D. Stefano, *Appl. Phys. Lett.*, 2007, **91**, 051921.

13. B. Lotz, A. J. Kovacs, G. A. Bassett and A. Keller, *Kolloid-Zeitschrift und Zeitschrift für Polymere*, 1966, **209**, 115-128.

14. U. Tritschler, S. Pearce, J. Gwyther, G. R. Whittell and I. Manners, *Macromolecules*, 2017, **50**, 3439-3463.

15. J. Schmelz, M. Karg, T. Hellweg and H. Schmalz, *ACS Nano*, 2011, **5**, 9523-9534.

16. J. Xu, H. Zhou, Q. Yu, G. Guerin, I. Manners and M. A. Winnik, *Chem.*, 2019, **10**, 2280-2284.

17. M. C. Arno, M. Inam, Z. Coe, G. Cambridge, L. J. Macdougall, R. Keogh, A. P. Dove and R. K. O'Reilly, *Journal of the American Chemical Society*, 2017, **139**, 16980-16985.

18. J. Cai, C. Li, N. Kong, Y. Lu, G. Lin, X. Wang, Y. Yao, I. Manners and H. Qiu, *Science*, 2019, **366**, 1095-1098.

19. A. M. Oliver, J. Gwyther, M. A. Winnik and I. Manners, *Macromolecules*, 2018, **51**, 222-231.

20. S. Pearce, X. He, M.-S. Hsiao, R. L. Harniman, L. R. MacFarlane and I. Manners, *Macromolecules*, 2019, **52**, 6068-6079.

21. J. Wang, J. H. Horton, G. Liu, S.-Y. Lee and K. J. Shea, *Polymer*, 2007, **48**, 4123-4129.

22. L. Yin and M. A. Hillmyer, *Macromolecules*, 2011, **44**, 3021-3028.

23. H. Schmalz, J. Schmelz, M. Drechsler, J. Yuan, A. Walther, K. Schweimer and A. M. Mihut, *Macromolecules*, 2008, **41**, 3235-3242.

24. J. Schmelz, A. E. Schedl, C. Steinlein, I. Manners and H. Schmalz, *Journal of the American Chemical Society*, 2012, **134**, 14217-14225.

25. Y. Cha, C. Jarrett-Wilkins, M. A. Rahman, T. Zhu, Y. Sha, I. Manners and C. Tang, *ACS Macro Lett.*, 2019, **8**, 835-840.

26. Y. He, J.-C. Eloi, R. L. Harniman, R. M. Richardson, G. R. Whittell, R. T. Mathers, A. P. Dove, R. K. O'Reilly and I. Manners, *Journal of the American Chemical Society*, 2019, **141**, 19088-19098.

27. M. Inam, G. Cambridge, A. Pitto-Barry, Z. P. L. Laker, N. R. Wilson, R. T. Mathers, A. P. Dove and R. K. O'Reilly, *Chem.*, 2017, DOI: 10.1039/C7SC00641A.

28. L. Sun, A. Pitto-Barry, N. Kirby, T. L. Schiller, A. M. Sanchez, M. A. Dyson, J. Sloan, N. R. Wilson, R. K. O'Reilly and A. P. Dove, *Nat. Commun.*, 2014, **5**, 5746.

29. G. Rizis, T. G. M. van de Ven and A. Eisenberg, *ACS Nano*, 2015, **9**, 3627-3640.

30. I. van der Meulen, E. Gubbels, S. Huijser, R. Sablong, C. E. Koning, A. Heise and R. Duchateau, *Macromolecules*, 2011, **44**, 4301-4305.

31. M. Bouyahyi, M. P. F. Pepels, A. Heise and R. Duchateau, *Macromolecules*, 2012, **45**, 3356-3366.

32. L. van der Mee, F. Helmich, R. de Bruijn, J. A. J. M. Vekemans, A. R. A. Palmans and E. W. Meijer, *Macromolecules*, 2006, **39**, 5021-5027.

33. J. A. Wilson, S. A. Hopkins, P. M. Wright and A. P. Dove, *Polymer Chemistry*, 2014, **5**, 2691-2694.

34. G. Ceccorulli, M. Scandola, A. Kumar, B. Kalra and R. A. Gross, *Biomacromolecules*, 2005, **6**, 902-907.

35. I. van der Meulen, M. de Geus, H. Antheunis, R. Deumens, E. A. J. Joosten, C. E. Koning and A. Heise, *Biomacromolecules*, 2008, **9**, 3404-3410.

36. J. Calabrese, M. A. Cushing and S. D. Ittel, *Inorg. Chem.*, 1988, **27**, 867-870.

37. M. Eriksson, L. Fogelström, K. Hult, E. Malmström, M. Johansson, S. Trey and M. Martinelle, *Biomacromolecules*, 2009, **10**, 3108-3113.

38. T. Vilgis and A. Halperin, *Macromolecules*, 1991, **24**, 2090-2095.

Chapter Three – Co-crystallisation-driven self-assembly of P(VL-*co*-PDL) polymers: controlling self-nucleation

3.1 Abstract

2D nanomaterials are of great interest owing to their large surface area and distinct surface chemistry. The successful development of 2D graphene materials has led to intense study in various applications such as catalysis, solar cells, electronics, and biomedicine. Many other synthetic approaches have been investigated to access 2D nanomaterials, including transition metal dichalcogenides (TMDs), black phosphorus (BP) nanosheets, and 2D metal-organic frameworks (MOFs), however, strategies towards 2D organic materials remain underdeveloped. The advent of crystallization-driven self-assembly has enabled easier access to a wide range of precisely defined 1D and 2D materials, with control across two dimensions. Herein, poly(δ-valerolactone) block copolymers are synthesised and explored for the preparation of cylindrical micelles by CDSA for the first time, providing both biocompatible and biodegradable characteristics. To overcome the homogeneous self-nucleation during the initial study of PVL CDSA, a random copolymer with PDL and VL as the crystalline core was next synthesised. Temperature-controlled CDSA was demonstrated as a result of PVL and PPDL fractions crystallising in different temperature ranges, thereby establishing an approach to manipulate self-nucleation during CDSA. Applying this method, epitaxial growth from PVL seeds with P(PDL-co-VL)$_{45}$-*b*-PDMA$_{270}$ and P(PDL-co-VL)$_{45}$ was achieved, resulting in precisely size-controlled 2D platelet micelles.

3.2 Introduction

3.2.1 Polymer self-nucleation in solution

In general, the crystallisation of a semicrystalline polymer from the melt state involves two steps: primary nucleation and crystal growth. The primary nucleation is considered as the dominant phase of the overall crystallisation. The production of polymer self-nuclei occurs from partial melting experiments or an unerased segmental orientation of the melt.[144] Self-nucleation is a technique employed to enhance the production of self-nuclei during the primary nucleation and was first introduced in 1966.[145] Since then, the specific protocols for self-nucleation such as annealing at different temperatures or for extended periods of time have been shown to have a significant impact on the crystal morphology.[146, 147]

As an alternative to the solidification of semicrystalline polymers, polymer crystallisation in solution has also been studied as a pathway of self-assembly.[127] However, controllable nucleation during polymer crystallisation in solution remains challenging due to the extraordinary effect of experimental conditions such as varying solvents and temperature on the nucleation barrier.[148] The standard protocol for self-assembly of semicrystalline polymers in solution is to first heat the semicrystalline polymer above the melting temperature (T_m), followed by cooling the solution below the crystallisation temperature (T_c), leading to crystallisation-driven self-assembly (CDSA).[149] During this process, random self-nucleation occurs owing to the lack of controlled polymer crystallisation during CDSA, resulting in micelles without defined sizes.

3.2.2 'Living' CDSA

To achieve length-controlled micelles, a CDSA 'seeded growth' technique has been reported.[105] During this approach, fragmented micelles are generated by sonication of pre-existing cylindrical micelles, giving the 'seeds'. The exposed crystalline surfaces of the seeds then act as nuclei for further epitaxy crystallisation, where any random self-nucleation during polymer crystallisation in solution is bypassed.[100] This overall process allows for the preparation of monodisperse micelles and is defined as 'living' CDSA. The method has since been extended into the preparation of precisely size-controlled 2D micelles, by increasing the ratio of crystalline polymer in the added unimer solution.[82, 83]

To date, poly(ferrocenyldimethylsilane) (PFS) block copolymers have received the most extensive studies for the preparation of various size and dimension-controlled nanostructures.[150-153] Meanwhile, fewer reports describing living CDSA of biodegradable crystalline polymers such as polylactide (PLA)[97, 106], polycaprolactone (PCL)[95] and polycarbonate[98] have mostly been limited to the formation of cylindrical and platelet micelles (**Figure 3.1**). Crystalline polymers such as polyethylene (PE)[90] and poly(3-hexylthiophene) (P3HT)[154] have also been studied for 'living' CDSA as a result of their degradability and optical applicability respectively. However, there is still a substantial need for extending the scope of 'living' CDSA with other organic crystalline polymers with varying applications.

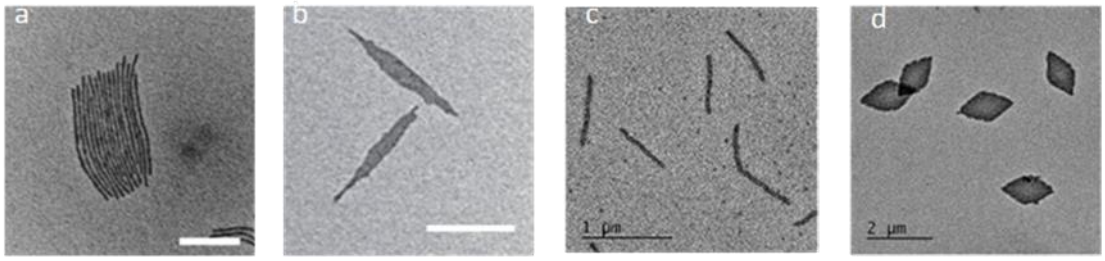

Figure 3.1 Examples of sized controlled 1D and 2D micelles prepared by 'living' CDSA of (a,b) PFS polymers[83, 105] and (c,d) PLLA polymers[97, 106], scale bar 500nm.

3.2.3 Poly(δ-valerolactone) and its copolymers

Poly(δ-valerolactone) (PVL) is a biocompatible and biodegradable material, and in recent years synthetic methods for its preparation in a controlled manner using metal-free catalysts have been rapidly developed. [155-157] On account of its comparable alkyl chain length in the polymer backbone, PVL exhibits a similar hydrophobicity and crystallinity to poly(ε-caprolactone) (PCL) and polylactide (PLA).[158, 159] Hence, the thermal properties of PVL have not only been studied as the homopolymer, but also as copolymers with other small cyclic esters.[160] Jorge et al. studied the crystallisation and melting behaviour of poly(ε-caprolactone-*co*-δ-valerolactone) as an approach to reduce the crystallinity of PCL. The copolymers remained highly crystalline over a broad composition range of ε-caprolactone-*co*-δ-valerolactone. [161] This is a rare report of a co-crystallisation system between ε-caprolactone and δ-valerolactone which inspires similar studies in CDSA. James et al. reported a successful synthetic method for the preparation of random poly(pentedecalactone-co-δ-valerolactone) with tunable thermal and degradation properties. [162] Although the co-crystallisation of pentadecalactone and δ-valerolactone was not proven. Given the biocompatibility and biodegradability of PVL, its application in areas such as drug carriers has been investigated using as hydrogel blend. [163]

Nevertheless, a fundamental exploration of PVL self-assembly and the resultant properties of the micelles remain underexplored.

3.3 Results and Discussion

Due to the extensive reports of CDSA of PCL copolymers, I was interested to next explore poly(δ-valerolactone) (PVL) considering its crystallinity, biodegradability, biocompatibility, and overall similarity to poly(ε-caprolactone).[95] In order to be comparable with previous PCL CDSA studies, a PVL DP of 50 was targeted. Poly(*N,N*-dimethylacrylamide) (PDMA) was selected as the corona block, as it was studied previously in Chapter 2 and in the literature.[95]

3.3.1 Synthesis of PVL_{50}-*b*-$PDMA_{194}$

PVL block copolymers were synthesised by ring-opening polymerisation (ROP) of δ-valerolactone using a dual-headed initiator and chain transfer agent, followed by reversible addition-fragmentation chain transfer (RAFT) polymerisation of DMA (**Scheme 3.1**, **Table 3.1**).

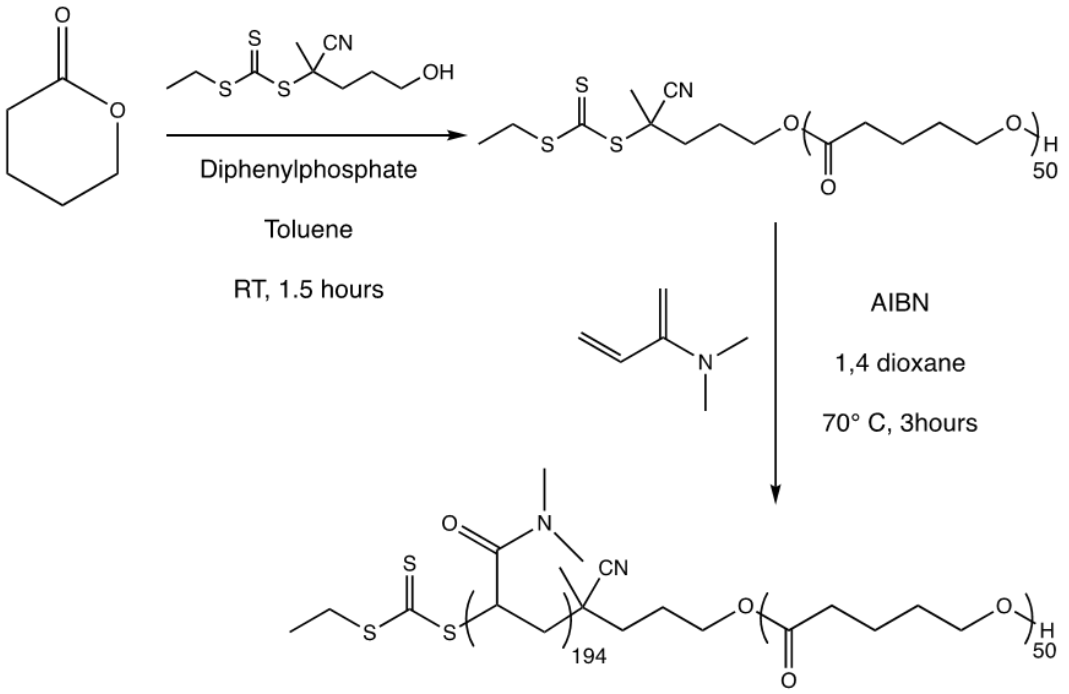

Scheme 3.1 Synthesis route of PVL_{50}-*b*-$PDMA_{194}$ block copolymer.

Table 3.1 Characterisation of PVL polymers.

Polymer	$M_{n,NMR}$ (Kg mol^{-1})	$M_{n,SEC}$ (Kg mol^{-1})	$Đ_M$
PVL_{50}	5.3	9.3	1.06
PVL_{50}-*b*-$PDMA_{194}$	24.5	28.7	1.10

The ROP of δ-valerolactone was performed in a N_2 filled glovebox. The reaction was catalysed by the commercially available organic catalyst diphenyl phosphate, following a previously reported protocol.[156] The conversion of δ-valerolactone reached 70% after 90 minutes, as determined by ^{1}H NMR spectroscopy monitoring and examing the changing ratios of the monomer C*H*$_2$OC=O resonance (δ =4.35) and the polymer C*H*$_2$OC=O resonance (δ =4.05). After purification by precipitation into n-hexane, the final

product was obtained after centrifugation. The final DP (50) of PVL was confirmed by end group analysis in ^{1}H NMR spectroscopy, by integrating the polymer C*H*$_2$OC=O resonances of (δ = 4.05) and the chain transfer reagent SC*H*$_2$CCN(CH$_3$) resonance (δ =3.69). (**Figure 3.2**) Size exclusion chromatography (SEC) analysis revealed a M_n of 9.3 kDa, a relatively low dispersity ($Đ_M$ = 1.06) and good overlap of the refractive index (RI) and ultraviolet (UV) (λ = 309 nm, corresponding to the π-π* electronic transition of the thiocarbonyl moiety) peak in the SEC traces, which signifies the retention of the RAFT end group (**Figure 3.3**).

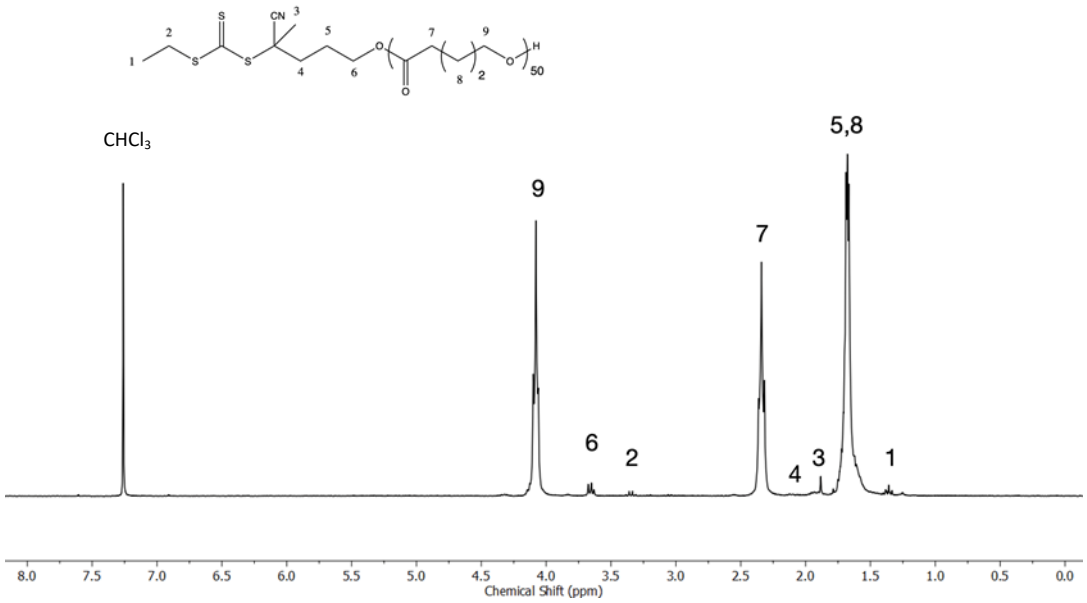

Figure 3.2 ^{1}H NMR spectrum ($CDCl_3$, 400MHz) of PVL_{50}.

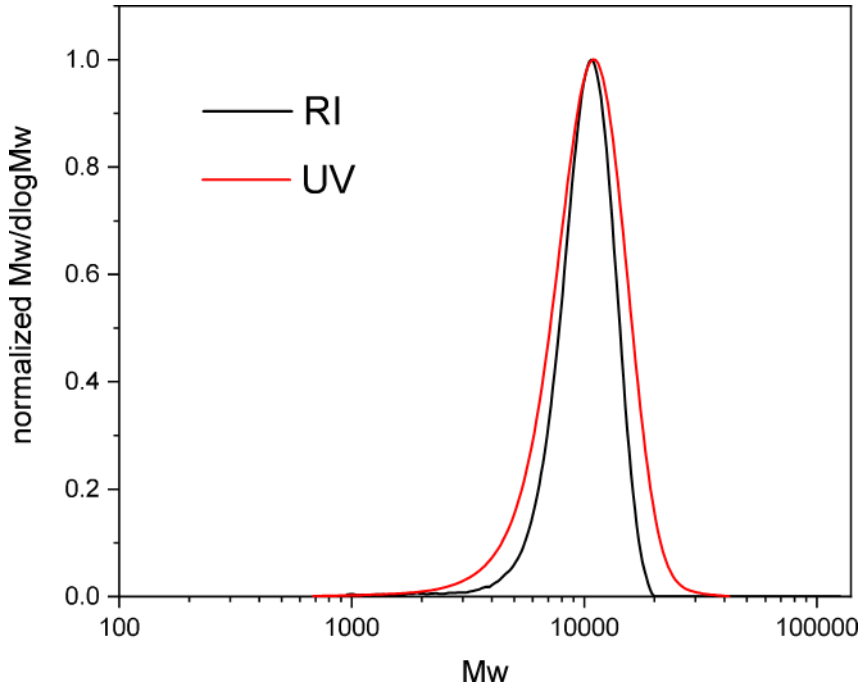

Figure 3.3 Overlaid RI and UV (λ = 309 nm) SEC chromatograms of PVL_{50} using $CHCl_3$ with 0.1% TFE as an eluent with polystyrene (PS) standards.

Subsequently, the PVL_{50} homopolymer was used as a macromolecular chain transfer agent to mediate the polymerisation of DMA by RAFT. The polymerisation was carried out in 1,4-dioxane at 70 °C to ensure full solubilisation of PVL and using 2,2-azobis(2-methylpropionitrile) (AIBN) as the radical initiator. After two hours, the polymer was purified by precipitation into hexane followed by centrifugation. A chain extension of DP 194 of the DMA hydrophilic block was confirmed by ^{1}H NMR spectroscopy, whereby the peak at δ = 2.90 ppm corresponding to the 6 protons of the dimethyl groups was compared to the α-methylene resonance of PVL (δ = 4.05 ppm) (**Figure 3.4**). SEC analysis in $CHCl_3$ was performed to characterise the resultant polymer, where a clear molecular weight shift compared to the PVL homopolymer could be observed. The retention of the RAFT end group was confirmed by the overlapping of the RI and UV traces (λ = 309 nm) (**Figure 3.5**).

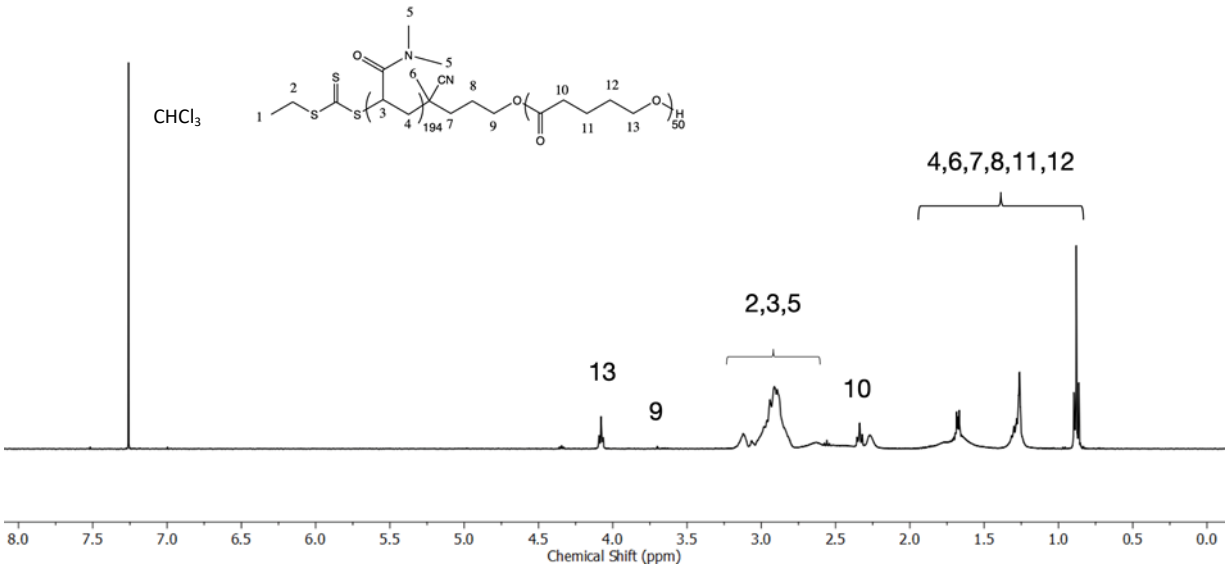

Figure 3.4 ^{1}H NMR spectrum ($CDCl_3$, 400MHz) of PVL_{50}-*b*-$PDMA_{194}$.

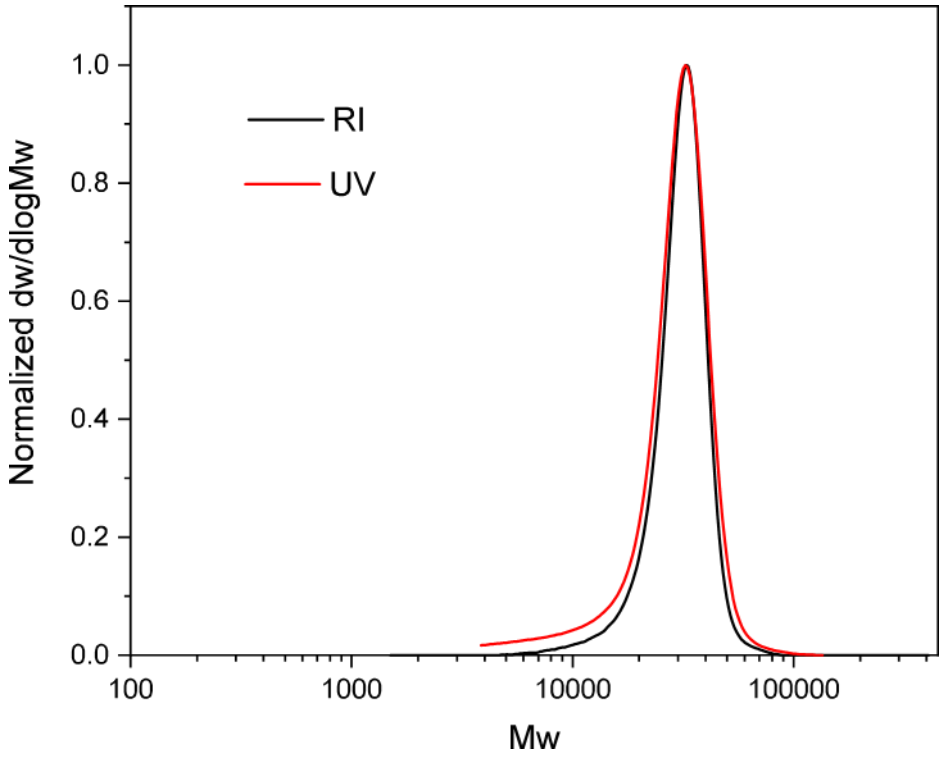

Figure 3.5 Overlaid RI and UV (λ = 309 nm) SEC chromatograms of PVL_{50}-*b*-$PDMA_{194}$ using $CHCl_3$ with 0.1% TFE as an eluent with polystyrene (PS) standards.

3.3.2 Crystallisation-driven self-assembly of PVL_{50}-*b*-$PDMA_{194}$

To date, the crystallisation of PVL polymers has not been studied in solution. Differential scanning calorimetry (DSC) analysis of PVL_{50} was therefore carried out to confirm a melting temperature, T_m, of *ca*. 57 °C and a crystallisation temperature, T_c of *ca*. 31 °C, in agreement with previous reports (**Figure 3.6**).[164] It should be emphasised, based on understanding from Chapter 2, that self-nucleation study of the PVL_{50}-*b*-$PDMA_{194}$ in solvents should be monitored by nano differential scanning calorimetry (NanoDSC) experiments. However, DSC values still provide a temperature window for choosing solvents with boiling temperatures exceeding the peak melting temperature of the PVL polymer.

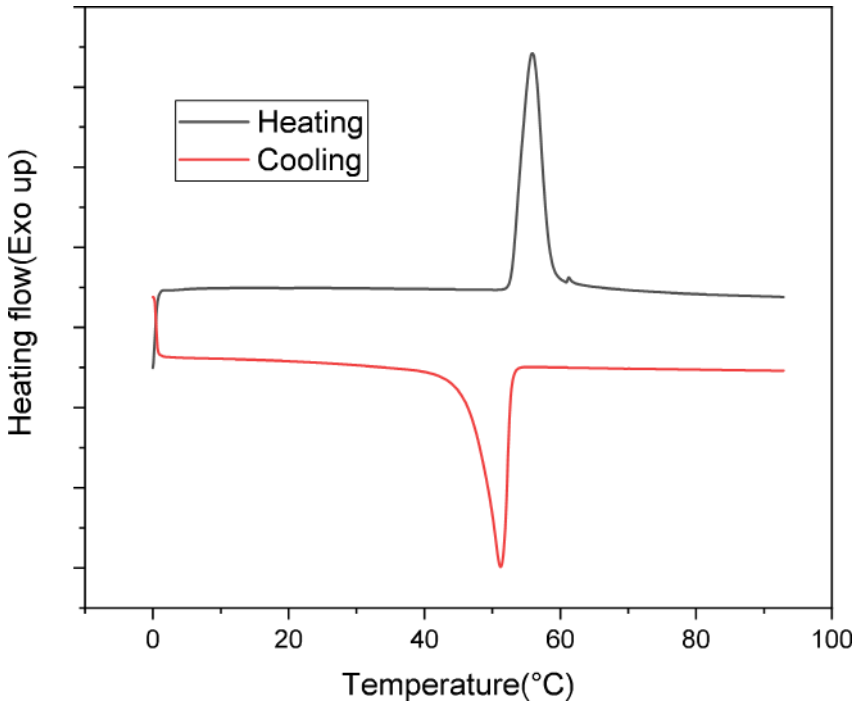

Figure 3.6 Differential scanning calorimetry thermograms of PVL_{50} second heating and cooling curve at a rate of 2 °C per minute.

Four solvents (ethanol, n-propanol, n-butanol and n-pentanol) were subsequently selected for the NanoDSC experiments, to act as selective solvents for the corona block while also having a boiling temperature exceeding the T_m (57 °C) of PVL as measured by DSC. Non-isothermal experiments in nanoDSC were performed as follows: PVL_{50}-*b*-$PDMA_{194}$ was heated in each solvent to 70 °C, before cooling down to 0 °C at a rate of 1 °C per minute. The melting and crystallisation temperatures from the second cycle were compared. (**Table 3.2**) Both the melting and crystallisation temperatures were decreased due to the solvent plasticising effect as discussed in Chapter 2. It is also notable that compared to the poly(pentadecalactone) (PPDL) polymers studied in Chapter 2, PVL_{50}-*b*-$PDMA_{194}$ doesn't have a wide crystallisation temperature window, which is due to the smaller number of carbons in each repeat unit. As the solvent plasticising effect increases, both crystallisation and melting peaks of PVL_{50}-*b*-$PDMA_{194}$ disappear as exemplified in cyclopentanol from NanoDSC. (**Figure 3.7**)

Table 3.2 Melting and crystallisation temperatures of PVL_{50}-*b*-$PDMA_{194}$ in different solvents measured from NanoDSC (second circle)

	ethanol	**n-propanol**	**n-butanol**	**cyclopentanol**
$T_{Melting}$(°C)	42	41	38	-
$T_{Crystallisation}$ (°C)	28	28	27	-
Solvent boiling point(°C)	78	97	118	138

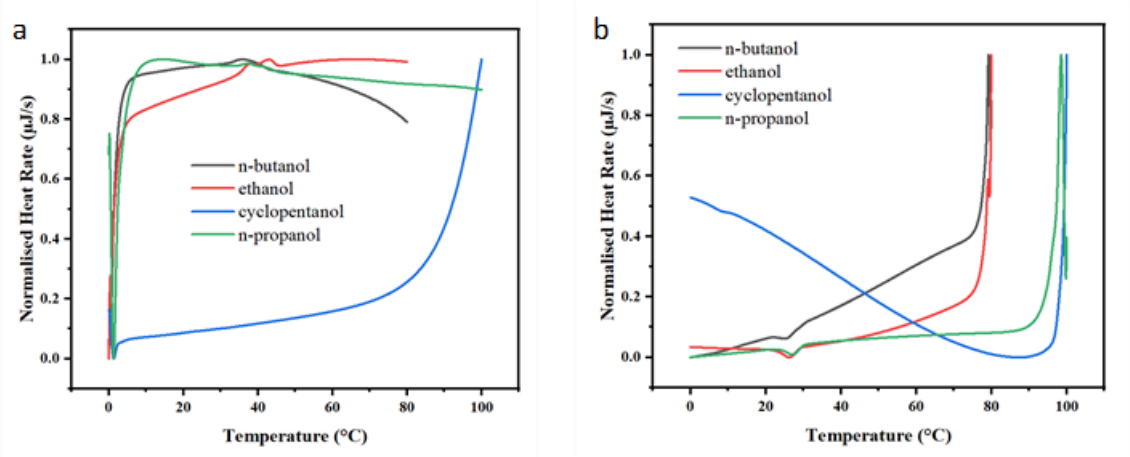

Figure 3.7 Nano Differential scanning calorimetry thermograms of PVL_{50}-b-$PDMA_{194}$ second heating(a) and cooling(b) curve at a rate of 1°C per minute.

Based on the crystallisation and melting temperatures of PVL_{50}-*b*-$PDMA_{194}$ obtained from the NanoDSC experiments, crystallisation-driven self-assembly of PVL_{50}-*b*-$PDMA_{194}$ was then explored in ethanol, n-propanol and n-butanol. A solution of 5 mg mL^{-1} PVL_{50}-*b*-$PDMA_{194}$ was heated to 70 °C in each solvent and annealed for three hours to allow a complete melting of the polymer in solution. The solutions were then slowly cooled down to room temperature to initiate the first phase of nucleation of PVL_{50}-*b*-$PDMA_{194}$. All solutions were then aged for three days to allow full crystallisation of the PVL_{50}-*b*-$PDMA_{194}$. Each sample was then diluted into a 0.5 mg mL^{-1} solution before being dropped on a TEM grid and stained before TEM analysis. Cylindrical structures were observed in each sample, although the cylinders formed in ethanol and n-propanol had rough edges, while n-butanol gave well-defined cylinders. (**Figure 3.8**)

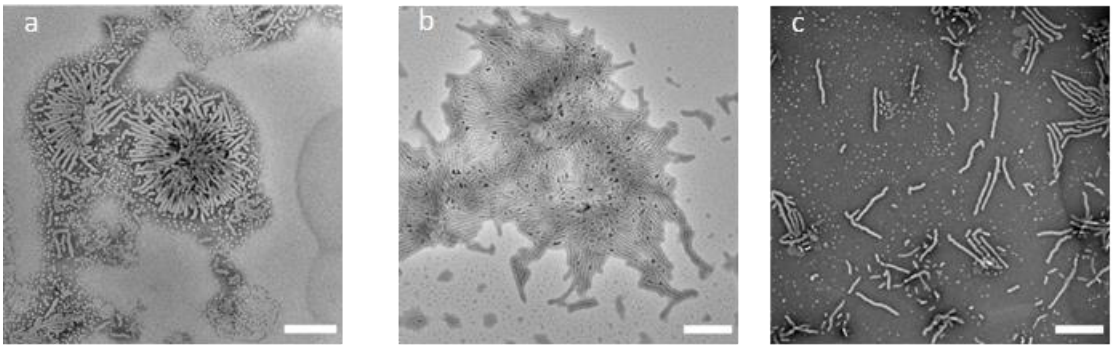

Figure 3.8 TEM micrographs of cylindrical micelles prepared using PVL_{50}-*b*-$PDMA_{194}$ by self-nucleation in ethanol (a), n-propanol (b), and n-butanol (c) heating at 70 °C for 3 hours and subsequently cooling down to room temperature. All samples were aged for 3 days, stained with 1 wt. % uranyl acetate in water. Scale bar = 500 nm.

Despite the similar crystallinity of PVL_{50}-*b*-$PDMA_{194}$ and PCL_{50}-*b*-$PDMA_{180}$, while well-defined cylinders of PCL_{50}-*b*-$PDMA_{180}$ could be obtained in ethanol,[95] the same did not occur for the PVL copolymer. This was attributed to the different polarities of PVL and PCL as the core-forming block, considering an overall 50 less repeating methylene moieties in PVL. As a consequence, the greater plasticising effect of ethanol on PVL_{50}-*b*-$PDMA_{194}$ than that on PCL_{50}-*b*-$PDMA_{180}$ has reduced its crystallinity, resulting in some spherical micelles with amorphous PVL core. Comparable CDSA result of PVL_{50}-*b*-$PDMA_{194}$ to PCL_{50}-*b*-$PDMA_{180}$ has shown in the less polar solvent n-butanol with a reduced plasticising effect.

To further achieve precisely size-controlled cylinders, a 'living' CDSA of PVL_{50}-*b*-$PDMA_{194}$ was studied. The procedure included two steps; first, the sonication of PVL_{50}-*b*-$PDMA_{194}$ formed from the self-nucleation process, followed by crystallisation of additionally added unimer onto the fragmental cylinders (**Scheme 3.2**).

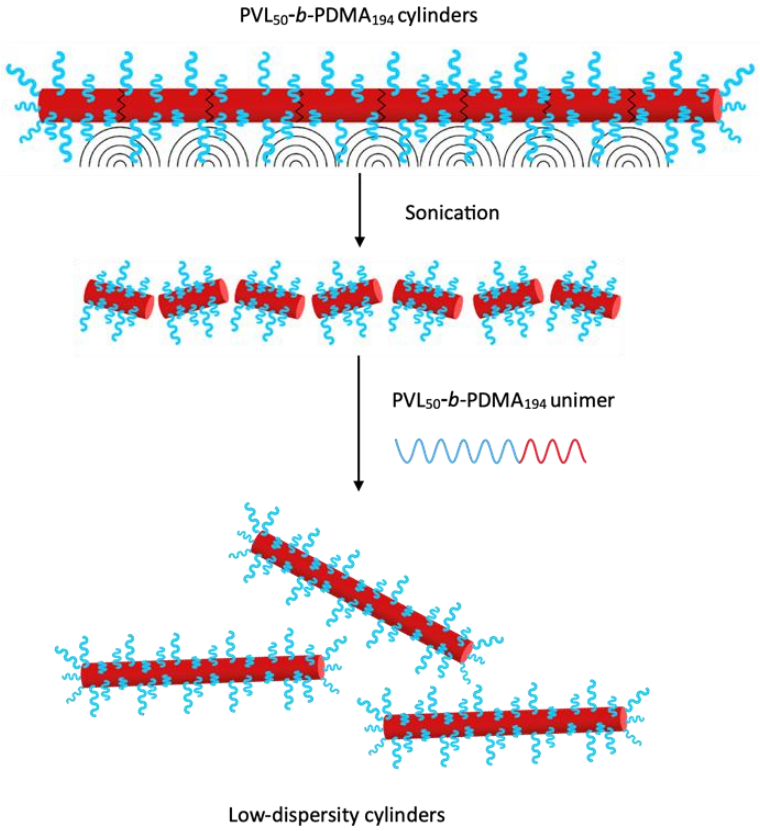

Scheme 3.2 Schematic steps of 'living' CDSA study of cylinders obtained by PVL_{50}-*b*-$PDMA_{194}$ self-nucleation in n-butanol.

The solution containing PVL_{50}-*b*-$PDMA_{194}$ cylinders was initially sonicated with a sonicator probe at 0 °C in order to minimise the melting of the polymer during the process. The solution was sonicated continuously for 3 minutes in total, with breaks for 20 minutes every 20 seconds to allow the solution to cool down. A small aliquot was removed every minute for TEM analysis to monitor the transition of cylinder length. Results from TEM images indicated a controlled fragmentation process of the micelles, without any recombination from the exposed crystallisation surface of the fragment micelles. (**Figure 3.9**) The distribution of the fragmented micelles was calculated by the number-average lengths, L_n, and weight-average lengths, L_w. Both lengths were calculated by counting 1,000 features from TEM images obtained from different areas

on the TEM grid. The values of each sonication period are summarised in **Table 3.3.** Notably, cylindrical micelles which experienced a sonication time longer than two minutes no longer appeared as cylindrical structures and were therefore not suitable for further study. The fractionated micelles from two minutes sonication were thus considered as 'seeds' in this study, having the lowest resultant length distribution during the sonication experiments.

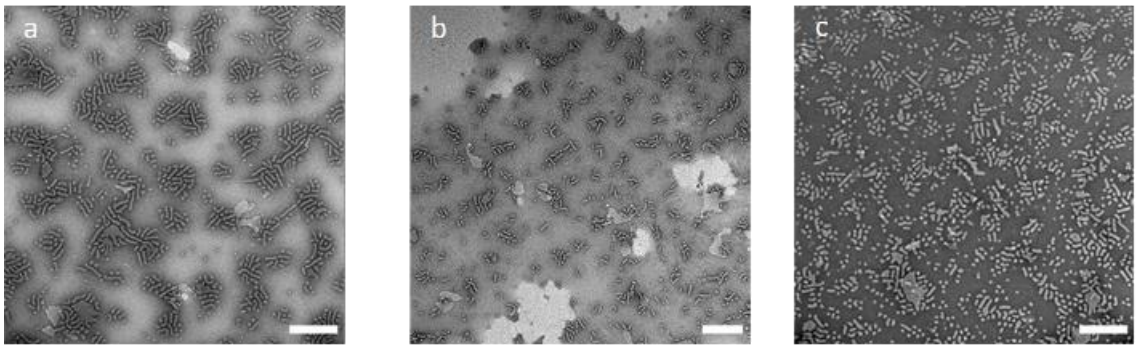

Figure 3.9 TEM micrographs of 'seeds' micelles prepared by sonicating PVL_{50}-*b*-$PDMA_{194}$ cylinder micelle in n-butanol 0 °C for using a sonic probe (a) 1, (b) 2 and (c) 3 mins. All samples were stained with 1 wt. % uranyl acetate in water. Scale bar = 500 nm.

Table 3.3 Distribution determined by TEM for PVL_{50}-*b*-$PDMA_{194}$ 'seeds' micelles.

Sonication time (seconds)	20	60	80	120
L_n(nm)	656	314	221	122
L_w(nm)	432	240	173	98
L_n /L_w	1.52	1.31	1.28	1.24

3.3.3 Growth experiments of PVL_{50}-*b*-$PDMA_{194}$ cylindrical micelles

In order to prepare cylindrical micelles with controlled length, an epitaxial growth process was studied with the seed micelles prepared above. By introducing unimer solution into the crystalline seed micelles solution, further crystallization could occur on the seed micelles' initiation sites to form controlled length cylindrical micelles instead of random self-nucleation which leads to polydisperse cylinders.

PVL_{50}-*b*-$PDMA_{194}$ was dissolved in a miscible solvent (THF) at different concentrations to serve as the unimer solution. This meant that while keeping the same volume of THF (10 µL), the ratio of seeds to unimer could be adjusted by using the different concentration solutions in order to target different length cylinders. However, after the addition of the unimer solution, there is a chance that homogeneous self-nucleation can occur because of the solvent change in quality. This will result in micelles with a broad dispersity due to the two competing kinetics of crystallization: the unimer crystallising onto the seed micelles, and random self-nucleation of the unimers. The propensity for self-nucleation was tested by forming a 30 mg mL^{-1} unimer solution in n-butanol, where seed micelles

were obtained. The solution was then aged for three days before the examination by TEM (**Figure 3.10a**). Cylindrical micelles from the random self-nucleation were observed indicating an uncontrollable epitaxial growth process. To verify this, 10 µL of the 30 mg mL^{-1} unimer was added into 1 mL of a 0.01mg mL^{-1} seeds solution in n-butanol. The solution was then aged for three days before characterisation by TEM (**Figure 3.10b, c**). Two different distributions of cylindrical micelles were observed deriving from the two competing crystallisation processes. One is formed by seeded growth and the other resulted from self-nucleation of PVL_{50}-*b*-$PDMA_{194}$ unimers. For most epitaxial growth, the solvent is the only adjustable parameter, although the self-nucleation is also governed by the properties of the crystalline core. As the PVL_{50}-*b*-$PDMA_{194}$ cylindrical micelles were established in n-butanol, it was considered that changing the epitaxial growth solvent was unlikely to have the desired effect in this case. Instead, an approach of introducing a PPDL component into the polymer to adjust the crystallinity of the core-forming block was investigated to optimise the self-nucleation of PVL in solution.

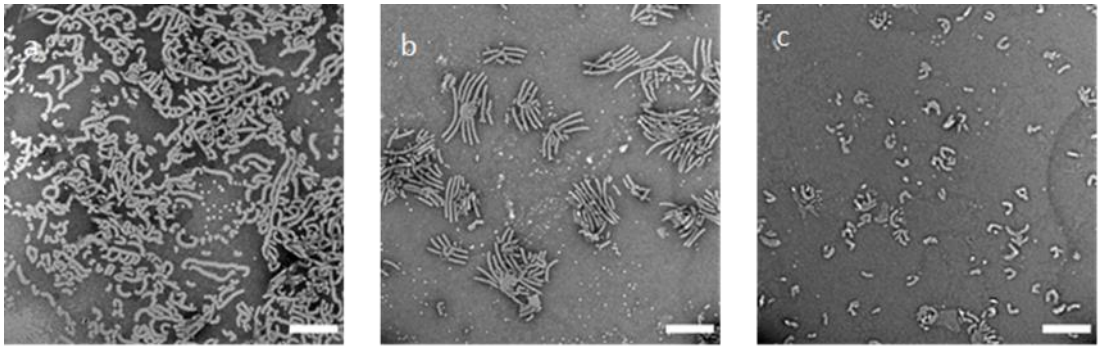

Figure 3.10 TEM micrographs of cylindrical micelles prepared by adding 10µL 30mg mL^{-1} PVL_{50}-*b*-$PDMA_{194}$ unimer into (a) n-butanol, (b) and (c) 1mL 0.01mg mL^{-1} seeds solution after three days ageing. All samples were stained with 1 wt. % uranyl acetate in water. Scale bar = 1 µm.

3.3.4 Random copolymerisation of pentadecalactone and valerolactone and chain extension reactions

In order to optimise the self-nucleation of PVL_n-*b*-$PDMA_m$ block copolymers in solvent, PDL was copolymerised with δVL as the core-forming block, and the properties of the copolymers during crystallisation-driven self-assembly were studied. The ROP of PDL and δVL was catalysed by $Mg(BHT)_2(THF)_2$ and initiated by a dual-head initiator and chain transfer agent (**Scheme 3.3**). The advantage of the $Mg(BHT)_2(THF)_2$ catalysed ROP of PDL as described in Chapter 2 is that it is an 'immortal' polymerization and can occur in ambient conditions.[140] However, all reactions were performed in dry and inert environments to be comparable and consistent with literature.[140]

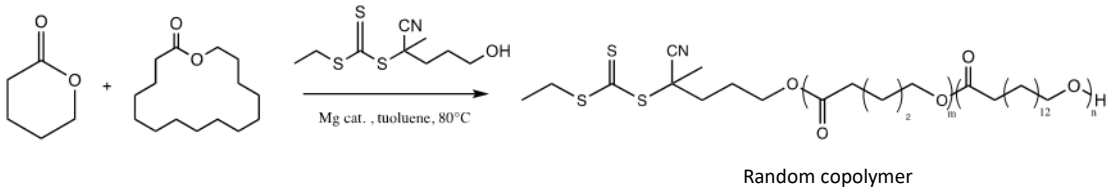

Scheme 3.3 Copolymerization of PDL and δVL catalyzed by $Mg(BHT)_2(THF)_2$

An equimolar mixture of PDL and δVL was heated to 80 °C in toluene with an overall concentration of 2 M, targeting a DP of 50 to be comparable with the PVL_{50}-*b*-$PDMA_{194}$ for further self-nucleation studies. The overall conversion of monomer was monitored by ^{1}H NMR spectroscopy periodically. The conversion of δVL reached 40% after 20 minutes, as confirmed by the changing ratios of the monomer $CH_2OC{=}O$ resonance (δ = 4.35ppm) and the polymer $CH_2OC{=}O$ resonance (δ = 4.05ppm). It should be noted here that due to the overlapping methylene resonances of both poly(pentadecalactone) and poly(δ-valerolactone), the calculation of individual monomer conversion was not possible from ^{1}H NMR spectroscopy. However, from the consistent integration of the α-

methylene resonance of PDL between 0 minutes and 20 minutes, it could be concluded at this point that the polymer chain was pure PVL. It was observed that the conversion increased by 16% in the next 24 hours, indicating a slow incorporation of PDL monomer. (**Figure 3.11**) This is probably due to the transesterification of PVL being energetically preferable over the ROP of PDL and thus severely slowing the incorporation of PDL monomer. The copolymers were also examined by SEC to confirm their number-average molecular weight (M_n) growth. (**Table 3.4**)

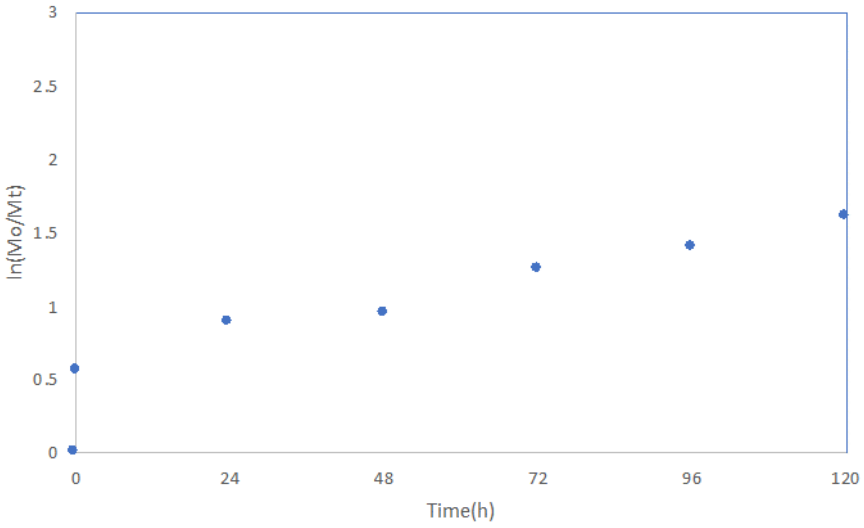

Figure 3.11 Kinetic plot for the copolymerization of pentadecalactone and valerolactone at 80 °C in toluene with $[PDL]_0$:$[VL]_0$:$[PDL]_0$:$[PDL]_0$ = 25:25:1:1, total monomer concentration= 2M.

Table 3.4 Copolymerisation of PDL and δVL at 1:1 mol% targeting DP50.

Time(h)	Conversion[a] (%)	M_n [b] (SEC) (kDa)	M_w [b] (SEC) (kDa)	$Đ_M$	M_n [c] (NMR) (kDa)
0.5	45	4.8	6.3	1.31	2.5
24	60	6.5	9.2	1.42	3.7
48	66	7.8	11.7	1.51	4.6
72	71	8.4	13.6	1.62	5.3
120	80	9.5	17.1	1.80	7.6

[a]Total monomer conversion determined by ^{1}H NMR spectroscopy. [b]Determined by SEC in $CHCl_3$ against poly(styrene) standards. [c]Determined by end-group analysis by ^{1}H NMR spectroscopy.

The dispersity of the copolymer was observed to increase as the incorporation of PDL increased. This is owing to both the side transesterification reactions and the unavoidable formation of cyclic species during the PDL polymerisation.[162] We attributed the low molecular weight tail from the SEC trace to these species (**Figure 3.12**). In order to determine that the polymer chain has a statistical distribution, it is important to calculate the integration of the carbonyl region of PDL and VL using quantitative ^{13}C NMR spectroscopy. Three different diad resonances could be identified corresponding to δVL*-PDL, PDL*-δVL and PDL*-PDL (δ = 173.5, 174.0 and 174.1 ppm, respectively). There are two main reactions in this polymerization in regards to PDL: 1) PDL incorporation into the chain end and 2) transesterification into the main chain after incorporation into the chain end. The carbonyl diad resonances δVL*-PDL and PDL*-δVL increased more

rapidly compared to PDL*-PDL, which indicated that the transesterification process was occurring faster than PDL incorporation onto the chain end. As the PDL polymerised, the increasing transesterification lead to a higher proportion of two adjacent PDL repeat units (PDL*-PDL) in the main copolymer chain. During a copolymerisation, the possibility of A*-B diad resonance of two monomers (A, B) is equivalent to $P(A^*\text{-}B) = f_A \times f_B$, where f_A and f_B are the mole fractions of monomers A and B respectively. (**Table 3.5**)[165] The copolymer can only be classed as completely statistical if the observed A*-B diad resonance is equal to P(A*-B). As such, the resultant copolymers have random architecture through transesterification side reactions.

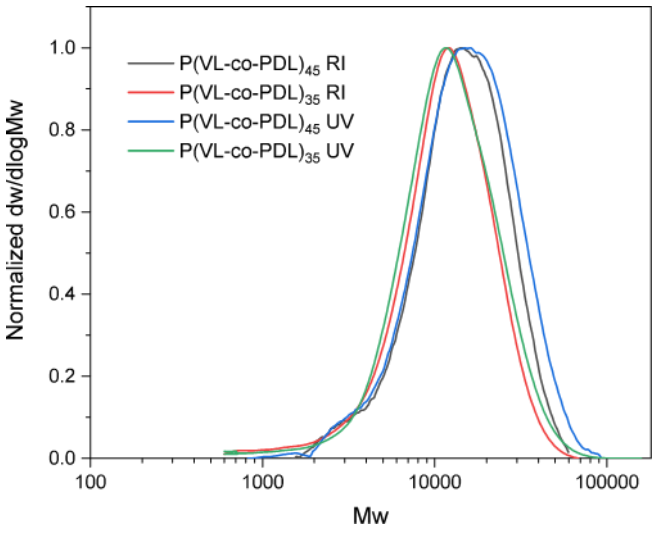

Figure 3.12 Overlaid RI and UV (λ = 309 nm) SEC chromatograms of P(PDL-*co*-VL)$_{35}$ (PDL:VL=3:5) and P(PDL-*co*-VL)$_{45}$ (PDL:VL=4:5) using $CHCl_3$ with 0.1% TFE as an eluent with polystyrene (PS) standards.

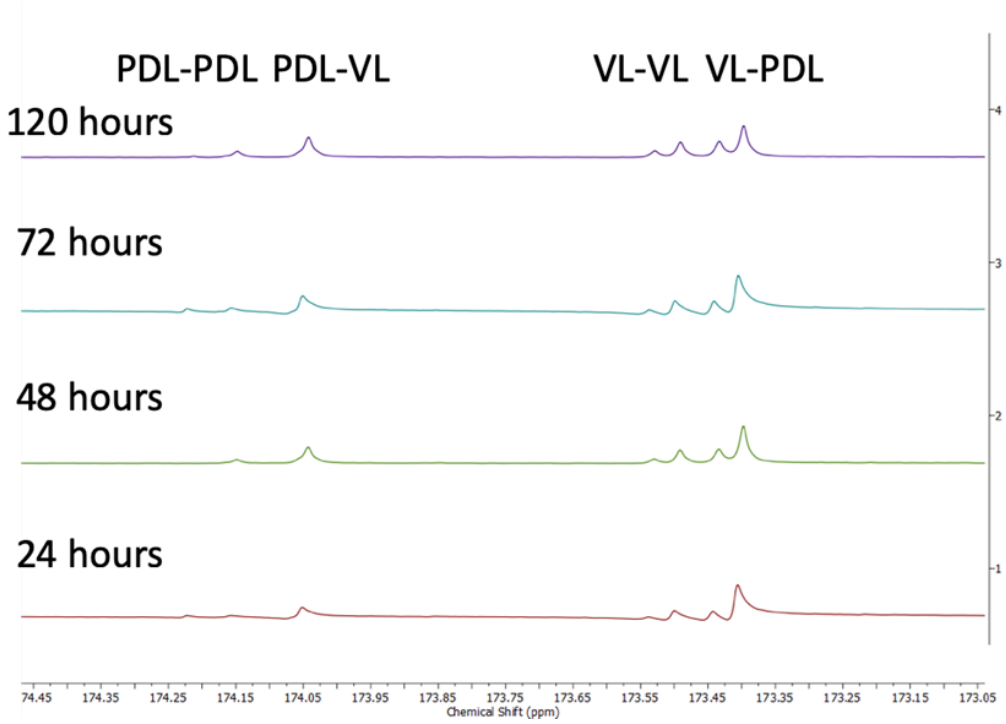

Figure 3.13 Quantitative ^{13}C NMR spectra of the carbonyl region during copolymerisation of ω-pentadecalactone with δ-valerolactone (125 MHz, $CDCl_3$, 298 K).

Table 3.5 Analysis of PDL and δVL copolymerisation at 1:1mol% targeting DP50 using ^{1}H NMR spectroscopy and quantitative ^{13}C NMR spectroscopy.

		Diads			
Time(h)	Conversion(%)	PDL*-PDL	PDL*-VL	VL*-VL	VL*-PDL
0.5	43	0.00	0.00	(0.04)	(0.96)
		(0.00)	(0.00)	(0.00)	(1.00)
24	60	0.09	0.12	0.24	0.55
		(0.08)	(0.20)	(0.20)	(0.52)
48	66	0.10	0.16	0.20	0.54
		(0.11)	(0.22)	(0.22)	(0.45)
72	71	0.11	0.20	0.21	0.48
		(0.14)	(0.23)	(0.23)	(0.40)
120	80	0.14	0.23	0.24	0.39
		(0.20)	(0.25)	(0.25)	(0.30)

[a]Total monomer conversion determined by ^{1}H NMR spectroscopy. [b]Determined by quantitative ^{13}C NMR spectroscopy, with * defining the carbonyl analysed and numbers in parentheses are theoretical values based on composition by the equation P(A*-B) = fa × fb.

The P(PDL-*co*-VL) random copolymer (DP=45) was then studied as a macromolecular chain transfer agent to mediate the RAFT polymerisation of DMA for investigation of

CDSA in aqueous conditions. Considering the different solubilities of PPDL and PVL, the polymerisation was first carried out in toluene at 80 °C, which are the same reaction conditions studied in Chapter 2 for the PPDL chain extension reaction. 2,2-Azobis(2-methylpropionitrile) (AIBN) was used as a radical initiator, and after two hours, the polymer was purified by precipitation into hexane followed by centrifugation. A chain extension of DP 270 of the DMA hydrophilic block was confirmed by ^{1}H NMR spectroscopy, through analysis of the peak at δ = 2.90 ppm corresponding to the 6 protons of the dimethyl groups, and the combined α-methylene resonances of the polylactones (δ = 4.05 ppm) (**Figure 3.14**). SEC analysis in $CHCl_3$ was also used to characterise the resultant polymer, which showed a clear low molecular weight peak overlapping with the P(PDL-co-VL) random copolymer in the UV trace (λ = 309 nm). This clearly indicated that a fraction of the P(PDL-co-VL) random copolymer had not initiated, likely a consequence of the poor solubility of the copolymer in toluene. (**Figure 3.15**).

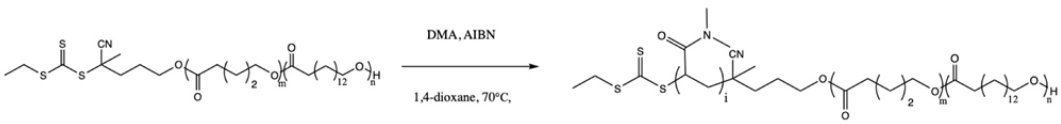

Scheme 3.4 Synthesis route of P(PDL-*co*-VL)$_n$-*b*-PDMA$_m$ block copolymer.

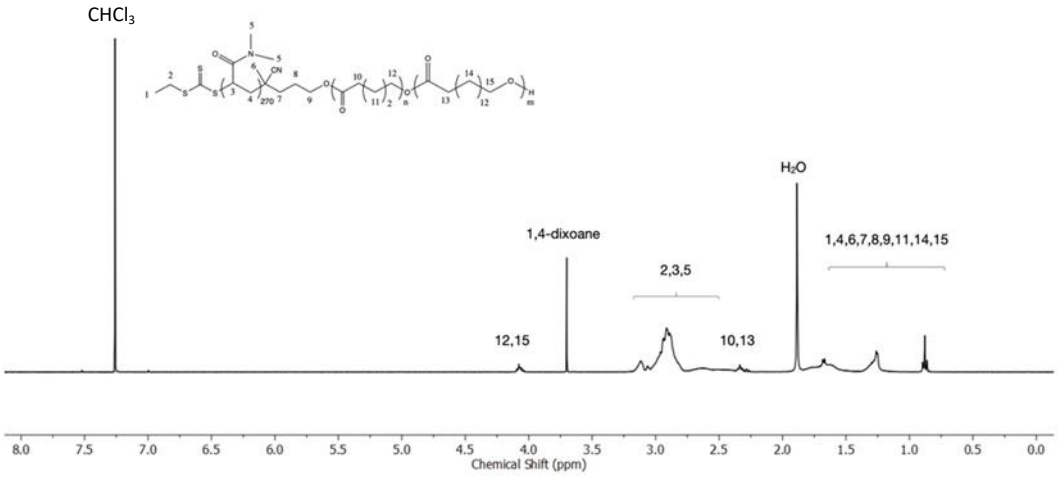

Figure 3.14 ^{1}H NMR spectrum ($CDCl_3$, 400MHz) of P(PDL-*co*-VL)$_{45}$-*b*-PDMA$_{270}$ resulted from toluene.

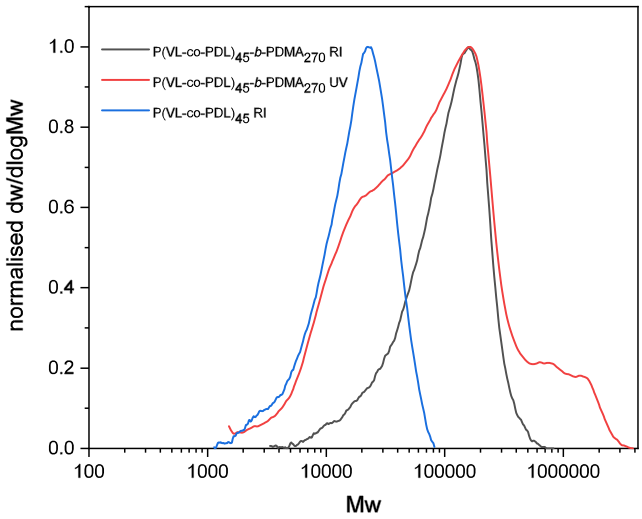

Figure 3.15 Overlaid RI and UV (λ = 309 nm) SEC chromatograms of P(PDL-*co*-VL)$_{45}$ and P(PDL-*co*-VL)$_{45}$-*b*-PDMA$_{270}$ conducted from toluene using $CHCl_3$ with 0.1% TFE as an eluent with polystyrene (PS) standards.

The chain extension reaction of P(PDL-*co*-VL)$_{45}$ was then investigated as per the conditions for PVL$_{50,}$ as discussed in 3.3.1. The P(PDL-*co*-VL)$_{45}$ and DMA were heated in

1,4-dioxane at 70 °C using 2,2-azobis(2-methylpropionitrile) (AIBN) as a radical initiator. After two hours, the polymer was purified by precipitation into hexane followed by centrifugation. A similar molecular weight percentage of the hydrophilic block (79%) was targeted, in order to allow comparison with the reported cylindrical micelles formed by polylactone block copolymers (76%), which corresponded to a DP 270 of DMA.[95] The chain extension of DP 270 of the DMA hydrophilic block was confirmed by ^{1}H NMR spectroscopy, through analysis of the peak at δ = 2.90 ppm corresponds to the 6 protons of the dimethyl groups and the α-methylene resonance of overlay polylactones (δ = 4.05 ppm). SEC analyse in $CHCl_3$ was also used to characterise the resultant polymer. (**Figure 3.16**) A small tailing was observed from the UV trace. However, there was no tailing or shoulder in the molecular weight distribution from the RI trace, suggesting that the initiation of P(PDL-*co*-VL)$_{45}$ was considerably increased compared to the polymerisation in toluene. A clear molecular weight shift compared to the P(PDL-*co*-VL)$_{45}$ copolymers could also be observed.

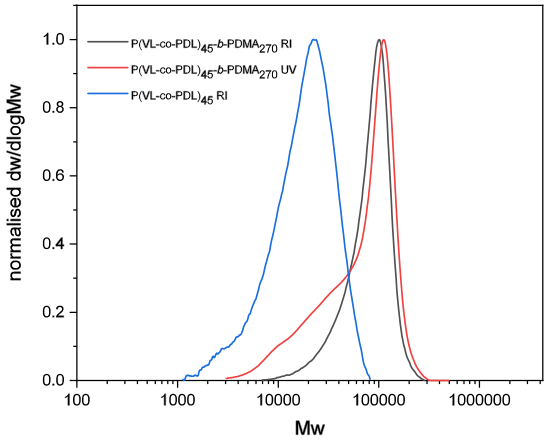

Figure 3.16 Overlaid RI and UV (λ = 309 nm) SEC chromatograms of P(PDL-*co*-VL)$_{45}$ and P(PDL-*co*-VL)$_{45}$-*b*-PDMA$_{270}$ conducted from 1,4-dioxane using $CHCl_3$ with 0.1% TFE as an eluent with polystyrene (PS) standards.

P(PDL-*co*-VL)$_{35}$ was next studied as a macromolecular chain transfer agent to mediate the polymerisation of DMA by RAFT following the same chain extension reaction procedure of P(PDL-*co*-VL)$_{45}$. DP 180 of the DMA hydrophilic block was confirmed by ^{1}H NMR spectroscopy, through analysis of the peak at δ = 2.90 ppm corresponds to the 6 protons of the dimethyl groups and the α-methylene resonance of overlay polylactones (δ = 4.05 ppm) (**Figure 3.17**). SEC analysis in $CHCl_3$ was also used to characterise the resultant polymer. (**Figure 3.18**) The overlapping of the RI and UV (λ = 309 nm) traces confirmed the retention of the RAFT end group, where a narrow distribution and no low molecular weight shoulder was observed. These experiments suggested that controlling the solubility of the copolymer was an important factor for control of the overall distribution, due to a better initiation from the RAFT end group.

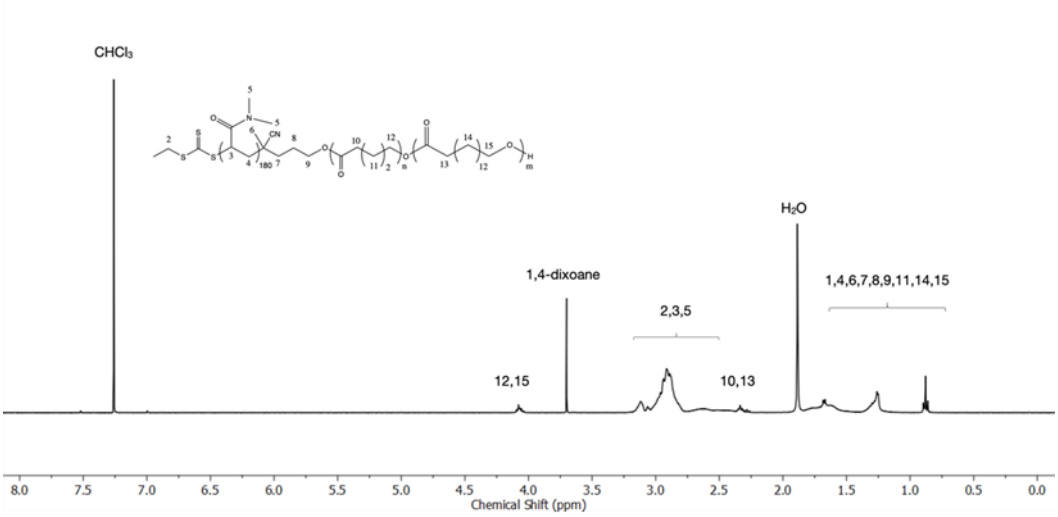

Figure 3.17 ^{1}H NMR spectrum ($CDCl_3$, 400MHz) of P(PDL-*co*-VL)$_{35}$-*b*-PDMA$_{180}$ resulted from 1,4-Dioxane.

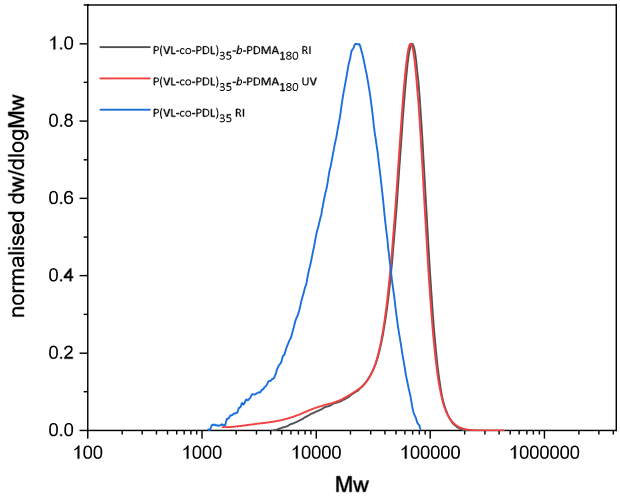

Figure 3.18 Overlaid RI and UV (λ = 309 nm) SEC chromatograms of P(PDL-co-VL)$_{35}$ and P(PDL-co-VL)$_{35}$-b-PDMA$_{180}$ conducted from 1,4-dioxane using $CHCl_3$ with 0.1% TFE as an eluent with polystyrene (PS) standards.

3.3.5 Crystallisation-driven self-assembly of P(PDL-*co*-VL)$_n$-*b*-PDMA$_m$

To explore the temperature window for the CDSA of P(PDL-*co*-VL)$_n$-*b*-PDMA$_m$ polymers, differential scanning calorimetry (DSC) was used to measure the melting and

crystallisation temperatures of P(PDL-*co*-VL)$_{35}$ and P(PDL-*co*-VL)$_{45}$ as per the previously described methodology in Section 3.3.2 (**Figure 3.19**). Both of the copolymers showed drastically lower crystallisation temperatures compared to the PPDL$_{25}$ homopolymers (**Table 3.6**). The observation of the crystallisation peaks during non-isothermal DSC scanning confirmed that the PPDL and PVL segments did not interfere during the crystallisation. This has opened up the possibility of utilising these polymers for further co-crystallisation studies in solution.

Table 3.6 Summary of melting and crystallisation temperatures of PPDL, PVL homopolymers, P(PDL-*co*-VL)$_{35}$ and P(PDL-*co*-VL)$_{45}$ copolymers.

	PVL$_{50}$	**PPDL$_{25}$**	**P(PDL-*co*-VL)$_{35}$**	**P(PDL-*co*-VL)$_{35}$**
***T$_c$*(°C)**	32	75	32	20
***T$_m$*(°C)**	55	92	73	91

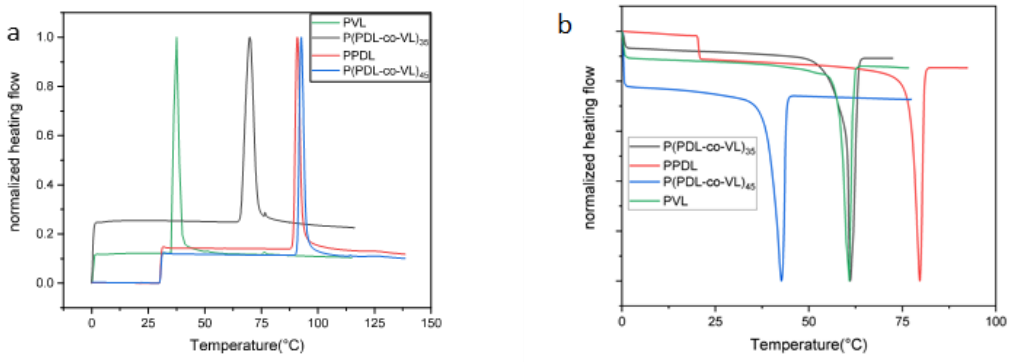

Figure 3.19 Differential scanning calorimetry thermograms of P(PDL-*co*-VL) copolymers overlay with PPDL and PVL homopolymers second (a) heating and (b) cooling curve at rate of 10°C per minute.

To further investigate the thermal properties of the block copolymers in solution, P(PDL-*co*-VL)$_{35}$-*b*-PDMA$_{180}$ and P(PDL-*co*-VL)$_{45}$-*b*-PDMA$_{270}$ were analysed by Nano differential scanning calorimetry (Nano DSC). The NanoDSC analysis was performed in n-butanol as a solvent, as the CDSA of both PPDL and PVL block copolymers had previously been conducted in this solvent, as noted in Chapter 2 and Section 3.3.3. P(PDL-*co*-VL)$_{35}$-*b*-PDMA$_{180}$ and P(PDL-*co*-VL)$_{45}$-*b*-PDMA$_{270}$ were heated in n-butanol to 70 °C before cooling down to 0 °C at a rate of 1 °C per minute. The melting and crystallisation temperatures measured from the second heating and cooling cycles were then compared with those from PPDL$_{25}$-*b*-PDMA$_{110}$ and PVL$_{50}$-*b*-PDMA$_{194}$ (**Table 3.7**). Notably, two distinct crystallisation peaks were observed at 35 °C and 8 °C from the second cooling curve of P(PDL-*co*-VL)$_{45}$-*b*-PDMA$_{270}$ representing the crystallisation of PPDL and PVL fractions, respectively (**Figure 3.20a**). Comparably, the second cooling curve of P(PDL-*co*-VL)$_{35}$-*b*-PDMA$_{180}$ showed two crystallisation peaks at a temperature of 28 °C and 0 °C, corresponding to the crystallisation of PPDL and PVL fractions respectively (**Figure 3.20a**). This provided evidence that during the CDSA of P(PDL-*co*-VL)$_{n}$-*b*-PDMA$_{m}$, the PPDL and PVL in the random copolymer main chain would be able to crystallise individually. Additionally, the crystallisation temperatures of the PPDL and PVL fraction in both block copolymers were decreased, compared to the 52 °C for PPDL$_{25}$-*b*-PDMA$_{110}$ and 28 °C for PVL$_{50}$-*b*-PDMA$_{194}$. This is owing to the interference between the crystallising of PPDL and PVL in the random copolymer chain, which is consistent with the DSC data presented in **Table 3.6**. Furthermore, only one melting peak from both the P(PDL-co-VL)$_{45}$-*b*-PDMA$_{270}$ and P(PDL-co-VL)$_{35}$-*b*-PDMA$_{180}$ heating curves was observed at 41 °C and 33 °C, respectively (**Figure 3.20b**). This indicates that the melting of the polymer occurs only during disassembly in solution, which is contributed by both PPDL

and PVL fractions. In this case, the PVL fraction is only able to melt when associating with PPDL. The melting in n-butanol of both block copolymers has dropped to lower temperatures compared to 73 °C of $PPDL_{25}$-*b*-$PDMA_{110}$ and 38 °C of PVL_{50}-*b*-$PDMA_{194}$ as well as the crystallisation temperature in n-butanol. The above information provided by the Nano DSC experiments has revealed the possibility for further CDSA of both P(PDL-co-VL)$_{45}$-*b*-$PDMA_{270}$ and P(PDL-co-VL)$_{35}$-*b*-$PDMA_{180}$ in n-butanol with an ability for greater control of self-nucleation using temperature.

Table 3.7 Summary of melting and crystallisation temperatures of PVL_{50}-*b*-$PDMA_{194}$, $PPDL_{25}$-*b*-$PDMA_{110}$, P(PDL-*co*-VL)$_{35}$-*b*-$PDMA_{180}$ and P(PDL-*co*-VL)$_{45}$-*b*-$PDMA_{270}$.

	PVL_{50}-*b*-$PDMA_{194}$	$PPDL_{25}$-*b*-$PDMA_{110}$	P(PDL-*co*-VL)$_{35}$-*b*-$PDMA_{180}$	P(PDL-*co*-VL)$_{45}$-*b*-$PDMA_{270}$
T_c(°C)	28	52	34,8	28,-2
T_m(°C)	38	75	36	41

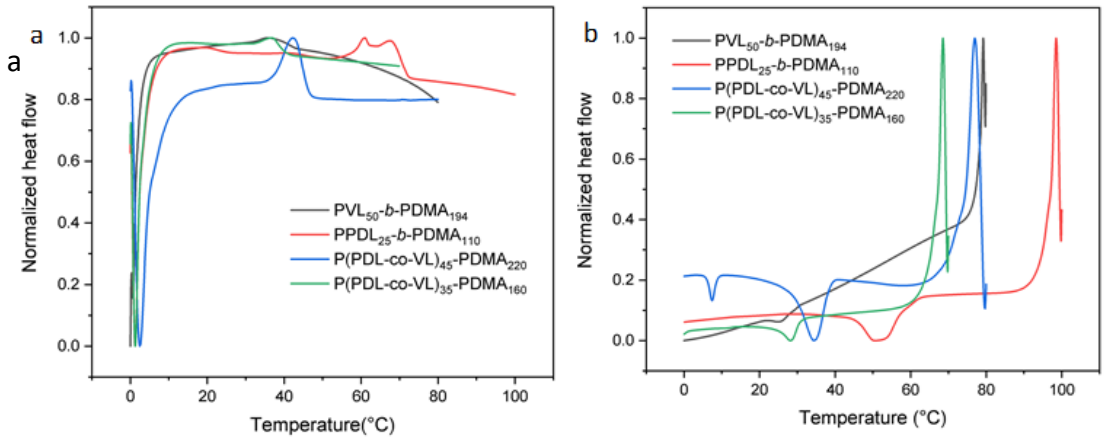

Figure 3.20 Nano Differential scanning calorimetry thermograms of P(PDL-*co*-VL)$_{45}$-*b*-PDMA$_{270}$ and P(PDL-*co*-VL)$_{35}$-*b*-PDMA$_{180}$ second (a) heating and (b) cooling curve at a rate of 1°C per minute in n-butanol.

Next, the self-nucleation of P(PDL-*co*-VL)$_{45}$-*b*-PDMA$_{270}$ and P(PDL-*co*-VL)$_{35}$-*b*-PDMA$_{180}$, were studied by heating both polymers in n-butanol at 70 °C (which is above the Tm measured by NanoDSC) for three hours at a concentration of 5 mg mL^{-1} and subsequently cooled down to room temperature. Both of the polymer solutions were then aged for three days at two different temperatures of 23 °C and -3 °C, where the former is between the T_c of PPDL and PVL fractions in n-butanol and the latter is below both crystallisation temperatures. All the samples were then examined by TEM at 0.5 mg mL-1 stained by 1 wt.% uranyl acetate water solution. It was observed from TEM images that both of P(PDL-co-VL)$_{45}$-*b*-PDMA$_{270}$ and P(PDL-co-VL)$_{35}$-*b*-PDMA$_{180}$ formed long cylindrical micelles after ageing at 23 °C (**Figure 3.21a, c**). On the contrary, very short cylindrical and spherical micelles were observed after ageing at -3 °C from the TEM images (**Figure 3.21b, d**). The formation of recognisably different length micelles from the same polymer simply by ageing at two different temperatures is attributed to the changes in self-nucleation rates. While ageing at 23 °C, which is above the T_c of the PVL

fraction in n-butanol, the self-nucleation of the PVL fraction is switched off. This leads to a relatively slow self-nucleation of the copolymer in solution, resulting in longer cylindrical micelles. Contrarily, ageing below both T_c of PPDL and PVL fractions at -3 °C, results in fast self-nucleation which produced short cylindrical and spherical micelles (**Scheme 3.5**). Moreover, a reduction in the length difference between the micelles from ageing at different temperatures for P(PDL-*co*-VL)$_{35}$-*b*-PDMA$_{180}$ compared to P(PDL-co-VL)$_{45}$-*b*-PDMA$_{270}$ was observed by TEM. This suggested that a less PPDL fraction in the copolymer chain diminished the changing of self-nucleation at two different temperatures. To conclude, crystallisation-driven self-assembly of P(PDL-*co*-VL)$_n$-*b*-PDMA$_m$ polymers has been demonstrated, where the self-nucleation in solution is controlled by two different semi-crystallised polymer segments. As a consequence of the different T_c of PPDL and PVL, self-nucleation during the higher temperature domain is governed by PPDL, whereas self-nucleation during the lower temperature domain is controlled by both PPDL and PVL. This has revealed that it is possible to control self-nucleation in solution simply through suppressing the crystallisation of the PVL fraction in solution by ageing at different temperatures.

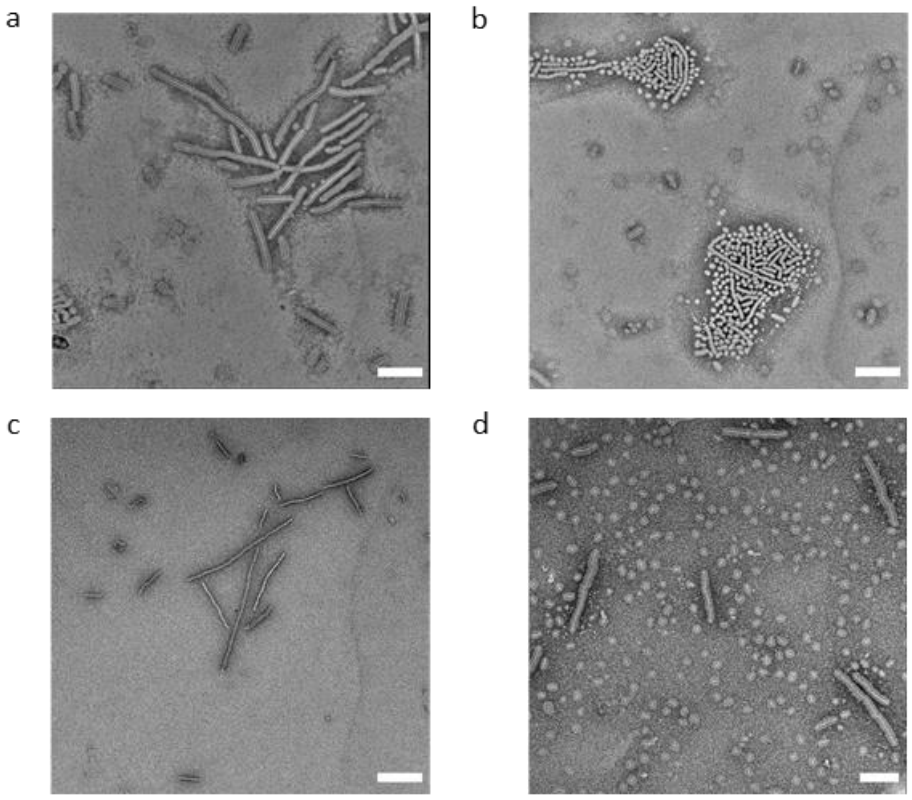

Figure 3.21 TEM micrographs of cylindrical micelles prepared using P(PDL-*co*-VL)$_{45}$-*b*-PDMA$_{270}$ (a) ageing at 23°C, (b) ageing at -3°C and P(PDL-*co*-VL)$_{35}$-*b*-PDMA$_{180}$ ageing at (c) 23°C, (d) ageing at -3°C for 3 days after self-nucleation in n-butanol heating at 70 °C for 3 hours and subsequently cooling down to room temperature. All samples were stained with 1 wt. % uranyl acetate in water. Scale bar = 1 µm.

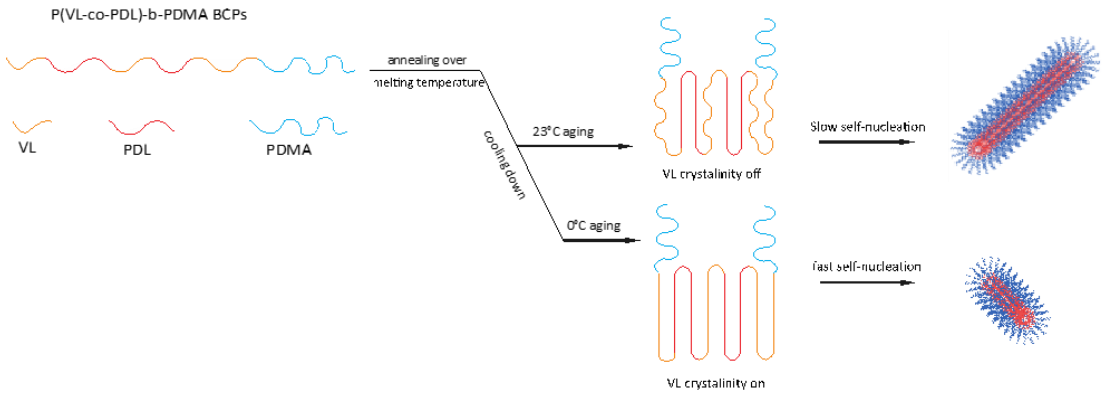

Scheme 3.5 Mechanism of different length cylindrical micelles formed by P(PDL-*co*-VL)$_n$-*b*-PDMA$_m$ polymers self-nucleation in n-butanol.

3.3.6 Epitaxial growth of P(PDL-*co*-VL)$_n$-*b*-PDMA$_m$ platelet micelles

As discussed in Section *3.3.3*, the challenge faced when attempting epitaxial growth of PVL$_n$-*b*-PDMA$_m$ block copolymers is the homogeneous self-nucleation after unimer is reintroduced into the seed solution, which is unavoidable because of the nature of PVL crystallinity. Herein, applying the knowledge of controllable self-nucleation of P(PDL-*co*-VL)$_n$-*b*-PDMA$_m$ polymers, an epitaxial growth mechanism was attempted. The PVL$_{50}$-*b*-PDMA$_{194}$ seeds produced from the procedure in Section 3.3.2 served as the self-nucleation sites for P(PDL-*co*-VL)$_n$-*b*-PDMA$_m$ and P(PDL-*co*-VL)$_n$ unimer to crystallise on. The blend of P(PDL-*co*-VL)$_n$-*b*-PDMA$_m$ and P(PDL-co-VL)$_n$ unimer is applied here to allow 2D epitaxial growth. By employing different ratios between seeds and unimers, precisely size-controlled platelets were targeted (**Scheme 3.6**).

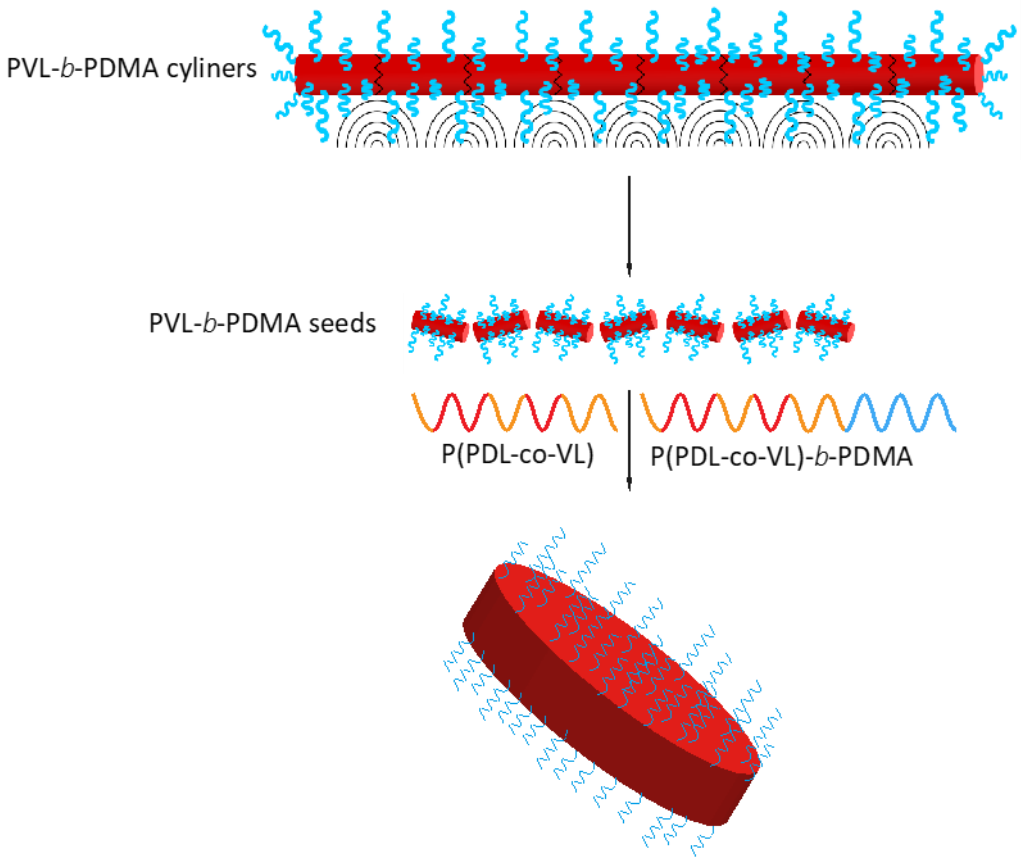

Scheme 3.6 Epitaxial growth of mixed P(PDL-*co*-VL)$_n$-*b*-PDMA$_m$ and P(PDL-*co*-VL)$_n$ unimer from PVL$_n$-*b*-PDMA$_m$ seeds into platelets micelles in n-butanol. Seeds were prepared at 0.01 mg mL^{-1} in n-butanol, with the addition of unimers at 10 mg mL^{-1} in THF.

Unimers were prepared by dissolving P(PDL-*co*-VL)$_{45}$-*b*-PDMA$_{270}$ and P(PDL-*co*-VL$_{45}$ (1:1) in THF at different concentrations. Adding the same volume of THF into a 0.01 mg mL^{-1} seeds solution in n-butanol, different ratios between unimers and seeds were achieved in order to manipulate the size of the resultant platelets. The solutions were aged for three days at room temperature to suppress the crystallinity of PVL, and to avoid homogeneous self-nucleation. A controlled linear epitaxial growth was observed from TEM analysis, where the length of the platelet micelles varied from 150 nm to 1500 nm (**Figure 3.22**). As expected, the size of the platelet micelles was proportional to the

amount of introduced unimer (**Figure 3.23**). Finally, the size dispersity of the platelet micelles was shown to be near monodisperse from statistical analysis of the TEM images (**Table 3.8**).

Table 3.8 Length dispersity of platelet micelles formed upon epitaxial growth of PVL_{50}-*b*-$PDMA_{194}$ seeds micelles.

m_{unimer}/ m_{seeds}	L_n(nm)	L_w(nm)	W_n(nm)	W_w(nm)	L_n / L_w	W_n / W_w
1	163	170	65	66	1.04	1.02
3	310	319	91	94	1.03	1.03
5	353	364	101	104	1.03	1.03
10	462	476	170	173	1.03	1.02
15	661	687	278	284	1.04	1.02
20	910	955	357	367	1.05	1.03
25	1120	1142	425	433	1.02	1.02
30	1530	156066	503	513	1.02	1.02

Calculation of L_n and L_w specified in experimental.

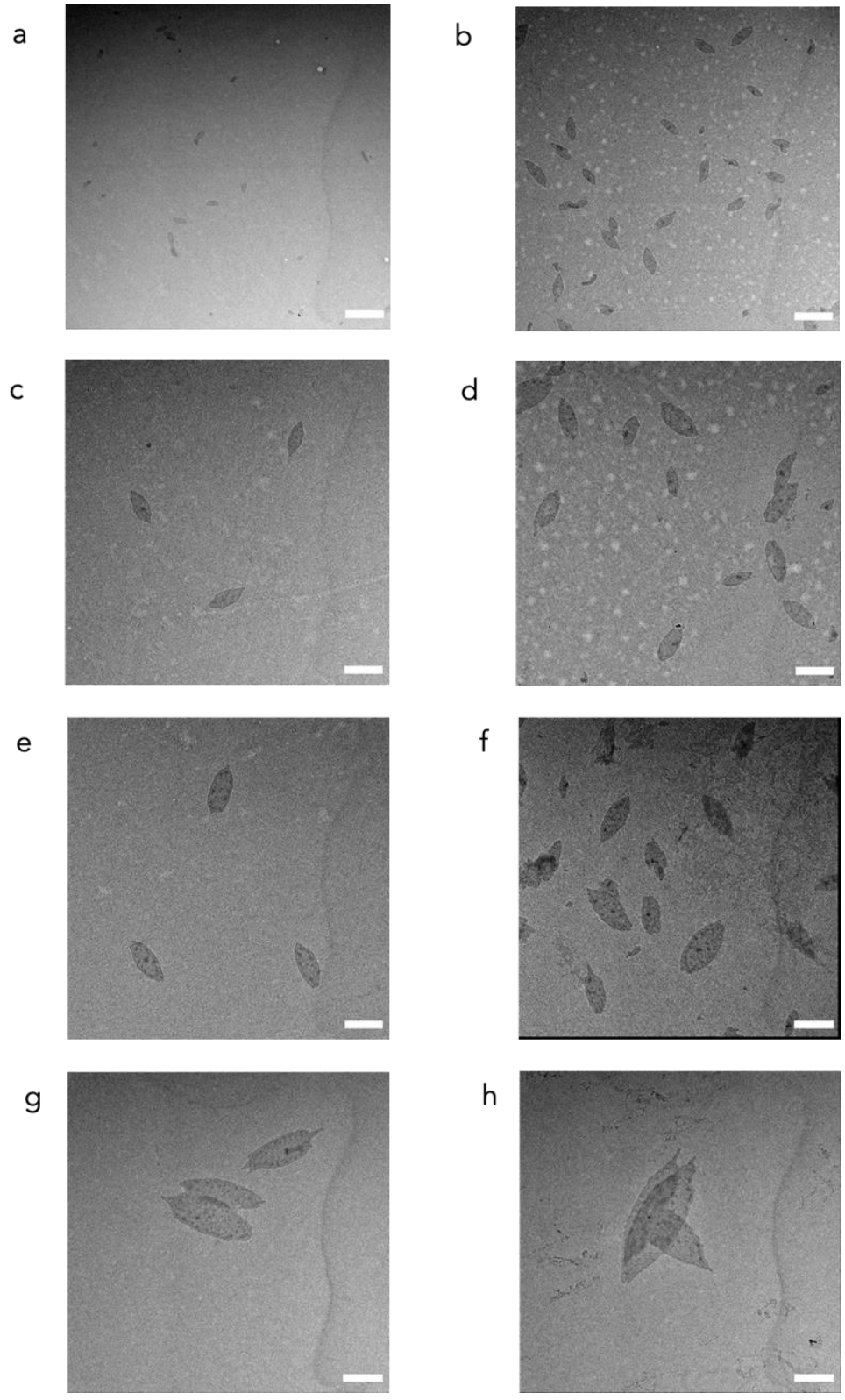

Figure 3.22 TEM micrographs of platelet micelles epitaxially grown from PVL_{50}-*b*-$PDMA_{194}$ seed micelles with a unimer/seed ratio of 1(a), 3(b), 5(c), 10(d), 15(e), 20(f), 25(g), 30(h). 1wt % uranyl acetate was used as a negative stain. Scale bar = 500 nm.

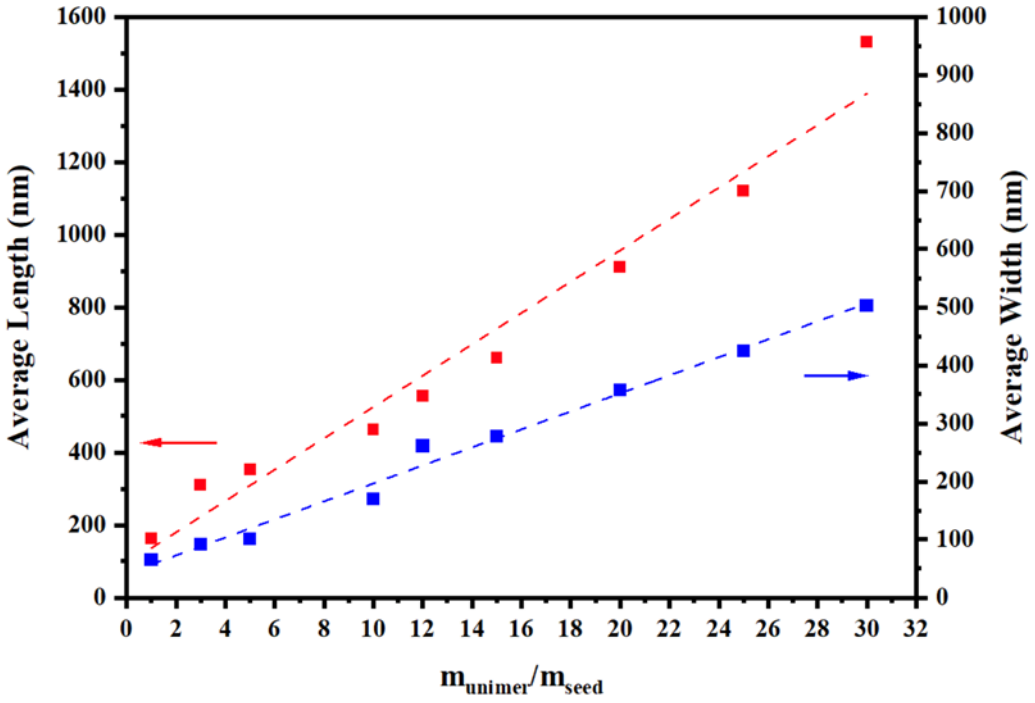

Figure 3.23 Plot showing the linear dependence of length and width of 2D P(PDL-*co*-VL)$_n$-*b*-PDMA$_m$ and P(PDL-*co*-VL)$_n$ blending platelet micelles epitaxially grown from PVL$_{50}$-b-PDMA$_{194}$ seed micelles upon the unimer-to-seed ratio.

3.4 Conclusions

The successful formation of cylindrical micelles was prepared by crystallisation-driven self-assembly of both PVL_n-*b*-$PDMA_m$ and P(PDL-*co*-VL)$_n$-*b*-$PDMA_m$ copolymers. In particular, the CDSA of P(PDL-*co*-VL)$_n$-*b*-$PDMA_m$ copolymers exhibited two self-nucleation domains due to the independent crystallisation of the PPDL and PVL fractions in the copolymer core. Controllable self-nucleation during CDSA of P(PDL-*co*-VL)$_n$-*b*-$PDMA_m$ polymers was then demonstrated by suppressing the crystallinity of PVL in the random copolymer chain at selected temperatures. This was confirmed by the change in length of cylindrical micelles as observed by TEM analysis. This method was then applied to overcome the homogenous self-nucleation of PVL_n-*b*-$PDMA_m$ during epitaxial growth. As a result, platelet micelles could be achieved by epitaxial crystallisation of the P(PDL-*co*-VL)$_n$-*b*-$PDMA_m$ copolymer onto PVL_n-*b*-$PDMA_m$ seed micelles, with controlled dimensions and a low dispersity in n-butanol. Therefore, this co-crystallisation-driven self-assembly approach shows great potential as a method to optimise self-nucleation for a wide range of crystalline cores whenever a copolymerisation is possible for the core-forming block.

3.5 Experimental

3.5.1 Materials

Chemicals and solvents were purchased from Sigma Aldrich, Acros, Fluka, Fisher Chemical, Alfa Aesar, or VWR. Dry solvents were purified using MBRAUN SPS solvent purification system. δ-Valerolactone, was dried over calcium hydride for 24 hours before vacuum distillation. ω-Pentadecalactone was dissolved in 75 wt.% toluene and dried overnight on molecular sieves. 1,4-dioxane, *N,N*-dimethylacrylamide (DMA) and 2,2'-azobis(2-methylpropionitrile) (AIBN) was recrystallised twice from methanol and stored in the dark at 4 °C.

3.5.2 Instrumentation

Proton (^{1}H) NMR spectra were recorded using a Bruker DPX-300 spectrometer or Bruker DPX-400 spectrometer. Carbon (^{13}C) NMR spectra were recorded using a Bruker DPX-400 spectrometer or Bruker DRX-500 spectrometer. All chemical shifts were recorded in parts per million (ppm) relative to a reference peak of chloroform solvent at δ = 7.26 ppm and 77.16 ppm for ^{1}H and ^{13}C NMR spectra respectively.

Size exclusion chromatography (SEC) was performed on an Agilent 390-MDS on PLgel Mixed-D type columns in series with refractive index (RI) detection. Weights were calculated using a calibration curve determined from poly(styrene) standards with chloroform (0.5% NEt_3) as eluent flowing at 1.0 mL.min^{-1} and sample concentration 3 mg mL^{-1}.

Differential scanning calorimetry (DSC) analysis was performed on a Mettler Toledo HP DSC827. Samples were run at a heating or cooling ramp series of 10 °C min^{-1} in triplicate

under a nitrogen atmosphere using 40 µL aluminium crucibles. T_c and T_m of various samples were obtained in the first runs and were taken as the midpoint of the inflection tangent.

Nano Differential scanning calorimetry (NanoDSC) was performed on a TA NanoDSC. 800µL samples were run at a heating or cooling ramp series of 1 °C min^{-1} in triplicate under a constant 3-atmosphere pressure. T_c and T_m of various samples were obtained in the second runs and were taken as the midpoint of the inflection tangent.

Samples for transmission electron microscopy (TEM) analysis were prepared by drop casting 10 µL of polymer in ethanol (0.5 mg/mL) onto a carbon/formvar-coated copper grid placed on filter paper. Samples were stained with a 1% uranyl acetate solution to facilitate imaging of the thin organic structures unless specified. Imaging for samples was performed on a Jeol 2100 transmission electron microscope operating at 120 kV. TEM images were analysed by ImageJ software, where at least 100 particles were counted for each sample to obtain the number-average length (L_n) and weight-average length (L_w). L_n and L_w were calculated by using the following equations:

$$L_n = \frac{\sum_{i=1}^{n} N_i L_i}{\sum_{i=1}^{n} N_i}$$

$$L_w = \frac{\sum_{i=1}^{n} N_i L_i^2}{\sum_{i=1}^{n} N_i L_i}$$

where L_i is the length of each counted cylindrical micelle and N_i is the number of the cylindrical micelles with the length L_i.

3.5.3 Synthesis of 4-cyano-4-(((ethylthio)carbonothioyl)thio)pentanoic acid (CEPA)

Following a previously reported procedure,[95] to an oven-dried round bottom flask, sodium ethanethiolate (10 g, 119 mmol, 1 eq) was added followed by the addition of dry diethyl ether (500 mL) with the resulting solution cooled to 0˚C. Carbon disulfide (7.74 mL, 131 mmol, 1.1 eq) was subsequently added dropwise over 10 min, producing a thick yellow precipitate of sodium S-ethyl trithiocarbonate. After 2 h of stirring at room temperature, solid iodine (15.1 g, 59.4 mmol, 0.5 eq) was added and the resultant reaction mixture was stirred for a further 2 h at room temperature. The reaction mixture was then washed with sodium thiosulfate solution (1 M, 3 × 100 mL), deionized water (3 × 100 mL) and finally with saturated sodium chloride solution (3 × 100 mL). The organic phase was dried over $MgSO_4$, filtered and evaporated to remove the solvent, leaving a residue of bis-(ethylsulfanylthiocarbonyl) disulfide (15.6 g, 56.8 mmol).

A solution of 4,4'-azobis(4- cyanovaleric acid) (ACVA) (23.9 g, 85.2 mmol, 1 eq) and bis-(ethylsulfanylthiocarbonyl) disulfide (15.6 g, 56.8 mmol, 0.67 eq) in ethyl acetate (500 mL) was heated to 80˚C overnight at reflux under an N_2 atmosphere. After removal of the volatile solvents in vacuo, purification was carried out using silica gel column chromatography (hexane : dichloromethane = 1:3) affording 4-cyano-4-(((ethylthio) carbonothioyl)thio)pentanoic acid (CEPA) as an orange red oil (24.4 g, 97.7 mmol, 86%).

^{1}H NMR (400 MHz, $CDCl_3$) δ/ppm: 3.35 (2H, q, $^3J_{H-H}$ = 7.6 Hz, SCH_2CH_3), 2.68 (2H, m, $C(CN)(CH_3)CH_2CH_2$), 2.3-2.6 (2H, m, $C(CN)(CH_3)CH_2CH_2$), 1.88 (3H, s, $C(CN)(CH_3)\ CH_2CH_2$), 1.36 (3H, t, $^3J_{H-H}$ = 7.6 Hz, SCH_2CH_3). ^{13}C NMR (100 MHz, $CDCl_3$) δ/ppm: 216.6 (*C*=S), 177.1

(*C*=O), 118.8 (C(*C*N)(CH_3)CH_2CH_2), 46.1 (*C*(CN)(CH_3)CH_2CH_2), 33.4 (C(CN)(CH_3)*C*H_2CH_2), 31.4 (S*C*H_2CH_3), 29.5(C(CN)(CH_3)CH_2*C*H_2), 24.8 (C(CN)(*C*H_3)CH_2CH_2), 12.7 (SCH_2*C*H_3).

3.5.4 Synthesis of 2-cyano-5-hydroxypentan-2-yl ethyl carbonotrithioate (CHPET)

To a flame-dried three-neck round bottom flask, 4-cyano-4-(((ethylthio)carbonothioyl)thio)pentanoic acid (CEPA) (14.1 g, 53.6 mmol, 1 eq) was added followed by the addition of dry tetrahydrofuran (500 mL) with the resulting solution cooled to -78 ˚C (mixture of dry ice and acetone). Borane tetrahydrofuran complex solution (1 M, 56.3 mL, 56.3 mmol, 1 eq) was subsequently added in a dropwise fashion over 30 min. The reaction mixture was left to stir for 1 h, after which the cooling bath was removed, and the reaction stirred overnight at ambient temperature under an N2 atmosphere. After 18 h of stirring, methanol (100 mL) was added in five portions and stirred for 10 min. after each addition or until no further bubbling was observed. After removal of the volatile solvents in vacuo, the organic residue was dissolved in diethyl ether (250 mL) and washed with saturated $NaHCO_3$ solution (3 × 250 mL) and then with brine (250 mL). Further extraction using diethyl ether from the collected aqueous layers was carried out. Combined organic layers were then dried over $MgSO_4$, filtered and evaporated to dryness. Purification was carried out using silica gel column chromatography (petroleum ether 40/60: ethyl acetate = 1:1) affording 2-cyano-5-hydroxypentan-2-yl ethyl carbonotrithioate (CHPET) as an orange-red oil (9.7 g, 39.1 mmol, 73%). ^{1}H NMR (300 MHz, $CDCl_3$) δ/ppm: 3.72 (2H, t, $^3J_{H-H}$ = 6 Hz, C*H*$_2$OH) 3.34 (2H, q, $^3J_{H-H}$ = 7.5 Hz, SC*H*$_2$$CH_3$), 2-2.3 (2H, m, C(CN)($CH_3$)C*H*$_2$$CH_2$), 1.89 (3H, s, C(CN)(C*H*$_3$)CH_2CH_2), 1.85 (2H, m, C(CN)(CH_3)CH_2C*H*$_2$), 1.35 (3H, t, $^3J_{H-H}$ = 7.5 Hz, SCH_2C*H*$_3$).

^{13}C NMR (75 MHz, $CDCl_3$) δ/ppm: 217.4 (*C*=S), 119.5 (C(*C*N)(CH_3)CH_2CH_2), 61.7 (*C*H_2OH) 46.9 (*C*(CN)(CH_3)CH_2CH_2), 35.7 (C(CN)(CH_3)*C*H_2CH_2), 31.3 (S*C*H_2CH_3), 27.9 (C(CN)(CH_3)CH_2*C*H_2), 24.9 (C(CN)(*C*H_3)CH_2CH_2), 12.8 (SCH_2*C*H_3).

3.5.5 Synthesis of PVL_{50}

In a nitrogen-filled glove box, solutions of diphenylphosphate (30 mg, 0.12 mmol) in dry toluene (3 mL) and dual-head CTA (15 mg, 0.06 mmol) in dry toluene (3 mL) were added to δ-valerolactone (540 µL, 6 mmol). After stirring for 1.5 hours at room temperature, the solution was removed from the glove box, precipitated three times into ice-cold diethyl ether and collected by centrifugation. It should be noted that the polymers must have no evidence of high or low molecular weight shoulders by SEC before proceeding with RAFT polymerizations and self-assembly. ^{1}H NMR (400 MHz, $CDCl_3$) δ/ppm: 4.07 (100 H, t, CH_2OH), 3.65 (2 H, CH_2OCO), 2.34 (100 H, t, OCOCH_2), 1.67 (230 H, m,OCO CH_2(C*H*$_2$)$_2$$CH_2$OH). SEC ($CHCl_3$, PS standard): M_n = 9.3 kDa, $Đ_m$ = 1.05.

3.5.6 Synthesis of PVL_{50}-*b*-$PDMA_{194}$

PVL_{50} (100 mg, 0.019 mmol), DMA (470.9 mg, 4.75 mmol) and AIBN (37.4 µL of a 10 mg mL^{-1} solution in 1,4-dioxane, 2.28 µmol) were dissolved in 1,4-dioxane (1 mL) and placed in an ampoule. After three freeze- pump-thaw cycles, the solution was heated for 2 hours at 70 ˚C. The reaction was quenched by immersion of the ampoule in liquid nitrogen and the polymer was precipitated in ice-cold diethyl ether three times before drying under vacuum. $M_{n,\,NMR}$ = 24.5 kDa, DP = 194. $M_{n,\,SEC}$ = 28.7 kDa, $Đ_M$ = 1.09. ^{1}H NMR (400 MHz, $CDCl_3$) δ (ppm) 4.03 (t, 100H, C*H*$_2$OH), 3.23-2.28 (m, 1250H, N(*CH*$_3$)$_2$, *CH*CH_2 from PDMA), 2.28-0.79 (m, 788H, OCOC*H*$_2$ (PVL), OCO(C*H*$_2$)$_4$OH (PVL), CHC*H*$_2$ (PDMA)).

3.5.7 Random copolymerisation of ω-pentadecalactone and δ-valerolactone

Using standard glovebox techniques, an ampoule was filled with $Mg(BHT)_2(THF)_2$ (120mg, 0.2 mmol), dual-head CTA (50 mg, 0.2 mmol), δ-valerolactone (648 µL, 6 mmol) and ω-pentadecalactone stock solution (75 wt.% toluene, 5.0 mmol). The ampoule was sealed and heated at 80 °C for a defined time period. The reaction was quenched with the addition of acidified (5% HCl) methanol. Chloroform was added to dissolve any solids and the polymer was precipitated in excess methanol.

^{1}H NMR (400 MHz, 298 K, CDCl3): δ =4.07 (m, C*H*$_2$OC=O), 2.33 (m, C*H*$_2$C=OO), 2.28 (m, C*H*$_2$C=OO), 1.67, 1.60, 1.27 and 1.24 (all remaining hydrogens) ppm. ^{13}C NMR (500 MHz, 298 K, CDCl3): δ = 174.14 (PDL*-PDL, $OCOCH_2$), 174.04 (PDL*-VL, $OCOCH_2$), 173.52 (PDL-VL*-PDL, $OCOCH_2$), 173.49 (VL-VL*-PDL, $OCOCH_2$), 173.43 (PDL-VL*-VL, $OCOCH_2$), 173.39 (VL-VL*-VL, $OCOCH_2$), 64.74 (PDL*-VL, OCH_2), 64.54 (PDL*-PDL, OCH_2), 64.04 (VL*-VL, OCH_2), 63.84 (VL*-PDL), 34.54 (PDL*-PDL, $OCOCH_2$), 34.45 (PDL*-VL, $OCOCH_2$), 33.94 (PDL-VL*-PDL, $OCOCH_2$), 33.90 (VL-VL*- PDL, $OCOCH_2$), 33.85 (PDL-VL*-VL, $OCOCH_2$), 33.82 (VL-VL*-VL, $OCOCH_2$), 29.78-29.40, 29.31 (PDL, CH_2), 28.24 (VL, OCH_2CH_2), 26.05 (VL, $OCOCH_2CH_2$), 25.15 (PDL, CH_2), 25.10 (VL, $OCOCH_2CH_2CH_2$) ppm.

3.5.8 Synthesis of P(PDL-co-VL)$_n$-*b*-PDMA$_m$ block copolymer.

P(PDL-co-VL)$_n$ (6.6 µmol), *N,N*-dimethylacrylamide, (316 µL, 1.98 mmol) and AIBN (13 µL of a 10 mg mL^{-1} solution in 1,4-dioxane, 0.79 µmol) and 1,4-dioxane (1.0mL) were combine in a dried ampoule under nitrogen. After three freeze-pump-thaw cycles, the solution was sealed under nitrogen and heated for 3 hours at 70 °C. The reaction was

quenched in liquid nitrogen and purified by precipitation three times into ice-cold diethyl ether. The resultant pale yellow solid was dried in vacuo before use.

$M_{n,\,NMR}$ = 24.5 kDa, DP = 194. $M_{n,\,SEC}$ = 28.7 kDa, $Đ_M$ = 1.09. ^{1}H NMR (400 MHz, $CDCl_3$) δ (ppm) 4.07 (t, C*H*$_2$OH), 3.28-2.23 (m, N(*CH*$_3$)$_2$, C*H*CH$_2$ from PDMA), 1.92-1.20 (m, OCOC*H*$_2$ (P(PDL-co-VL)), OCO(C*H*$_2$)$_n$OH (P(PDL-co-VL)), CHC*H*$_2$ (PDMA)).

3.5.9 Typical crystallisation-driven self-assembly method for the self-nucleation of PVL and P(PDL-*co*-VL) block copolymers

PVL and P(PDL-*co*-VL) block copolymers (10 mg) was added to 5 mL of solvent (5 mg mL^{-1}) in a 7 mL vial and heated at 70 °C without stirring for 3 hours before cooling to room temperature. Samples were imaged after 5 days of ageing at room temperature.

3.5.10 Sonication of PVL_{50}-*b*-$PDMA_{194}$ cylindrical micelles

Self-nucleated PVL_{50}-*b*-$PDMA_{194}$ cylindrical micelles in n-butanol were diluted (0.5 mg mL^{-1}) and sonicated using an ultrasonic bath or sonic probe at 0 °C. An aliquot of the assembly was taken at various time intervals and analysed by TEM. Seed micelles were obtained by 2 minutes of sonication using a sonic probe.

3.5.11 Typical crystallisation-driven self-assembly method for the epitaxial growth of PVL block copolymers

P(PDL-*co*-VL)$_n$-*b*-$PDMA_m$ dissolved in THF (10 mg mL^{-1}) was added to a dispersion of PVL_{50}-*b*-$PDMA_{194}$ seed micelles (0.01 mg mL^{-1}) and aged for 5 days before analysis by TEM. The unimer-to-seed ratio was altered by adding different volumes of unimer solution to the dispersion of seed micelles.

3.6 References

1. R. M. Michell, A. Mugica, M. Zubitur and A. J. Müller, in *Polymer Crystallization I: From Chain Microstructure to Processing*, eds. F. Auriemma, G. C. Alfonso and C. de Rosa, Springer International Publishing, Cham, 2017, DOI: 10.1007/12_2015_327, pp. 215-256.

2. D. J. Blundell, A. Keller and A. J. Kovacs, *J. Polym. Sci., Part B: Polym. Lett.*, 1966, **4**, 481-486.

3. A. T. Lorenzo, M. L. Arnal, J. J. Sánchez and A. J. Müller, *J. Polym. Sci. B Polym. Phys.*, 2006, **44**, 1738-1750.

4. A. J. Müller, V. Balsamo and M. L. Arnal, in *Block Copolymers II*, ed. V. Abetz, Springer Berlin Heidelberg, Berlin, Heidelberg, 2005, DOI: 10.1007/12_001, pp. 1-63.

5. B. Lotz, A. J. Kovacs, G. A. Bassett and A. Keller, *Kolloid-Zeitschrift und Zeitschrift für Polymere*, 1966, **209**, 115-128.

6. C. P. Price, A. L. Grzesiak and A. J. Matzger, *J. Am. Chem. Soc.*, 2005, **127**, 5512-5517.

7. J. J. Crassous, P. Schurtenberger, M. Ballauff and A. M. Mihut, *Polymer*, 2015, **62**, A1-A13.

8. J. B. Gilroy, T. Gädt, G. R. Whittell, L. Chabanne, J. M. Mitchels, R. M. Richardson, M. A. Winnik and I. Manners, *Nat. Chem.*, 2010, **2**, 566-570.

9. X. Wang, G. Guerin, H. Wang, Y. Wang, I. Manners and M. A. Winnik, *Science*, 2007, **317**, 644-647.

10. Z. M. Hudson, C. E. Boott, M. E. Robinson, P. A. Rupar, M. A. Winnik and I. Manners, *Nat. Chem.*, 2014, **6**, 893-898.

11. H. Qiu, Y. Gao, C. E. Boott, O. E. C. Gould, R. L. Harniman, M. J. Miles, S. E. D. Webb, M. A. Winnik and I. Manners, *Science*, 2016, **352**, 697-701.

12. H. Qiu, Z. M. Hudson, M. A. Winnik and I. Manners, *Science*, 2015, **347**, 1329-1332.

13. H. Qiu, G. Cambridge, M. A. Winnik and I. Manners, *J. Am. Chem. Soc.*, 2013, **135**, 12180-12183.

14. B. Kalra, A. Kumar, R. A. Gross, M. Baiardo and M. Scandola, *Macromolecules*, 2004, **37**, 1243-1250.

15. P. A. Rupar, L. Chabanne, M. A. Winnik and I. Manners, *Science*, 2012, **337**, 559-562.

16. Y. He, J.-C. Eloi, R. L. Harniman, R. M. Richardson, G. R. Whittell, R. T. Mathers, A. P. Dove, R. K. O'Reilly and I. Manners, *J. Am. Chem. Soc.*, 2019, **141**, 19088-19098.

17. X. He, Y. He, M.-S. Hsiao, R. L. Harniman, S. Pearce, M. A. Winnik and I. Manners, *J. Am. Chem. Soc.*, 2017, **139**, 9221-9228.

18. M. C. Arno, M. Inam, Z. Coe, G. Cambridge, L. J. Macdougall, R. Keogh, A. P. Dove and R. K. O'Reilly, *J. Am. Chem. Soc.*, 2017, **139**, 16980-16985.

19. J. R. Finnegan, X. He, S. T. G. Street, J. D. Garcia-Hernandez, D. W. Hayward, R. L. Harniman, R. M. Richardson, G. R. Whittell and I. Manners, *J. Am. Chem. Soc.*, 2018, **140**, 17127-17140.

20. J. Schmelz, A. E. Schedl, C. Steinlein, I. Manners and H. Schmalz, *J. Am. Chem. Soc.*, 2012, **134**, 14217-14225.

21. J. Gwyther, J. B. Gilroy, P. A. Rupar, D. J. Lunn, E. Kynaston, S. K. Patra, G. R. Whittell, M. A. Winnik and I. Manners, *Chem. Eur. J.*, 2013, **19**, 9186-9197.

22. R. Kakuchi, Y. Tsuji, K. Chiba, K. Fuchise, R. Sakai, T. Satoh and T. Kakuchi, *Macromolecules*, 2010, **43**, 7090-7094.

23. K. Makiguchi, T. Satoh and T. Kakuchi, *Macromolecules*, 2011, **44**, 1999-2005.

24. X. Lou, C. Detrembleur and R. Jérôme, *Macromolecules*, 2002, **35**, 1190-1195.

25. A. Nakayama, N. Kawasaki, Y. Maeda, I. Arvanitoyannis, S. Aiba and N. Yamamoto, *J. Appl. Polym. Sci.*, 1997, **66**, 741-748.

26. C. G. Pitt, M. M. Gratzl, G. L. Kimmel, J. Surles and A. Schindler, *Biomaterials*, 1981, **2**, 215-220.

27. M. Aubin and R. E. Prud'homme, *Polymer*, 1981, **22**, 1223-1226.

28. J. Fernández, A. Etxeberria and J.-R. Sarasua, *J. Appl. Polym. Sci.*, 2015, **132**.

29. J. A. Wilson, S. A. Hopkins, P. M. Wright and A. P. Dove, *Macromolecules*, 2015, **48**, 950-958.

30. A. A. Alghamdi, W. S. Saeed, A.-B. Al-Odayni, F. A. Alharthi, A. Semlali and T. Aouak, *Polymers*, 2019, **11**, 439.

31. Y. Ren, Z. Wei, T. Wu, Y. Bian, X. Leng, C. Zhou and Y. Li, *RSC Adv.*, 2016, **6**, 45791-45801.

32. J. A. Wilson, S. A. Hopkins, P. M. Wright and A. P. Dove, *Polymer Chemistry*, 2014, **5**, 2691-2694.

33. Z. Jiang, H. Azim, R. A. Gross, M. L. Focarete and M. Scandola, *Biomacromolecules*, 2007, **8**, 2262-2269.

Chapter Four – Determination of crystallisation of novel Poly(ζ-heptalactone) polymers: from bulk to solution

4.1 Abstract

Polyesters have been studied in the interest of their mechanical and thermal properties for a wide range of potential industrial applications. As biodegradable materials, polyesters have also received significant attention for biological applications such as tissue engineering and drug delivery. Therefore, exploring the thermal properties and self-assembly behaviour of polyesters are of great interest. Poly(ζ-heptalactone) (PHL), synthesised from the non-commercially available monomer η-heptalactone, has not been extensively studied to date. In this work, the ring-opening polymerisation of η-heptalactone was demonstrated, achieving well-controlled PHL homopolymers, and isothermal DSC experiments revealed their crystallisation kinetics and melting temperatures. In order to prepare micelles from this underexplored polyester, three diblock copolymers (poly(*N*,*N*-dimethylacrylamide)-*b*-poly(η-heptalactone), *N*-isopropylacrylamide-*b*-poly(η-heptalactone) and 2-(dimethylamino)ethyl methacrylate-*b*-poly(η-heptalactone)) were subsequently synthesized. Self-nucleation of these polymers during crystallisation in solution was investigated by NanoDSC. Finally, different morphologies prepared by crystallisation-driven self-assembly were compared in an effort to examine the corona effect on self-nucleation of PHL copolymers.

4.2 Introduction

4.2.1 Polymer self-nucleation in bulk

In the field of polymer crystallisation in bulk, polymer nucleation has received extensive studies in the literature. There are two different types of polymer nucleation: homogeneous and heterogeneous. Homogeneous nucleation requires a spontaneous aggregation of chain segments and the production of a new surface, which suffers from a high energy barrier.[1-3] Conversely, heterogeneous nucleation occurs in the presence of a substantial amount of heterogeneities, such as impurities or additives, and as such, the energy barrier is largely reduced in this process.[4-6] On account of the importance of nucleation in both processes, self-nucleation was developed as a technique to produce crystal fragments to serve as nuclei. It was first studied as a technique to control the nucleation of polyethylene,[7] and has since been extended as a differential scanning calorimetry (DSC)-based thermal protocol to study polymer nucleation.[8, 9] There are three different domains defined within a DSC-based self-nucleation study, depending on the applied self-nucleation temperature (T_s). Domain I is where T_s is high enough to afford a complete and isotropic melt of the polymer. Domain II can normally be recognised as two sub-domains; one is where the majority of the polymer has melted under T_s, but some crystals are left as nuclei, and the second is when the fully melted crystals retain their melt memory under T_s. Domain III is when only partial melting is produced from a low T_s. The unmelted crystals in this domain will often be annealed (**Figure 4.1**).

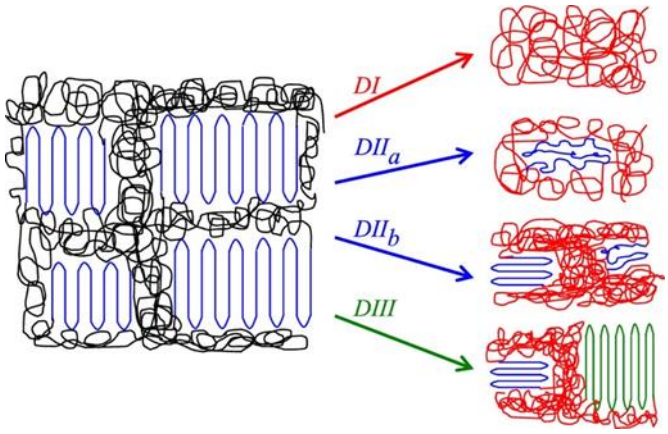

Figure 4.1 Different self-nucleation domains.[9]

In addition to DSC studies, polarised light optical microscopy (PLOM) is often utilised to observe the different forms of nuclei within the different self-nucleation domains. For example, poly(butylene succinate) (PBS) crystallising from different domains was observed using this technique, and the formation of small nuclei was illustrated during domain II, while crystals were obtained from domain III (**Figure 4.2**). Studying polymer self-nucleation in bulk is not only essential in order to understand polymer crystallisation, but also offers an approach to manipulate crystallisation processes. Hence, it is essential to comprehensively understand polymer self-nucleation, particularly when studying the crystallisation of a yet unexplored polymer.

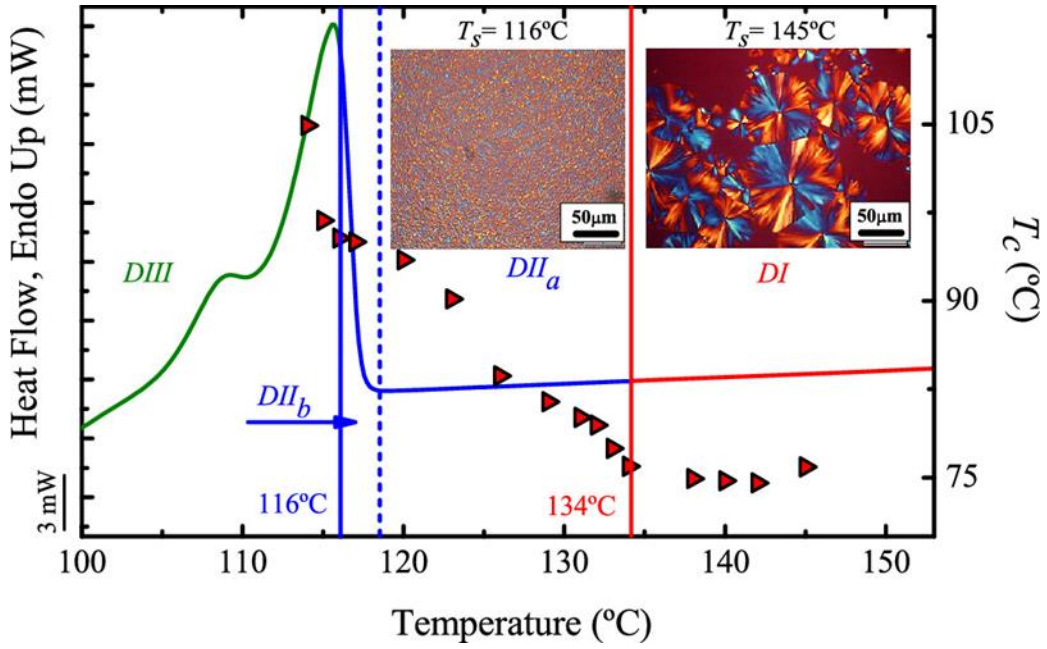

Figure 4.2 A plot of the self-nucleation domains for PBS homopolymer. Inserts show PLOM micrographs taken during cooling from Ts = 145 °C (Domain I) and Ts = 116 °C (Domain II).[10]

4.2.2 Poly(ζ-heptalactone) (PHL)

As biocompatible and biodegradable materials, polyesters have drawn great attention in many applications.[11] Thus far, most studies have been devoted to polycaprolactone and polylactide on account of their industrial availability. [12-14] Consequently, ring-opening polymerisation (ROP) is a well-established method for the production of well-defined polyesters from lactones. The ROP technique has been extensively employed for the synthesis of small ring lactones (~4-7 membered rings) and macrolactones using various catalysts which span inorganic, organic and enzymatic.[15-17] Among those lactones, η-heptalactone has been largely understudied thus far, as it is not a commercially available material. The enzymatic ROP of ζ-heptalactone has been reported, catalysed by Novozym 435.[18] The polymerisation was performed at 45°C in

toluene at a concentration of 2 mol L^{-1}. Benzyl alcohol was selected as the initiator with a monomer/initiator molar ratio of 50/1. The ζ-heptalactone reached 80% conversion in 15 minutes. Preliminary materials characterisation including polydispersity (2.8) by size-exclusion chromatography analysis and thermal properties by differential scanning calorimetry analysis were also conducted. However, a thorough study of η-heptalactone has not yet been carried out, and thus the ability to predictably synthesise low polydispersity poly(ζ-heptalactone) (PHL) with predictable molecular weights and subsequent study of the resultant thermal properties remain unknown. Given the similarity in structure to ε-caprolactone (PCL), PHL could be expected to feature comparable properties, while exhibiting different degradability from its slightly longer alkyl chain in the backbone when compared to PCL. This suggests that self-assembly of PHL copolymers could be a candidate for a wide range of biological applications. Aiming at this, synthesis of PHL block copolymers is discussed in this chapter. The crystallisation of PHL polymers was studied both in bulk and in solution. Finally, crystallisation-driven self-assembly of three PHL copolymers was explored.

4.3 Results and discussion

As ζ-heptalactone is not commercially available, it was first synthesised and characterised. The first aim was to obtain low polydispersity poly(ζ-heptalactone) (PHL) with predictable molecular weight, and therefore ROP kinetics of the HL polymerisation was studied as catalysed by an organocatalyst diphenyl phosphate. A range of different DPs of PHL homopolymers were targeted for further investigation of crystallisation kinetics.

4.3.1 Synthesis of η-heptalactone

η-heptalactone was synthesised by Baeyer-Villiger oxidation following a literature procedure. (**Scheme 4.1**)[18] Cycloheptanone and 3-chloroperbenzoic acid were mixed in CH_2Cl_2 and the suspension was heated under reflux. The consumption of cycloheptanone was monitored by ^1H NMR spectroscopy. The reaction was stopped after three days in order to prevent the occurrence of a competing hydrolysis reaction. The reaction mixture was cooled down in an ice bath and filtered over Celite. The crude product was washed and dried, and the organic layer was evaporated in vacuo to remove the solvent. The product was then distilled over CaH_2 to afford the dry ζ-heptalactone for future ring-opening polymerisations. The pure product was confirmed with ^1H NMR and ^{13}C NMR spectroscopy. (**Figure 4.3**)

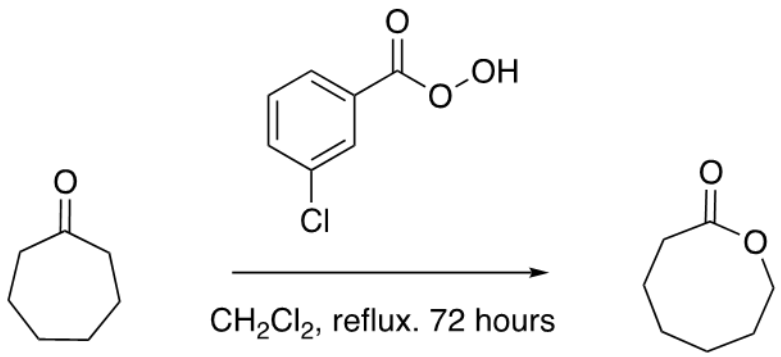

Scheme 4.1 Baeyer-Villiger oxidation of cycloheptanone.

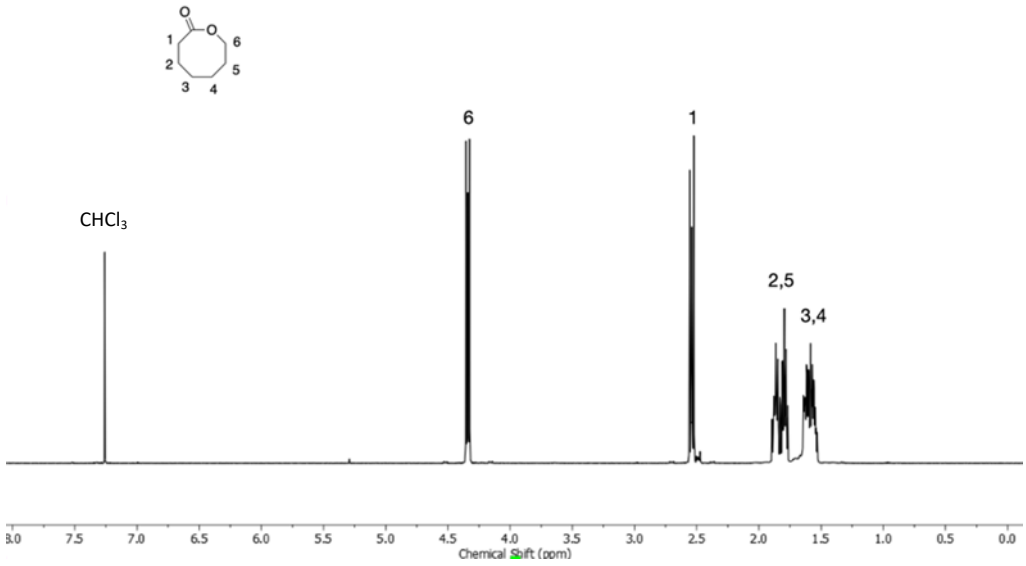

Figure 4.3 ^{1}H NMR spectrum ($CDCl_3$, 400MHz) of ζ-heptalactone.

4.3.2 ROP of HL

The homopolymerisation of η-heptalactone is lack of study thus far as a consequence of its non-commercial availability, with only limited successful reports of the polymerisation catalysed by lipase. [18] In this chapter, diphenyl phosphate (DPP) was selected as the catalyst and the polymerisation was initiated by a dual-head initiator and chain transfer agent in order to be consistent with our previously reported PCL work and Chapter 3. (**Scheme 4.2**)[19] Initially, the ROP of ζ-heptalactone was attempted at a

monomer concentration of 1 M in toluene as solvent at room temperature in an N_2 filled glovebox. Aliquots were taken periodically, and monomer conversion was monitored by ^{1}H NMR spectroscopy. The polymerisation exhibited first-order kinetics, however with only very low conversion (35%) after 5 hours (**Figure 4.4a**). Next, the polymerisation was performed with an increased monomer concentration of 4 M in toluene, aiming at a faster rate. The polymerisation reached 70% conversation after 4 hours while still exhibiting first-order kinetics (**Figure 4.4b**). Using these conditions, different DPs of PHL were targeted for further crystallisation study (**Table 4.1**). The polymer molecular weights were determined by end group analysis in ^{1}H NMR spectroscopy, comparing the ratio between the polymer $CH_2OC{=}O$ resonances of (δ = 4.05 ppm) and the chain transfer reagent $SCH_2CCN(CH_3)$ resonance (δ =3.69 ppm) (**Figure 4.5**). Size exclusion chromatography (SEC) analysis revealed low dispersities ($Đ_M$ < 1.2) and good overlap of the refractive index (RI) and ultraviolet (UV) (λ = 309 nm, corresponding to the π-π* electronic transition of the thiocarbonyl moiety) peak in the SEC traces, which signifies the retention of the RAFT end group (**Figure 4.6**).

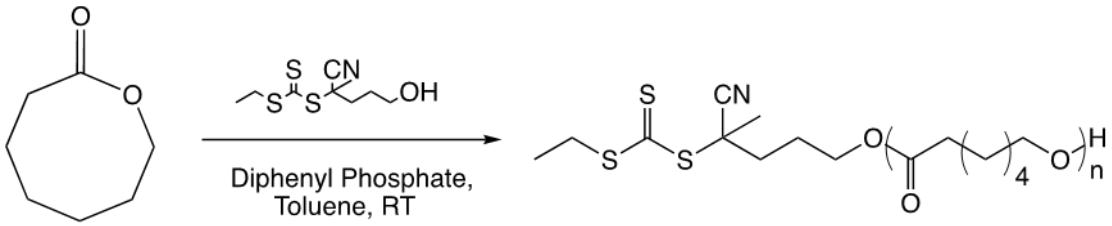

Scheme 4.2 ROP of ζ-heptalactone catalysed by DPP.

Table 4.1 Ring-opening polymerisation of ζ-heptalactone (4M) at room temperature targeting DP100 catalysed by DPP.

Time(h)	Coversion(%)	M_n[a](GPC) (kDa)	M_w[a](GPC) (kDa)	$Đ_M$	M_n[b](NMR) (kDa)
1	15	6.2	7.01	1.11	2.2
2	35	9.9	11.4	1.11	4.7
4	70	16.6	19.6	1.15	9.2
5	90	20.8	22.7	1.17	11.8

[a]Determined by SEC in $CHCl_3$ against poly(styrene) standards. [b]Determined by end-group analysis by ^1H NMR spectroscopy.

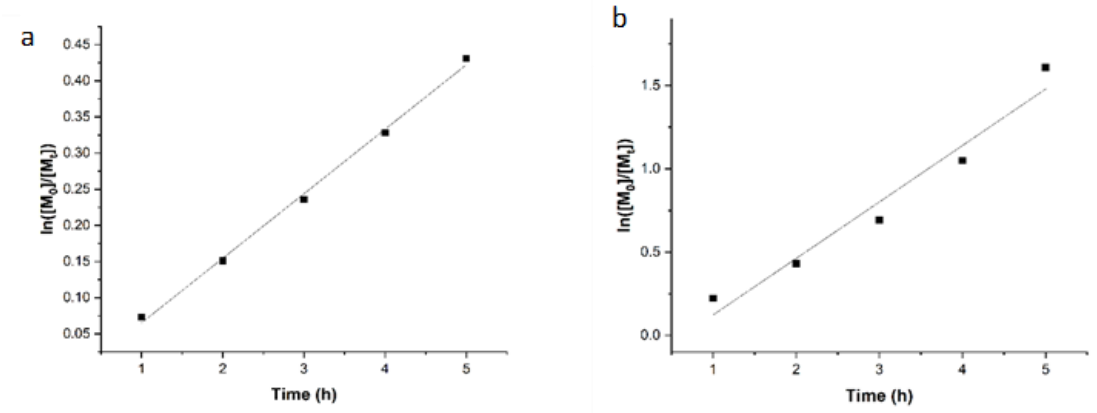

Figure 4.4 Kinetic plot for the polymerisation of ζ-heptalactone using DPP as a catalyst at room temperature in toluene with $[HL]_0$:$[CTA]_0$:$[cat.]_0$ = 100:1:1 and initial monomer concentration = 1 M(a) and 4 M (b)

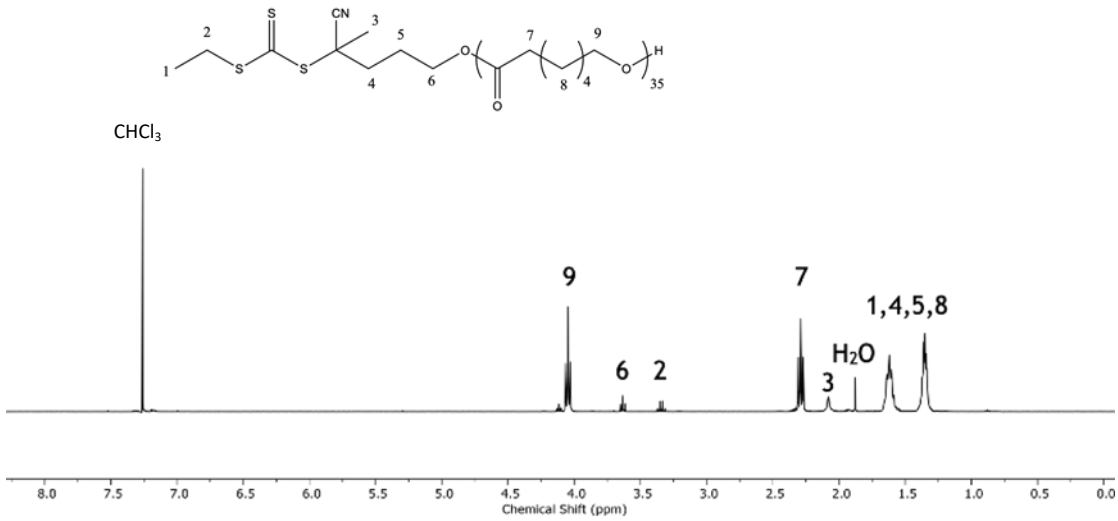

Figure 4.5 ^{1}H NMR spectrum ($CDCl_3$, 400MHz) of poly(ζ-heptalactone)$_{35}$.

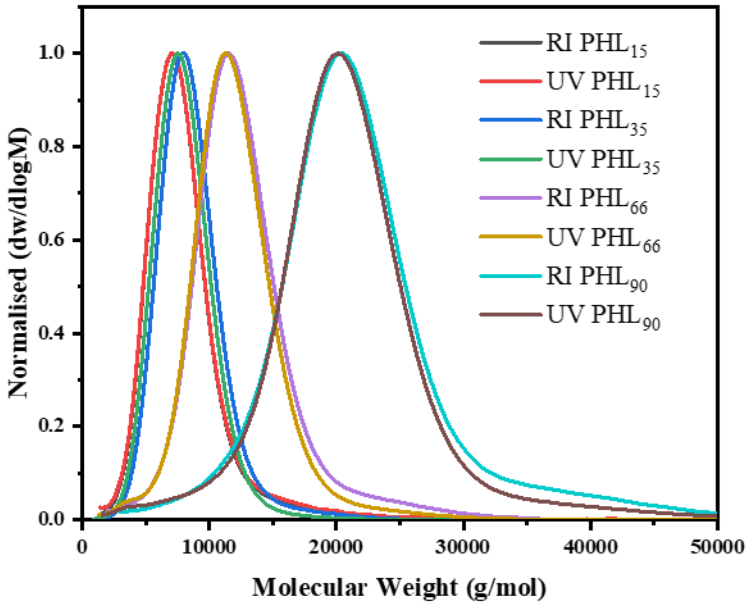

Figure 4.6 Overlaid RI and UV (λ = 309 nm) SEC chromatograms of PHL using $CHCl_3$ with 0.1% TFE as an eluent with polystyrene (PS) standards.

4.3.3 Self-nucleation study on PHL homopolymer crystallisation

The crystallisation kinetics and self-nucleation of the PHL polymers were determined through the combination of two techniques: differential scanning calorimetry (DSC) and

polarised light optical microscopy (PLOM). Non-isothermal DSC experiments were firstly performed to establish temperature windows for further thermal study. All four PHL homopolymers (PHL_{15}, PHL_{35}, PHL_{66}, PHL_{90}) were sealed in standard aluminium pans and subjected to a heating/cooling rate of 20 °C per minute under a 20 mL per minute nitrogen flow. It could be observed that both the crystallisation temperature (T_c) from a temperature of 36.6 °C to 41.7 °C and melting temperature (T_m) from a temperature of 55.1 °C to 62.0 °C are increasing with the polymer DP (**Figure 4.7**).

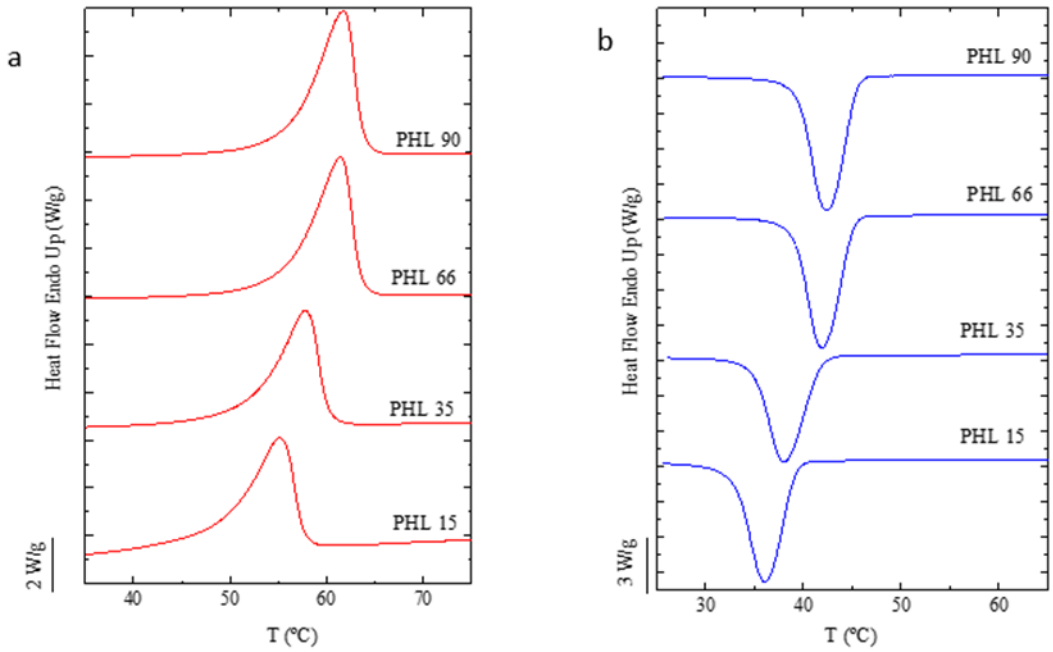

Figure 4.7 DSC thermograms (second heating curve) showing the (a)T_m and (b) T_c of the PHL homopolymers.

Isothermal differential scanning calorimetry experiments were then performed to investigate the overall crystallisation kinetics of the PHL homopolymers. The objective of an isothermal DSC experiment is to determine the minimum isothermal crystallisation

temperature $T_{c,min}$. After heating to a temperature (75 °C) high enough to remove any thermal history, all samples were quenched to the T_c values obtained from the non-isothermal DSC experiments at a rate of 60 °C min^{-1}. The samples were then immediately heated to temperatures above the T_m measured from the non-isothermal DSC experiments. Any detected melting enthalpy from this heating scan indicates that the sample was able to crystallise during the first cooling step to T_c. As such, this indicates T_c value should not be considered as $T_{c,min}$. A higher T_c value will then be explored following the same protocol.

Once the $T_{c,min}$ was determined, the isothermal crystallisation experiments were performed, following the procedure described in the literature. [20] The polymers were first heated from room temperature up to 30 °C above their melting point at a rate of 10 °C min^{-1}, and held for 3 minutes to remove the thermal history. The polymers were then quenched to the predetermined T_c at a rate of 60 °C min^{-1} and kept at this temperature to allow saturated isothermal crystallisation. Finally, the polymers were heated back to 30 °C above the T_m at 10 °C min^{-1} to observe the isothermal crystallisation at this T_c value. The equilibrium melting temperature of the sample could be calculated from the final melting runs by employing the Hoffman-Weeks extrapolation.

Following the above procedure, isothermal crystallisation kinetics of PHL homopolymers (PHL_{15}, PHL_{35}, PHL_{66}, PHL_{90}) were determined by isothermal DSC experiments. Isothermal crystallisation was performed at the various T_c values of each polymer (**Figure 4.8**). It was clearly demonstrated that the crystallisation rate was dominated by the cooling temperature, and that the cooling range increased with the molecular weight of PHL subjecting to its increasing melting temperature (**Figure 4.9**).

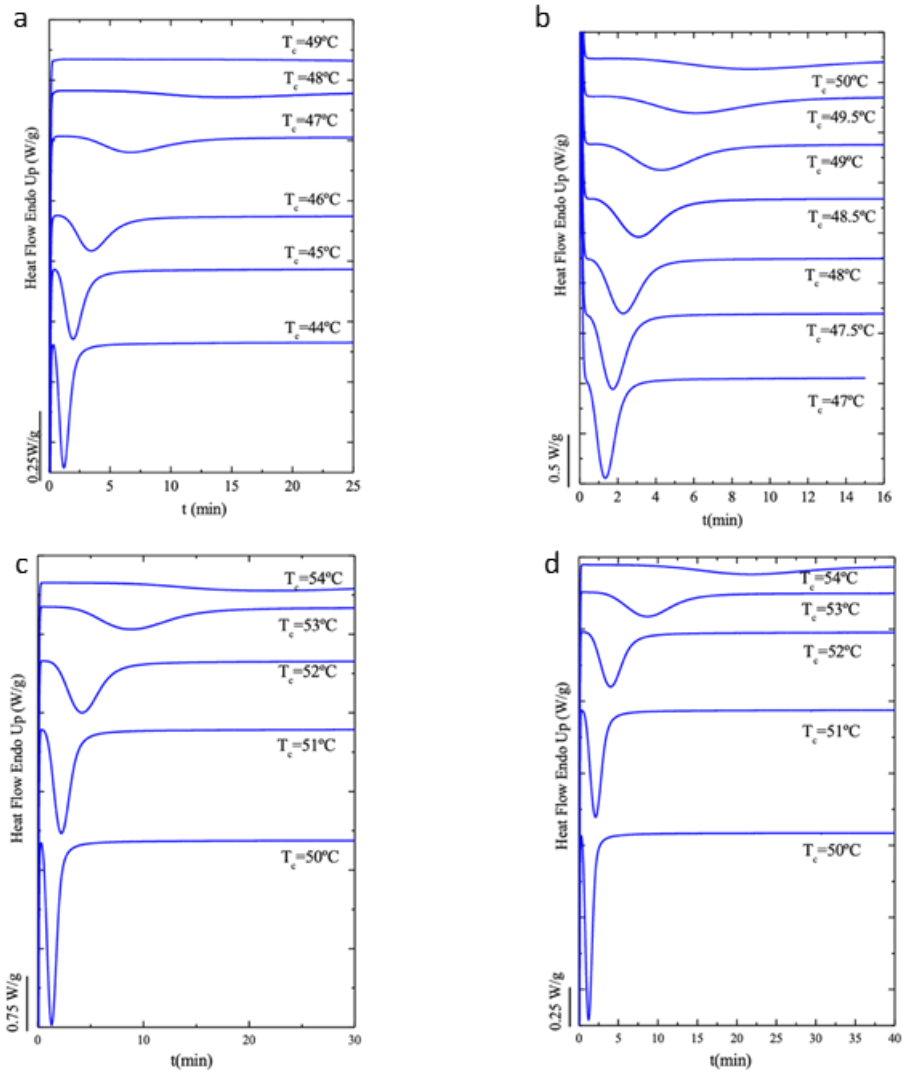

Figure 4.8 Isothermal crystallisation of (a) PHL_{15}, (b) PHL_{35}, (c) PHL_{66} and (d) PHL_{90} at different T_c.

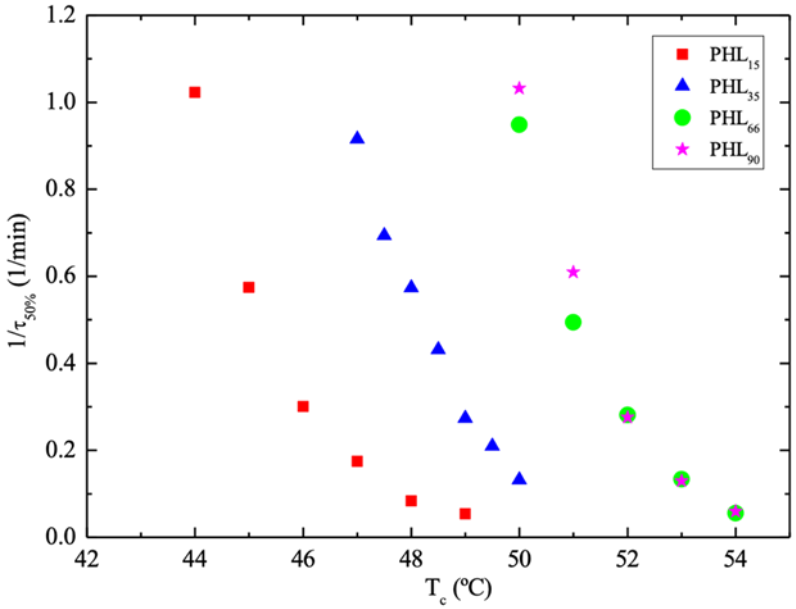

Figure 4.9 Overall crystallization versus isothermal crystallization temperature of PHL homopolymers. τ50% is the crystallisation half-life.

The Hoffman−Weeks extrapolation is a commonly used method employed to estimate the equilibrium melting temperature (T_m°).[21] The measured T_m values of the PHL homopolymers crystallised at different crystallisation temperatures (T_cs) are plotted against T_c, and the intercept of the linear extrapolation to the line $T_m = T_c$ gives T_m°.(**Figure 4.10**) The Hoffman−Weeks equation can be abbreviated to:

$$T_m = T_m^\circ\left(1 - \frac{1}{\beta}\right) + \frac{T_c}{\beta}$$

Equation 4.1 Hoffman−Weeks extrapolation

where T_m is the experimental melting temperature of crystal formed at temperature T_c, β is the thickening parameter.

The determined T_m and T_c were then compared with other lactones, both T_m and T_c increased with the increasing number of methylene units, which correlates with literature (**Table 4.2**).[22]

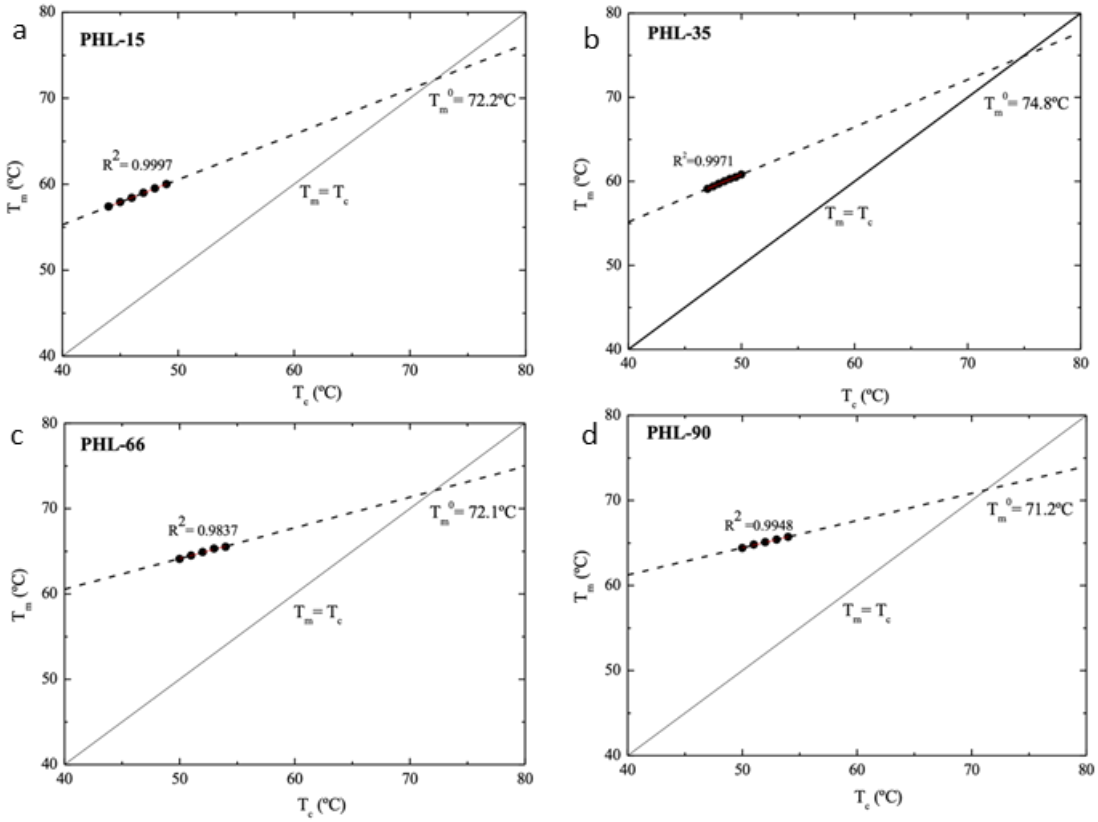

Figure 4.10 Estimated equilibrium melting temperature (T_m°) from Hoffman–Weeks extrapolation of (a) PHL_{15}, (b) PHL_{35}, (c) PHL_{66} and (d) PHL_{90}.

Table 4.2 T_m and T_c of different polylactones.

	PVL	**PCL**	**PHL**	**PPDL**
T_m (°C)	57.9	68.9	71.2	97.4
T_c (°C)	37.2	38.9	40.0	75.2

T_m and T_c of poly(δ-valerolactone) (PVL), poly(ε-caprolactone) (PCL) and poly(pentadecalactone) (PPDL) were predicted by literature.[22]

In order to understand the self-nucleation of PHL polymers, polarised light optical microscopy (PLOM) experiments were also carried out to observe the PHL nuclei from different crystallisation domains. When crystalline polymers were quenched from a homogenous melt into a low temperature, a sphere-shaped superstructure could be observed using PLOM and described as a spherulite. The spherulite observed by PLOM generally has two main characteristic patterns: extinction rings and Maltese crosses.(**Figure 4.11a**)[23] The average size of spherulites could vary as a function of crystallisation time and temperature during isothermal crystallisation. As such, PLOM could be used to evaluate the average growth rate of spherulites to further understand the self-nucleation kinetics of crystalline polymers. However, during the preliminary experiments of PHL homopolymers quenched from their $T_{c,min}$, the growth of spherulites could not be observed from PLOM as they are appeared to be highly dense (**Figure 4.11b,c**). Further PLOM experiments are yet to be performed to study the self-nucleation of PHL polymers crystallisation at different temperatures.

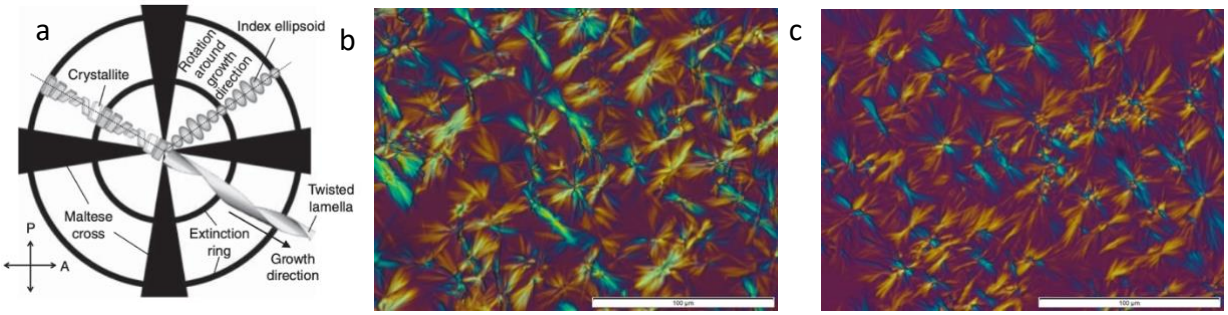

Figure 4.11 Illustration of (a) a typical spherulite, (b) PHL_{15} and (c) PHL_{35} self-nucleation from super cooling observed by polarised light optical microscopy (PLOM).

4.3.3 Synthesis of PHL diblock copolymers

On account of having a longer repeating carbonyl chain, the prepared PHL_{35} was subsequently used as a macro-chain transfer agent for RAFT polymerisation, chosen to maintain a similar hydrophobicity to PVL_{50} in Chapter 3. Three different monomers: *N*,*N*-dimethylacrylamide (DMA), *N*-isopropylacrylamide (NIPAm) and 2-(Dimethylamino)ethyl methacrylate (DMAEMA) were investigated in order to understand the effect of corona chemistry on self-nucleation during crystallisation-driven self-assembly in solution (**Scheme 4.3**). As such, the same final DP was targeted for each monomer (**Table 4.3**).

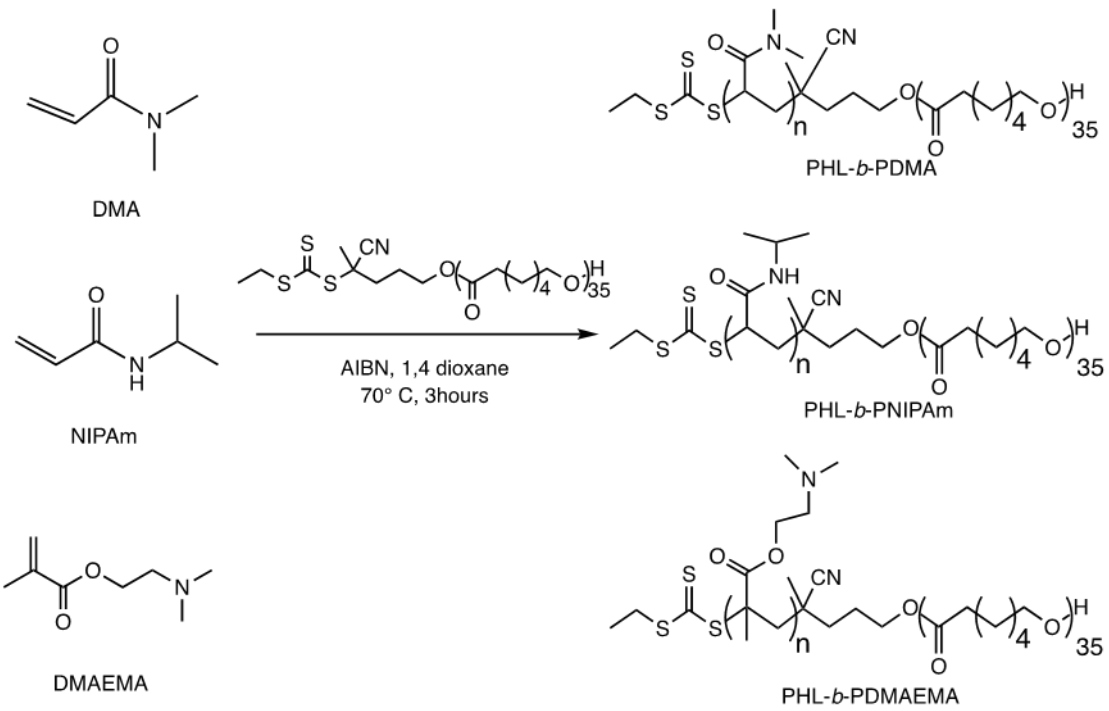

Scheme 4.3 Synthesis route of PHL block copolymers.

Table 4.3 Synthesis of PHL copolymerisation with different second blocks.

Monomer	PHL:monomer	Time (h)	Coversion (%)	M_n[a](GPC) (kDa)	M_w[a](GPC) (kDa)	$Đ_M$	M_n[b](NMR) (kDa)
DMA	1:175	3	79	29.8	36.5	1.22	18.6
NIPAm	1:175	6	82	27.4	37.2	1.22	20.5
DMAEMA	1:175	16	76	29.4	38.0	1.23	26.7

[a]Determined by SEC in $CHCl_3$ against polystyrene standards. [b]Determined by end-group analysis by ^{1}H NMR spectroscopy.

All polymerisations were carried out in 1,4-dioxane at 70 °C to ensure full solubilisation of PHL, using 2,2-azobis(2-methylpropionitrile) (AIBN) as the radical initiator. The polymerisation of DMA was quenched after two hours with a final conversion of 90%. The polymer was purified by precipitation into n-hexane followed by centrifugation to isolate the pure product. A chain extension of DP 138 (targeted 150) of the DMA hydrophilic block was confirmed by ^{1}H NMR spectroscopy, whereby the peak at δ = 2.90 ppm corresponds to the 6 protons of the dimethyl groups and the α-methylene resonance of PVL (δ = 4.05 ppm) (**Figure 4.12**). SEC analysis in $CHCl_3$ was also used to characterise the resultant polymer, where a clear molecular weight shift compared to the PVL homopolymer could be observed. The retention of RAFT group was confirmed by the overlapping of the RI and UV traces (λ = 309 nm) (**Figure 4.13**). A low molecular weight tail is observed in UV trace, indicating the presence of PHL homopolymer. This is due to inefficient initiating from the reduced solubility of PHL in 1,4-dioxane compared to PVL in Chapter 3.

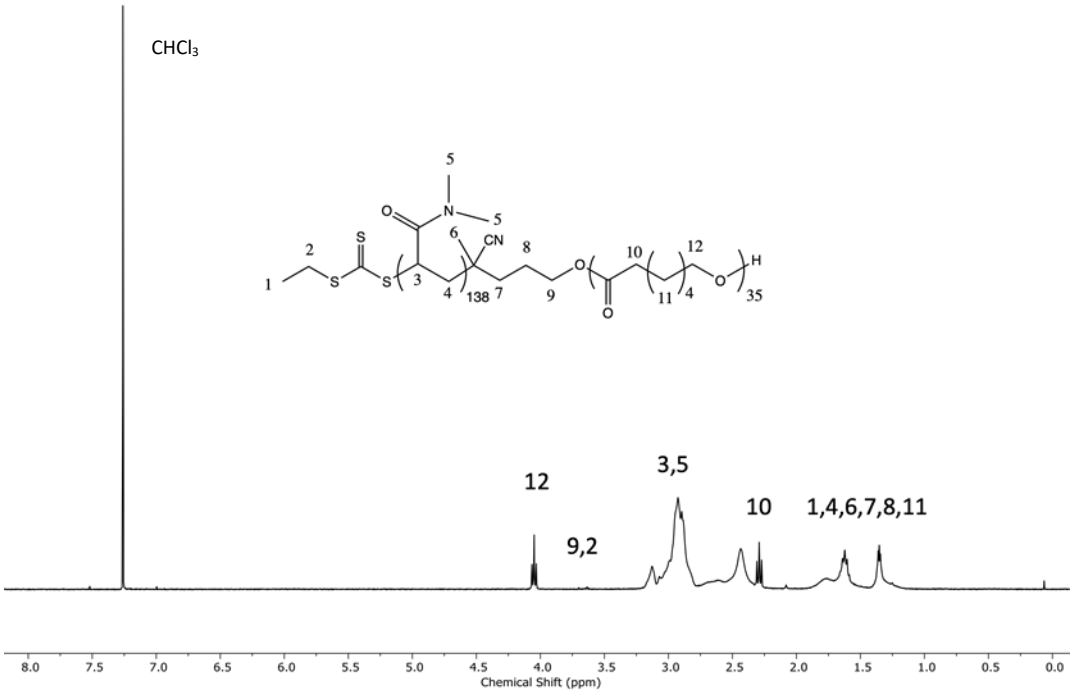

Figure 4.12 ^{1}H NMR spectrum ($CDCl_3$, 400MHz) of PHL_{35}-*b*-$PDMA_{138}$.

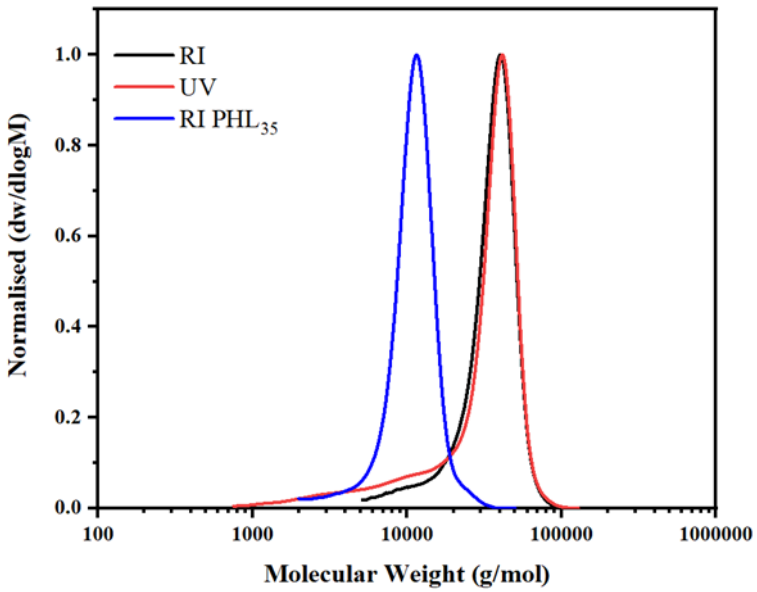

Figure 4.13 Overlaid RI and UV (λ = 309 nm) SEC chromatograms of PHL_{35}-*b*-$PDMA_{138}$ using $CHCl_3$ with 0.1% TFE as an eluent with polystyrene (PS) standards.

The polymerisation of NIPAm was quenched after six hours, reaching 80% conversion. The polymer was purified by precipitation into hexane followed by centrifugation as above. A chain extension of DP 143 of the NIPAm hydrophilic block was confirmed by ^{1}H NMR spectroscopy. The peak at δ = 1.12 ppm corresponds to the 6 protons of the dimethyl groups and the α-methylene resonance of PHL (δ = 4.05 ppm) (**Figure 4.14**). SEC analysis in $CHCl_3$ was also used to characterise the resultant polymer, where a clear molecular weight shift compared to the PVL homopolymer could be observed. The retention of RAFT group was confirmed by the overlapping of the RI and UV traces (λ = 309 nm) (**Figure 4.15**).

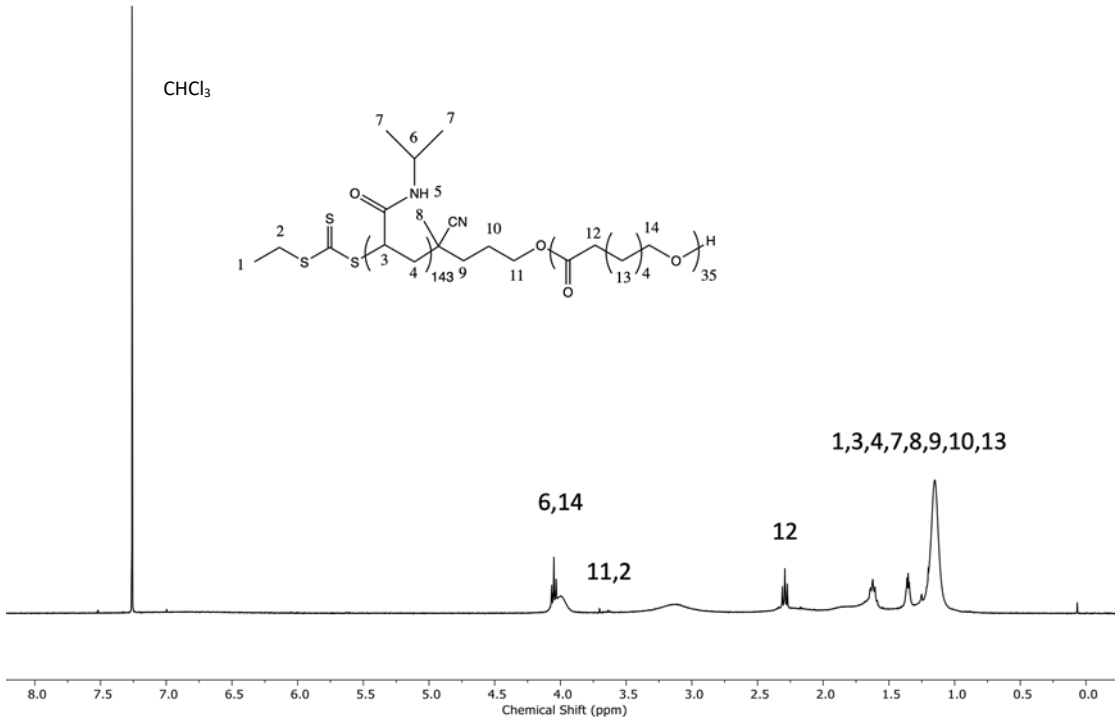

Figure 4.14 ^{1}H NMR spectrum ($CDCl_3$, 400MHz) of PHL_{35}-*b*-$PNIPAm_{143}$.

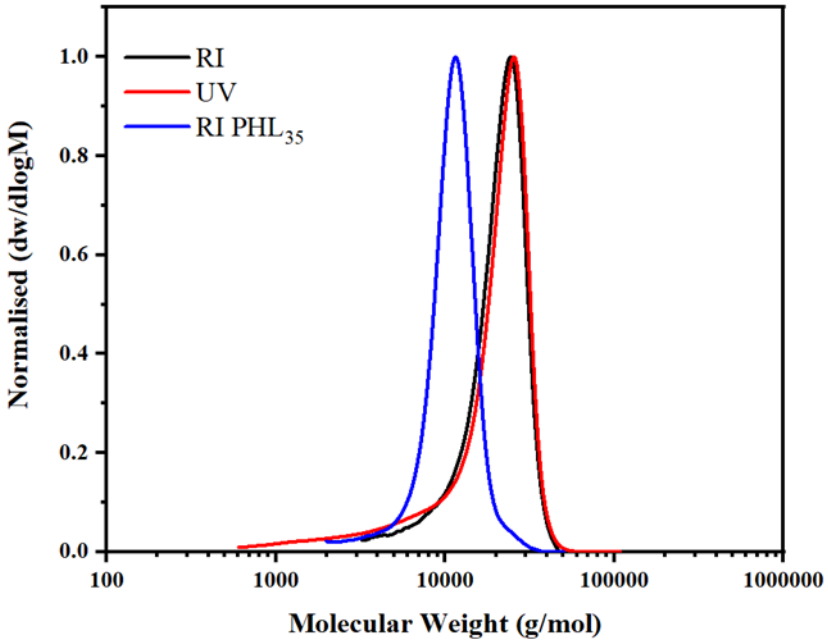

Figure 4.15 Overlaid RI and UV (λ = 309 nm) SEC chromatograms of PHL_{35}-*b*-$PNIPAm_{143}$ using $CHCl_3$ with 0.1% TFE as an eluent with polystyrene (PS) standards.

The same procedure was followed for the polymerisation of DMAEMA. The conversation of DMAEMA reached 76% after sixteen hours. The polymer was purified by precipitation into n-hexane, followed by centrifugation to isolate the pure product. A chain extension of DP 131 of the DMAEMA hydrophilic block was confirmed by ^{1}H NMR spectroscopy. The peak at δ = 2.28 ppm corresponds to the 6 protons of the dimethyl groups and the α-methylene resonance of PHL (δ = 4.05 ppm) (**Figure 4.16**). SEC analysis in $CHCl_3$ was also used to characterise the resultant polymer, where a clear molecular weight shift compared to the PHL homopolymers could be observed. The retention of RAFT group was confirmed by the overlapping of the RI and UV traces (λ = 309 nm) (**Figure 4.17**).

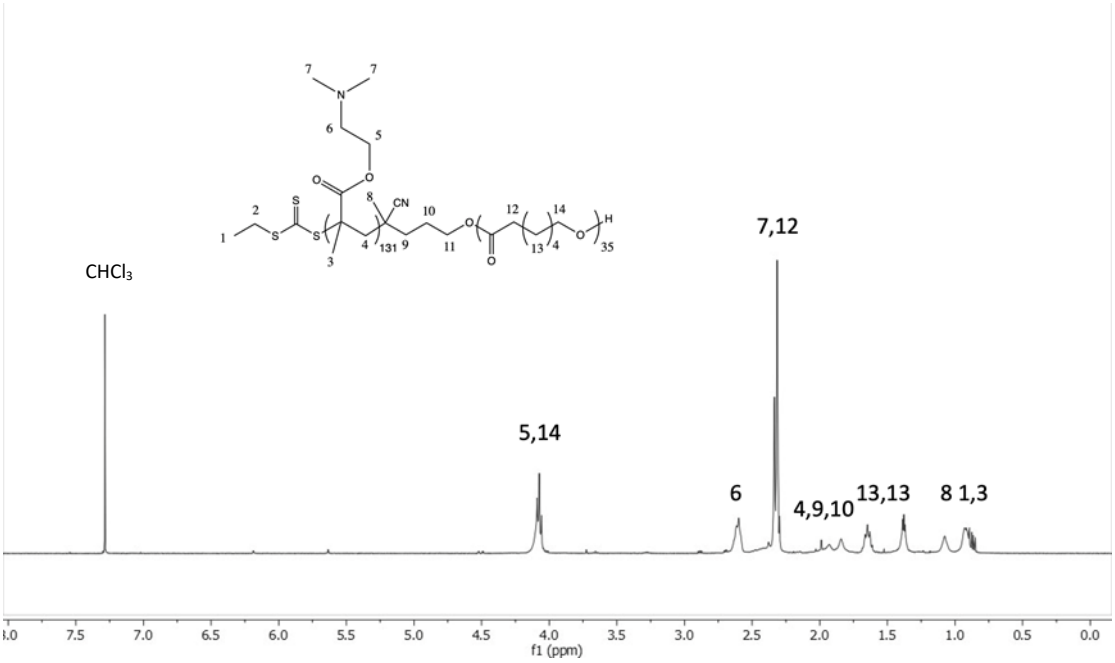

Figure 4.16 ^{1}H NMR spectrum ($CDCl_3$, 400MHz) of PHL_{35}-*b*-$PDMAEMA_{131}$.

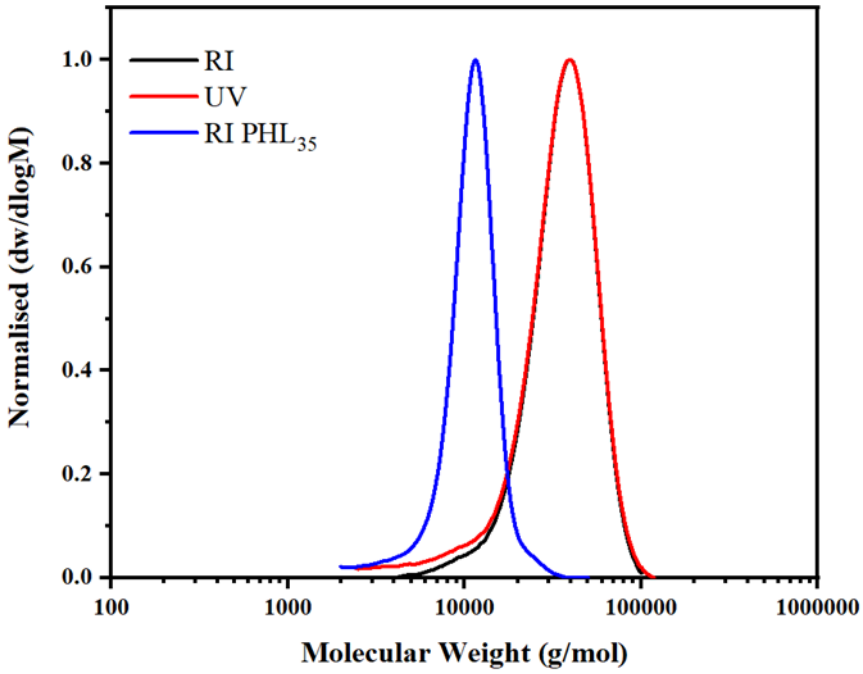

Figure 4.17 Overlaid RI and UV (λ = 309 nm) SEC chromatograms of PHL_{35}-*b*-$PDMAEMA_{131}$ using $CHCl_3$ with 0.1% TFE as an eluent with polystyrene (PS) standards.

4.3.5 CDSA of PHL diblock copolymers

The crystallisation-driven self-assembly of PHL copolymers has never been reported to date, and therefore the next objective was to explore the CDSA of this novel system. NanoDSC experiments were first performed in order to understand the thermal behaviour of PHL diblock copolymers in solution. The temperature window examined in the nanoDSC experiments exceeded the melting temperature of the PHL homopolymer obtained from the initial DSC measurements. Non-isothermal experiments in nanoDSC were performed as such: PHL_{35}-*b*-$PDMA_{138}$, PHL_{35}-*b*-$PNIPAm_{143}$ and PHL_{35}-*b*-$PDMAEMA_{131}$ were heated in ethanol to 70 °C before cooling down to 0 °C at 1 °C per minute. The melting and crystallisation temperatures from the second cycle were compared (**Table 4.4**, **Figure 4.18**). Both the melting and crystallisation temperatures of all three polymers suffered a decrease due to the solvent plasticising effect, which is consistent with observations in Chapter 2 and Chapter 3. It is of note that with different corona chemistries, both the T_m and T_c in ethanol decreased while the solubility of corona block increased. As the melting temperature of PHL copolymers in NanoDSC represents from the disassembly of micelles and melting of core-forming block, where the disassembly of micelles could be associated by a more soluble corona block, hence, a lower temperature is required. Meanwhile, a lower temperature is required for the polymer to crystallise from solvent with a more soluble corona block.

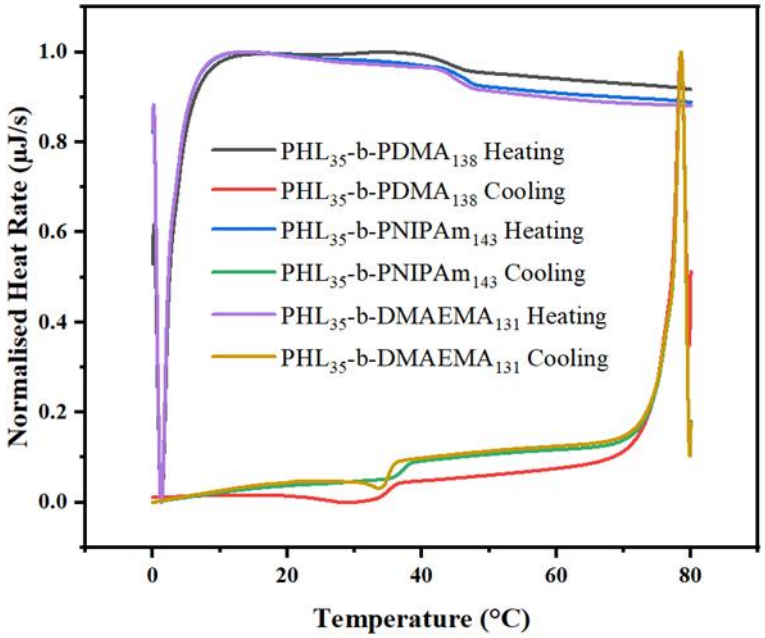

Figure 4.18 Nano Differential scanning calorimetry thermograms of PHL block copolymers in ethanol, second heating and cooling curve at a rate of 1°C per minute.

Table 4.4 Summary of melting and crystallisation temperatures of PHL_{35}-b-$PDMA_{140}$, PHL_{35}-b-$PNIPAm_{140}$, PHL_{35}-b-$PDMAEMA_{140}$ in ethanol measured by Nano Differential scanning calorimetry (second cycle).

	PHL_{35}-*b*-$PDMA_{138}$	**PHL_{35}-*b*-$PNIPAm_{143}$**	**PHL_{35}-*b*-$PDMAEMA_{131}$**
T_m(°C)	42	41	38
T_c(°C)	35	33	31

Based on the NanoDSC experiments of the PHL diblock copolymers, crystallisation-driven self-assembly of PHL_{35}-*b*-$PDMA_{138}$, PHL_{35}-*b*-$PNIPAm_{143}$ and PHL_{35}-*b*-$PDMAEMA_{131}$ were then explored in ethanol, as this is a model solvent for reported the CDSA of PCL_{50}-

b-PDMA$_{190}$.[19] 5mg/mL of each PHL copolymer was heated to 70 °C in ethanol and annealed for three hours to allow complete melting of the polymer in solution. The solutions were then slowly cooled down to room temperature to initiate the first phase of nucleation of the PHL copolymers. All solutions were then aged for three days to allow full crystallisation of PHL copolymer, and then diluted to 0.5 mg/mL, dropped on a TEM grid and stained for TEM analysis. Cylindrical structures were observed from PHL$_{35}$-*b*-PNIPAm$_{143}$, while mixed morphologies of cylinders and lamellae were seen in PHL$_{35}$-*b*-PDMA$_{138}$ and spheres from PHL$_{35}$-*b*-PDMAEMA$_{131}$ (**Figure 4.19**). During the CDSA of PHL$_{35}$-*b*-PDMA$_{138}$ the less soluble corona block leads to a partial phase separation before the crystallisation process. The PHL, therefore, undergoes a crystallisation of confinement, resulting in lamellae. At the same time, some of the PHL$_{35}$-*b*-PDMA$_{138}$ was able to form a phase separation (micellisation) of the semi-crystalline core in solution, resulting in cylindrical micelles. In the case of PHL$_{35}$-*b*-PNIPAm$_{143}$, with an increased solubility of the corona block, all polymer chains were able to self-assemble from core crystallisation. This allows the formation of homogenous low curvature cylindrical micelles. However, when the steric repulsion of the corona is too strong, such as for the PHL$_{35}$-*b*-PDMAEMA$_{131}$, the PHL block is not able to crystallise until phase separation is caused by a critical low temperature. Spherical micelles with an amorphous core are the result of this process. This suggests block copolymer self-nucleation could also be modified by the solubility of corona block, leading to different morphologies in CDSA.

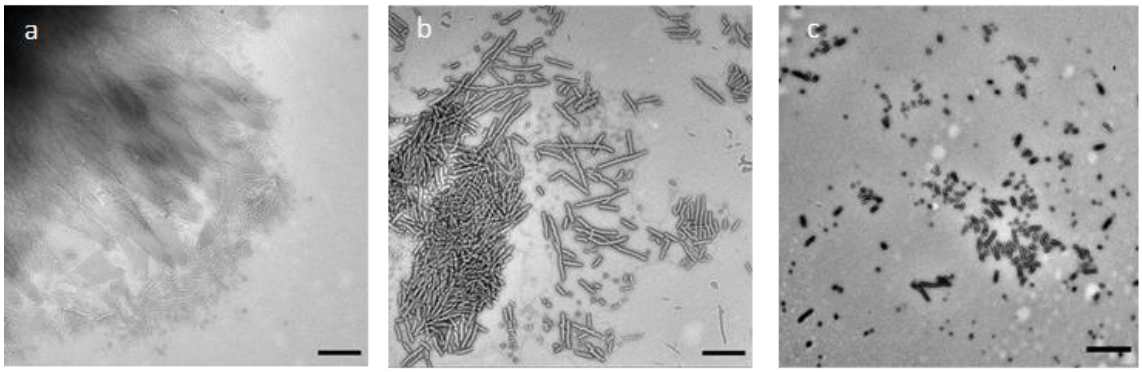

Figure 4.19 TEM micrographs of cylindrical micelles prepared using (a) PHL_{35}-*b*-$PDMA_{138}$, (b) PHL_{35}-*b*-$PNIPAm_{143}$, (c) PHL_{35}-*b*-$PDMAEMA_{131}$ by self-nucleation in ethanol heating at 70 °C for 3 hours and subsequently cooling down to room temperature. All samples were aged for 3 days, stained with 1 wt. % uranyl acetate in water. Scale bar = 500 nm.

4.4 Conclusions

The ring-opening polymerisation of ζ-heptalactone has been investigated using the commercially available organic catalyst diphenyl phosphate. First-order kinetics of the reaction and controlled molecular weight polymers were achieved, as well as a low polydispersity. Crystallisation and melting temperature of different poly(ζ-heptalactone) (PHL) homopolymers were demonstrated from isothermal DSC experiments along with well-established crystallisation kinetics. PHL block copolymers of different corona block were then synthesised for further exploration of PHL polymer crystallisation in solution. NanoDSC experiments revealed the correlation between corona solubility and self-nucleation in the solution for the PHL copolymers. The self-nucleation of PHL copolymers in solution driven by different corona chemistries played an important role in associating phase separation and polymer crystallisation. The staggered phase separation and polymer crystallisation could result in various shapes of nanoparticles prepared by CDSA. This suggests a method to demonstrate the corona effect during CDSA with same core-forming block copolymers.

4.5 Experimental

4.5.1 Materials

Chemicals and solvents were purchased from Sigma Aldrich, Acros, Fluka, Fisher Chemical, Alfa Aesar, or VWR. Dry solvents were purified using MBRAUN SPS solvent purification system. η-heptalactone was dried over calcium hydride for 24 hours before vacuum distillation. 1,4-dioxane, *N,N*-dimethylacrylamide (DMA) and 2-(dimethylamino)ethyl methacrylate (DMAEMA) were purified by passing through basic alumina before use. *N*-Isopropylacrylamide (NIPAm) was recrystallised twice from n-hexane. 2,2'-azobis(2-methylpropionitrile) (AIBN) was recrystallised twice from methanol and stored in the dark at 4 °C.

4.5.2 Instrumentation

^{1}H and ^{13}C nuclear magnetic resonance (NMR) spectra were recorded at 400 MHz on a Bruker DPX-400 spectrometer in $CDCl_3$ unless otherwise stated. Chemical shifts are reported as δ in parts per million (ppm) downfield from the internal standard trimethylsilane.

Size exclusion chromatography (SEC) was performed on an Agilent 390-MDS on PLgel Mixed-D type columns in series with refractive index (RI) detection. Weights were calculated using a calibration curve determined from poly(styrene) standards with chloroform (0.5% NEt_3) as eluent flowing at 1.0 $mL.min^{-1}$ and sample concentration 3 mg mL^{-1}.

Nano Differential scanning calorimetry (NanoDSC) was performed on a TA NanoDSC. 800µL samples were run at a heating or cooling ramp series of 1 °C min^{-1} in triplicate under a constant 3 atmosphere pressure. T_c and T_m of various samples were obtained in the second runs and were taken as the midpoint of the inflection tangent.

Samples for transmission electron microscopy (TEM) analysis were prepared by drop casting 10 µL of polymer in ethanol (0.5 mg mL^{-1}) onto a carbon/formvar-coated copper grid placed on filter paper. Samples were stained with a 1% uranyl acetate solution to facilitate imaging of the thin organic structures unless specified. Imaging for samples was performed on a Jeol 2100 transmission electron microscope operating at 120 kV. TEM images were analysed by ImageJ software.

4.5.3 Synthesis of ζ-heptalactone

The cycloheptanone (223 mmol) and m-chloroperbenzoic acid (275 mmol) were mixed in CH_2Cl_2 (250 mL). The suspension was heated under reflux for three days. The reaction mixture was cooled in an ice bath, and the solids were filtered over Celite and washed with CH_2Cl_2 (2 × 50 mL). The filtrate was washed with 10% $Na_2S_2O_3$ solution (2 × 200 mL), saturated Na_2CO_3 solution (2 × 200 mL), and saturated NaCl solution (1 × 200 mL). The organic layer was dried with $MgSO_4$, filtered, and evaporated in vacuo. The resulting liquid was distilled over CaH_2 to afford the lactone in yields of around 70%.

^{1}H NMR (400 MHz, 298 K, $CDCl_3$): δ = 4.28 (t, 2H, C*H*$_2$O), 2.48 (t, 2H, C*H*$_2$C=OO), 1.75 (m, 4H, C*H*$_2$), 1.52 (m, 4H, C*H*$_2$) ppm. ^{13}C NMR (125 MHz, 298 K, $CDCl_3$): δ = 176.4 (O*C*OCH_2), 64.3 (OCO*C*H_2), 31.0 (*C*H_2COO), 30.5 (OCH_2*C*H_2), 28.0 (*C*$H_2$$CH_2$COO), 25.4 (*C*$H_2$$CH_2$ CH_2COO) and 23.5 (O$CH_2$$CH_3$*C*$H_2$) ppm.

4.5.4 Synthesis of poly(ζ-heptalactone)

In a nitrogen-filled glove box, solutions of diphenylphosphate (10 mg, 0.04 mmol) in dry toluene (1 mL) and dual-head CTA (9.92 mg, 0.04 mmol) in dry toluene (1 mL) were added to ζ-heptalactone (490 µL, 4 mmol). After stirring at room temperature for a defined time period, the solution was removed from the glove box, precipitated three times into ice-cold methanol and collected by centrifugation. It should be noted that the polymers must have no evidence of high or low molecular weight shoulders by SEC before proceeding with RAFT polymerizations and self-assembly. ^{1}H NMR (400 MHz, $CDCl_3$) δ/ppm: 4.04-4.11 (t, C*H*$_2$OH), 3.63 (m, C(CN)C*H*$_2$CH$_2$), 3.33 (q, SC*H*$_2$CH$_3$), 2.28 (t, OCOC*H*$_2$), 1.61-1.35 (m, OCOCH$_2$(C*H*$_2$)$_3$CH$_2$OH).

4.5.5 Synthesis of PHL_{35}-*b*-$PDMA_{138}$

PHL_{35} (100 mg, 0.021 mmol), DMA (366.8 mg, 3.70 mmol) and AIBN (41.4 µL of a 10 mg mL^{-1} solution in 1,4-dioxane, 2.52 µmol) were dissolved in 1,4-dioxane (1 mL) and placed in an ampoule. After three freeze- pump-thaw cycles, the solution was heated for 3 hours at 70 °C. The reaction was quenched by immersion of the ampoule in liquid nitrogen and the polymer was precipitated in ice-cold diethyl ether three times before drying under vacuum. ^{1}H NMR (400 MHz, $CDCl_3$) δ (ppm) 4.04 (t, 70H, C*H*$_2$OH), 3.13-2.29 (m, 1050H, N(*CH*$_3$)$_2$, C*H*CH$_2$ (PDMA), OCOC*H*$_2$ (PHL)), 1.96-1.35 (m, 567H, OCOC*H*$_2$ (PHL), OCOCH$_2$(C*H*$_2$)$_4$CH$_2$OH (PHL), CHC*H*$_2$ (PDMA)).

4.5.6 Synthesis of PHL_{35}-*b*-$NIPAm_{143}$

PHL_{35} (100 mg, 0.021 mmol), NIPAm (418.7 mg, 3.70 mmol), 1,3,5-trioxane (18.9 mg, 0.21 mmol) and AIBN (41.4 µL of a 10 mg mL^{-1} solution in 1,4-dioxane, 2.52 µmol) were

dissolved in 1,4-dioxane (1 mL) and placed in an ampoule. After three freeze- pump-thaw cycles, the solution was heated for 6 hours at 70 °C. Conversion was monitored by the ratio of NIPAm and 1,3,5-trioxane. The reaction was quenched by immersion of the ampoule in liquid nitrogen and the polymer was precipitated in ice-cold diethyl ether three times before drying under vacuum. ^{1}H NMR (400 MHz, $CDCl_3$) δ (ppm) 7.0-5.6 (br, 140H, N*H*CH$(CH_3)_2$), 4.04-4.00 (t, 210H, C*H*$_2$OH(PHL), NHC*H*$(CH_3)_2$ (NIPAM)), 2.29-1.35 (m, 711H, OCOCH$_2$(C*H*$_2$)$_4$CH$_2$OH (PHL), C*H*C*H*$_2$ (PNIPAm)), 1.13 (m, 842H, NHCH$(CH_3)_2$ (NIPAM)).

4.5.5 Synthesis of PHL_{35}-*b*-$PDMAEMA_{131}$

PHL_{35} (100 mg, 0.019 mmol), DMA (470.9 mg, 4.75 mmol) and AIBN (37.4 µL of a 10 mg mL^{-1} solution in 1,4-dioxane, 2.28 µmol) were dissolved in 1,4-dioxane (1 mL) and placed in an ampoule. After three freeze- pump-thaw cycles, the solution was heated for 16 hours at 70 °C. The reaction was quenched by immersion of the ampoule in liquid nitrogen and the polymer was precipitated in ice-cold diethyl ether three times before drying under vacuum. $M_{n,\,NMR}$ = 24.5 kDa, DP = 194. $M_{n,\,SEC}$ = 28.7 kDa, $Đ_M$ = 1.09. ^{1}H NMR (400 MHz, $CDCl_3$) δ (ppm) 4.03 (t, 100H, C*H*$_2$OH), 3.23-2.28 (m, 1250H, N(*CH*$_3$)$_2$, C*H*CH$_2$ from PDMA), 2.28-0.79 (m, 788H, OCOC*H*$_2$ (PVL), OCO(C*H*$_2$)$_4$OH (PVL), CHC*H*$_2$ (PDMA)).

4.5.6 Typical crystallisation-driven self-assembly method for the self-nucleation of PHL block copolymers

PHL block copolymers (10 mg) was added to 5 mL of ethanol (5 mg mL^{-1}) in a 7 mL vial and heated at 70 °C without stirring for 3 hours before cooling to room temperature. Samples were imaged after 5 days of ageing at room temperature.

4.6 Acknowledgements

Differential scanning calorimetry and polarised light optical microscopy study were carried out by Asier Olmos and Maira Caputo.

4.7 References

1. B. Wunderlich, *Macromolecular Physics V2*, Elsevier, 2012.
2. L. Mandelkern, *Crystallization of Polymers: Volume 2, Kinetics and Mechanisms*, Cambridge University Press, 2004.
3. A. C. Zettlemoyer, *Nucleation.* 1969.
4. R. Cormia, F. Price and D. Turnbull, *J. Chem. Phys.*, 1962, **37**, 1333-1340.
5. A. Sharples, *Polymer*, 1962, **3**, 250-252.
6. A. Sharples, 1966.
7. D. C. Bassett and D. C. Bassett, *Principles of polymer morphology*, CUP Archive, 1981.
8. B. Fillon, J. Wittmann, B. Lotz and A. Thierry, *J. Polym. Sci. B Polym. Phys.*, 1993, **31**, 1383-1393.
9. R. Michell, A. Mugica, M. Zubitur and A. Müller, in *Polymer Crystallization I*, Springer, 2015, pp. 215-256.
10. L. Sangroniz, D. Cavallo and A. J. Müller, *Macromolecules*, 2020, **53**, 4581-4604.
11. A.-C. Albertsson and I. K. Varma, *Biomacromolecules*, 2003, **4**, 1466-1486.
12. L. Ghasemi-Mobarakeh, M. P. Prabhakaran, M. Morshed, M. H. Nasr-Esfahani and S. Ramakrishna, *Mater. Sci. Eng. C.*, 2010, **30**, 1129-1136.
13. K. Fukushima and Y. Kimura, *Polym. Int.*, 2006, **55**, 626-642.
14. M. Aider, *LWT-FOOD SCI TECHNOL*, 2010, **43**, 837-842.
15. K. S. Bisht, L. A. Henderson, R. A. Gross, D. L. Kaplan and G. Swift, *Macromolecules*, 1997, **30**, 2705-2711.
16. M. Bouyahyi, M. P. F. Pepels, A. Heise and R. Duchateau, *Macromolecules*, 2012, **45**, 3356-3366.
17. S. M. Guillaume and J.-F. Carpentier, *Catal. Sci. Technol.*, 2012, **2**, 898-906.

18. L. van der Mee, F. Helmich, R. de Bruijn, J. A. J. M. Vekemans, A. R. A. Palmans and E. W. Meijer, *Macromolecules*, 2006, **39**, 5021-5027.

19. M. C. Arno, M. Inam, Z. Coe, G. Cambridge, L. J. Macdougall, R. Keogh, A. P. Dove and R. K. O'Reilly, *J. Am. Chem. Soc.*, 2017, **139**, 16980-16985.

20. A. T. Lorenzo, M. L. Arnal, J. Albuerne and A. J. Müller, *Polym. Test.*, 2007, **26**, 222-231.

21. H. Marand, J. Xu and S. Srinivas, *Macromolecules*, 1998, **31**, 8219-8229.

22. B. Lebedev and A. Yevstropov, *Die Makromolekulare Chemie*, 1984, **185**, 1235-1253.

23. S. Nojima and H. Marubayashi, in *Polymer Morphology*, 2016, 165-180.

Chapter Five – Conclusions and Outlook

This thesis has been focused on expanding the scope of crystallisation-driven self-assembly (CDSA) of degradable polylactone-contained polymers to prepare both 1D and 2D nanomaterials. In particular, studies into self-nucleation of block copolymers bearing a polylactone block have been considered in detail.

The first interest has been placed on the solvent effect, which is one of the most common factors in CDSA. This is demonstrated by $PPDL_{25}$-*b*-$PDMA_{110}$ cylindrical micelles prepared by self-nucleation in several solvents with different polarities. Nano DSC experiments have shown self-nucleation rates could be adjusted by different solvent polarities, which could tune the length of cylindrical micelles. With further study and optimisation, this work offers great potential to determine precise thermal conditions and manipulate the self-nucleation rates in CDSA, purely by changing the solvent.

However, manipulating the self-nucleation by the solvent is not applicable in epitaxial crystallisation, which is generally carried out in the same solvent after polymer self-nucleation. This has been discovered by the unavoidable homogenous self-nucleation during the attempted epitaxial crystallisation of PVL block copolymers. Herein, a new method to control the polymer self-nucleation is introduced, where a core-forming block with a random architecture of PVL and PPDL was studied in CDSA. Following the independent crystallisation of PPDL and PVL fragments at different temperature ranges revealed by NanoDSC, significant change in length of cylindrical micelles was resulted from temperature-controlled self-nucleation, where the crystallisation of PVL in the random copolymer chain could be suppressed at a selected temperature. This method was then proven to efficiently overcome the homogenous self-nucleation of PVL_n-*b*-$PDMA_m$ during epitaxial growth by the successful preparation of the blending P(PDL-co-

VL)$_n$-*b*-PDMA$_m$ and PVL$_n$-*b*-PDMA$_m$ platelet micelles with highly controlled dimensions and a low dispersity in n-butanol. Therefore, this co-crystallisation-driven self-assembly approach has overall drawn a pathway to optimise homogenous self-nucleation for a wide range of crystalline cores whenever a copolymerisation is possible for the core-forming block.

Based on the study of self-nucleation of PPDL and PVL, one more lactone, ζ-heptalactone was studied. The T_m and T_c of PHL homopolymers were determined by isothermal DSC experiments which are in line with other polylactones. Following this, the corona chemistry of PHL copolymers has been shown to play an important role in associating phase separation and polymer self-nucleation. With further comparable experiments to other polylactones, this could allow predicting the conditions for CDSA of different polylactones while aiming at specific nanostructures.

Given the high interest in the preparation of precisely size-controlled micelles, further research will investigate the epitaxial growth of these polylactone-contained polymers, based on the understanding of their self-nucleation outlined in this thesis. Especially for PPDL block copolymers, the controlling self-nucleation method shown in the epitaxial growth of PVL should allow for the formation of controlled 1D cylindrical and 2D platelet morphologies. It is also expected degradation and biocompatibility studies of these nanostructures prepared by different polylactones were monitored for future use in biorelevant applications.